PhD degree in Molecular Medicine

European School of Molecular Medicine (SEMM),

University of Milan and University of Naples “Federico II”

Faculty of Medicine, Department Scienza della salute

Settore disciplinare: BIO/11

POLYCOMB ROLE IN CELLULAR PROLIFERATION AND TRANSFORMATION

Andrea Piunti

IFOM-IEO Campus, Milan

Matricola n. R08897

Supervisor: Dr. Diego Pasini

IFOM-IEO Campus, Milan

Anno accademico 2012-2013

TABLE OF CONTENTS

LIST OF ABBREVIATIONS

AdoHcy: S-adenosylhomocysteine

bp: base pairs

BrdU: Bromodeoxyuridine

CDK: Cyclin dependent kinase

CG: Cytidine-Guanine dinucleotide

ChIP: chromatin immunoprecipitation

ChIP-chip: chromatin immunoprecipitation-microarray chip

ChIPseq: ChIP-sequencing

CldU: Chlorodeoxyuridine

cKO: Conditional knockout

CMP: 5'-cytosine mono-phosphate

CpG: cytosine/guanine di-nucleotides

Ctrl: shRNA control

DAPI: 4',6-diamidino-2-phenylindole

dCTP: 5'-deoxycytosine triphosphate

Dpc: days post-coitum

DNA: Deoxyribonucleic acid

DLBCL: Diffused large B-cell lymphomas

DKO: double knockout

DMEM: Dulbecco's modified eagle medium

DZNep: 3-deazaneplanocin A

EMT: Epithelial to Mesenchymal Transition

ER: Estrogen receptor

ERT^2: Estrogen receptor Type 2

ES: embryonic stem

ESS: Endometrial Stromal Sarcomas

EtOH: Ethanol

FACS: Fluorescence-activated cell sorting

FBS: Fetal Bovine Serum

FC: Fold change

Fx: floxed

FDR: false discovery rate

G34R: Glycine to arginine substitution in position 34

GEO: Gene Expression Omnibus

H2AK119ub1: mono-ubiquitylation of lysine 119 on histone H2A

H3K27me3: tri-methylation of lysine 27 on histone H3

H3K4me3: methylation of lysine 4 on histone H3

H3K27R: Lysine to arginine mutation on histone H3 position 27

HSC: Hematopoietic stem cells

iBAQ: intensity based absolute quantification score

IdU: Iododeoxyuridine

IOD: Inter-origin distances

IP: immunoprecipitation

kb: kilobase

λ: wave length

Linc: Large intervening non coding

LC: liquid chromatography

LT: Large T antigen

K27M: Lysine to Methionine substitution in position 27

KO: Knockout

MeCN: acetonitrile

MEF: mouse embryonic fibroblasts

mHSC: mouse hematopoietic stem cells

min: minute

miRNA(s): microRNA(s)

MS: mass spectrometry

N: number of replicates

ncRNA: non-coding RNA

NPC: Neuronal precursors cells

nSC: Neural stem cells

OHT: 4-hydroxytamoxifen

ONor O/N : over night

p-val: p-value

PAI: Protein Abundance Index

PBS: phosphate buffered saline

PcG: Polycomb group proteins

PCR: polymerase chain reaction

PRC1: Polycomb repressive complex 1

PRC2: Polycomb repressive complex 2

PRE: Polycomb responsive element

PTM: post-translational modifications

R26: Rosa 26

R-loops: RNA loops

RMA: Robust Multi-array Average

RNAi: RNA interference

RT: Room Temperature

SA-βGal: Senescence-associated β-galactosidase

SD: Standard deviation

SDS: sodium dodecyl sulfate

SDS: sodium dodecyl sulfate-polyacrylamide gel electrophoresis

SCF: Stem cell factor

SE: standard error

shRNA: short hairpin RNA

SLLC: Squamous Lung Cell Carcinoma

ssDNA: single stranded DNA

SV40 ER: SV40 early region

T-ALL: T-cell acute lymphoid leukemia

T641F: Threonine to phenylalanine substitution in position 641

T641N: Threonine to asparagine substitution in position 641

T641S: Threonine to serine substitution in position 641

TBS: TRIS-buffered saline

TFA: trifluoroacetic acid

TrxG: Trithorax group proteins

TSC: Tobacco smoke condensate

TSG: Tumour suppressor gene

TTF: Tip tail fibroblasts

Ubq: ubiquitin

Vi: internal volume

Wt: wild type

FIGURE INDEX

Abstract

The Polycomb Group proteins (PcGs) are present in cells nuclei as two main repressive complexes named Polycomb Repressive Complex 1 (PRC1) and 2 (PRC2). Both have been involved in several cellular functions among which the ability to promote cellular proliferation is the main PcG feature that links their activity to cancer development. Both complexes are directly involved in repressing the transcription of the Ink4aArf locus that encodes for the tumor suppressive proteins p16 and p19/Arf (p14/Arf in humans), potent inhibitors of cell growth via the positive regulation of pRb and p53 functions. Thus, since the activity of both PRC1 and PRC2 complexes is frequently enhanced in different type of human tumors, inhibition of PcG function has been proposed for many years as a potential strategy for cancer treatment. Yet, the fact that the pro-proliferative role of PcG proteins depends on the repression of the pRb and p53 pathways, of which most if not all tumors are defective, generates a scientific paradox for the effectiveness of PcG inhibition in cancer treatment. In this thesis, with the help of my colleagues, (from now on referred as we) I will present data showing how PcGs genetic depletion dramatically impairs cellular proliferation independently on the expression of the Ink4a/Arf locus or p53 and pRb activities. We also genetically demonstrate, in cell culture and *in vivo*, that PcGs activity is required for both the transformation and the maintenance of the transformed phenotype obtained by expression of potent oncogenes such as H-RASV12 or c-MYC in cells defective for the pathways of p53 and pRb. Finally we suggest a potential mechanism to explain the reduced proliferation/tumorigenic potential involving DNA replication control by PcG proteins. We show defects both in fork progression and fork symmetry along with increased replication origin numbers in PcGs knockout transformed cells. Collectively these data strongly support PcGs as master regulators of cellular proliferation and transformation independently on the impairment of main tumor suppressive pathways and

introduce a novel general mechanism through which PcGs regulate these processes. Overall this work supports PcGs as druggable targets in tumors where oncosuppressive pathways are de-regulated and proliferation, ergo DNA replication, is enhanced.

Aims

The aims of this thesis mainly consist in dissecting Polycomb proteins role in the regulation of cellular proliferation and transformation. Precisely we try to elucidate the contribution of the main subunits of the Polycomb repressive complexes to cellular proliferation and transformation using primary cell lines genetically defecting the main negative regulators of cell cycle and the most known tumor suppressor genes. This allows us to study whether Polycomb proteins may play a role in a situation of uncontrolled proliferation, the hallmark feature of tumors. We next investigate the role of these proteins in both formation and maintenance of tumors generated by primary cell lines defective in tumor suppressive genes and fully transformed with well-known potent oncogenes. Last we try to elucidate the molecular mechanism that links Polycomb proteins to both controlled and uncontrolled proliferation by analyzing transcriptional changes induced by Polycomb loss as well as followed by deeply investigating a putative role of Polycomb proteins in S-phase and particularly in DNA replication.

CHAPTER 1: Introduction

1.1 Polycomb group proteins

The group of Polycomb proteins (PcG) is a biochemically heterogeneous family classified by their ability to induce, when mutated, homeotic transformations in *Drosophila melanogaster*[2-6]. Mutations of PcG proteins induce developmental defects that are all accounted by spatial-temporal deregulation of homeotic genes expression[2]. Trithorax Group proteins (TrxG) form a second class of developmental regulators that counteract the effects of PcG mutations. PcG and TrxG proteins act on common regulatory pathways and, at least from Drosophila studies, they are not involved in determining the ON and OFF state of target genes but they play an essential role in maintaining a pre-set repressed (PcG) or active (TrxG) transcriptional state throughout development functioning as pivotal factors in cellular memory[3, 5, 6].

PcG proteins are highly conserved in evolution. Orthologues can be found in plants, worms, insects, amphibians, fishes and mammals and in all classes PcGs exhibit important developmental functions[2, 4]. PcG proteins are biochemically associated in two distinct multiprotein complexes named Polycomb Repressive Complex (PRC) 1 and 2[7]. The PRC1 complex includes a large number of subunits with different biochemical proprieties (Ring, Chromo and Zinc finger domains)[7]. The minimal core PRC1 complex for *in vitro* activities requires Polyhomeotic (Ph), Polycomb (Pc), Posterior Sex Comb (PSC), and RING1[8-10]. Nevertheless, the great increase in genes redundancy found in mammals suggests the existence of different forms of PRC1 that could have cell type specific functions and or compensatory effects. Genetic mouse models for some PRC1 subunits support such hypothesis. For example, *Ring1b*-/- (RING1 in flies) mice are embryonic lethal at E9.5[11] while Knock Out (KO) mice for the proto-oncogene *BMI1* (PSC in flies) are viable but present strong developmental defects in the hematopoietic and nervous system[12].

The core of the PRC2 complex is formed by the three PcG proteins EZH2, EED and SUZ12 and by the histone binding proteins RbAp46/48[13-16]. KO mice for *EZH2*, *EED* and *SUZ12* are embryonic lethal during gastrulation[17-19] stressing the developmental role of PRC2 also in mammals. Additional subunits of PRC2 include, PHF1[20, 21], MTF2[22-24] and the DNA binding proteins AEBP2[13] and JARID2[22, 23, 25-27].

The use of high-throughput approaches such as Chromatin Immunoprecipitation (ChIP) coupled to microarray hybridization (ChIP-chip) or to next generation sequencing (ChIP-seq) demonstrated that PcG proteins directly associates to promoters of important regulator of cell fate and development[1, 28-31]. While PcG target genes are highly conserved in different organisms (mouse vs. human) the large amount of PcG targets differ between cell types[1, 32, 33]. For example, using a ChIP on chip approach to follow PRC2 activity during the differentiation of mouse Embryonic Stem (ES) cells into Neuronal Precursor Cells (NPC) and their further terminal differentiation into Neurons, the Dirk Schübeler laboratory showed that at each differentiation step, despite a constant number of regulated genes, PRC2 exchanged approximately 50% of target genes[32]. This suggests that the downstream pathways are lineage specific and undergo dynamic regulation during differentiation. The mechanisms that regulate these processes are still enigmatic and likely involve several different factors and signals.

1.2 Epigenetics: histones and DNA modifications

Within the cell nucleus, the DNA is tightly associated with histone proteins and form, together with other non-histone proteins, hyper condensed structures defined as chromatin[34]. Both histones and DNA present different modifications of which the best characterized include histones methylation, acetylation, ubiquitination, and phosphorylation as well as cytosine methylation (and its oxidized form) of DNA CpG di-nucleotides [35]. The work of several laboratories have put a tremendous effort to identify and characterize the enzymatic activities that catalyze deposition and removal of histones and DNA modifications demonstrating that: 1) chromatin modifications play an essential

role in regulating DNA transcription and genome stability; 2) Modifications are not stable and can be actively reverted by specific enzymatic activities; 3) At least in some cases, chromatin modifications are self-sufficient and can be maintained independently of the DNA sequence[36] linking chromatin modifying factors with epigenetic regulation of transcription.

The term epigenetic was coined by Conrad Waddington in 1942 more than ten years before Watson and Crick proposed the structure of the DNA and two years before Oswald Avery, Colin MacLeod, and Maclyn McCarty demonstrated that the DNA was the source of hereditary information. Waddington defined epigenetic as "*a branch of biology that study the casual interactions between genes and their products*" [37] while a more recent definition proposed by Levenson and Sweatt links epigenetic directly to chromatin modifications by defining it as: "*the mechanism for the stable maintenance of gene expression that involves physically 'marking' DNA or its associated proteins*" allowing " *genotypically identical cells to be phenotypically distinct*" [38]. Indeed, several chromatin-modifying factors play essential roles in regulating epigenetic phenomena such as gene imprinting and X-chromosome inactivation[39].

PcG proteins (as well as their counterpart TrxG) belong to this class and execute their transcriptional activity by modifying the chromatin surrounding their association sites[7, 40]. The PRC2 complex, through its catalytic subunit EZH2, modifies histone H3 by di- and tri-methylating (me2/me3) lysine (K) 27[13-16]. Such activity requires a minimal PRC2 complex formed by EZH2, EED and SUZ12[19, 41] and it is essential for PRC1 binding to the same target sites [42]. It has been proposed that the chromo-domain proteins of the PRC1 complex (CBX4, CBX6, CBX7 and CBX8) bind H3K27me3 and mediate PRC1 recruitment[13, 15, 43]. PRC1, through the ubiquitin ligase activity of RING1B, mediates ubiquitylation (ubq) of histone H2A K119 (in mammals)[44] inducing stable transcriptional repression possibly thought chromatin compaction and inhibition of SWI/SNF chromatin remodeling activity [8, 45].

1.3 Polycomb group proteins in tumors

Cancer is a heterogeneous disease that at a molecular level involves a multitude of different regulatory pathways and proteins. In general, at malignant stages, cancer cells acquire unlimited replicative potential, angiogenesis capabilities, the ability to evade apoptosis, self-sufficiency in growth signals, insensitivity to growth inhibition and acquire invasive (metastatic) proprieties[46, 47]. To achieve this, cells undergo a multistep process which gradually leads to a loss of cellular identity towards the acquisition of cancer cell capabilities. In both sporadic and hereditary cancers a large number of genetic alterations have been characterized and for many of these mutations the oncogenic proprieties were validated in mouse models [48-52]. Such genetic mutations are required but not fully sufficient for cancer development since most cancer models retain latency periods before the onset of the disease in order to accumulate additional genetic or epigenetic events to allow full cancer development [53]. Chromatin-modifying proteins seem to play an important role in this process. A classic example is the 11q23 translocation in leukemia involving the Mixed Lineage Leukemia gene *MLL,* a TrxG protein and a histone H3K4 specific methyltrasferase [54]. Among these factors, PcG proteins have critical roles in the development of several cancers [55, 56].

The first evidence of a PcG protein having a direct role in cancer formation was the identification of BMI1 as a proto-oncogene that cooperate with MYC in the formation of B-cell Lymphomas [57]. Since then, the attention at role of PcG proteins in human cancer gradually increased and raised dramatically together with the discovery of the enzymatic activities of both PRC1 and PRC2 complexes[13-16, 44].

Together with BMI1, the best-characterized PcG protein in human cancer is the catalytic subunit of the PRC2 complex EZH2. Ten years later the discovery of BMI1 oncogenic proprieties, EZH2 was identified as a direct downstream target of the pRB/E2F pathway and one of the most frequent over-expressed genes in malignant prostate cancer [58, 59].

Despite several subunits of both PRC1 and PRC2 complexes have critical roles in regulating PRCs activities, the cancer related attention of the scientific community mainly focused on BMI1 and EZH2. Whether this is a bias or a consequence of unproductive results is unclear. Some contradicting results on other PRC1 components suggest that PcG oncogenic proprieties might reside in single subunits rather than complexes activities. In addition few Polycomb proteins have been proposed as tumor suppressor in specific tumour types[60-62]. This unexpected and less known face of PcG proteins is in contradiction with the extensively characterized oncogenic role of PcGs. This intriguing observation may find an explanation in uncharacterized functions of PcG proteins that remain to be investigated.

1.4 Polycomb in Prostate Cancer

EZH2 was identified as one of the most frequent and highly expressed gene in malignant prostate cancers [58]. High EZH2 expression strongly correlates with metastatic tumors and poor survival making EZH2 a potential marker for prostate cancer prognosis [58]. Like EZH2, also BMI1, RING1B and CBX7 [63, 64] are found highly expressed in prostate tumors. Using RNAi and ectopic expression approaches, different studies have characterized the role of PcGs in the proliferation of prostate cancer cells. EZH2 RNAi in different cell lines demonstrates its essential role in cancer cell proliferation [58, 64-66]. Similar effects were also reported for CBX7 [63]. Importantly, overexpression of both EZH2 and CBX7 promote cell proliferation and transformation of benign cells [58, 63, 67]. Interestingly, despite CBX7 expression only give a slight proliferative advantage to LNCaP cells (androgen-sensitive human prostate adenocarcinoma cells), it cooperates with C-MYC to promote insensitivity to androgen dependent growth inhibition [63]. In contrast, the expression of MEL18 (the mammalian paralog of BMI1) is frequently lost in prostate tumors suggesting a tumor suppressive function [68]. It is not clear if loss of MEL18 expression has any causative role in prostate cancer but this observation could odd with the redundant roles of MEL18 and BMI1 in regulating normal hematopoiesis and INK4A-ARF expression [69-71]. In addition

Bmi1 and Akt pathways are found potentiated in high grade prostate tumors and Bmi1 phosphorylation by Akt enhanced its E3 ligase activity and, it's supposed, also its oncogenic ability in an Ink4a/Arf independent, DNA damage repair dependent manner[72].

The mechanisms that contribute to PcG over-expression in prostate cancer are still poorly understood. The frequent deregulation of the pRB/E2F pathway likely contributes to PcG overexpression [59]. Specific amplifications of both the *EZH2* and *BMI1* loci correlate with high protein expression [73, 74]. In addition, loss of expression of the micro RNA (miR) 101 in metastatic prostate tumors correlates with high EZH2 expression [75]. In this work, the authors showed that in breast and prostate cancer cells miR-101 targets EZH2 mRNA and negatively regulates its translation [75].

The mechanisms by which PcG proteins could promote prostate cancer development are also still poorly understood. Growth inhibition induced by CBX7 RNAi correlates with increased ARF and p16 expression [63]. Other evidences have been presented on a direct role of EZH2 in repressing PSP94, a small protein abundantly secreted by the prostatic gland that inhibit tumor growth and metastases whose expression is silenced in prostate cancers [76]. In addition, an extensive worked aimed to identify genes directly regulated by EZH2 found *ADRB2* as an important EZH2 target [66]. ADRB2 is a ß-adrenerigic receptor whose expression is directly silenced by EZH2 in metastatic prostate cancers. Loss of ARDB2 expression induce cell invasion in benign prostate cells while its constitutive expression counteract the proliferative and metastatic proprieties induced by EZH2 overexpression. Such regulatory pathway is not restricted to prostate cells and is conserved in a model of mammary epithelial cell transformation [66]. An additional target of polycomb repression is the Ras GTPase-activating protein DAB2IP linking PcGs to RAS signaling pathway [77]. Finally, a study aimed to identify PcG regulated genes in prostate tumors identified a signature of 14 PcG direct targets that, when silenced, predicts poor patients survival [78]. Despite the prognostic relevance of this finding, the link between repression of these targets and cancer development has not been investigated. Moreover it has also been

shown that in prostate cancer cells Ezh2 represses a complex miRNA network whom would, if de-repressed or ectopically express, target members of PRC1 leading to their silencing and loss of oncogenic potential[79]. More recently it has been proposed that Ezh2 can regulate tumorigenicity of castration-resistant prostate cancer cells in a "solo" mode. This consists in its ability to promote tumors in a PRC2 independent manner acting as transcriptional co-activator for different transcription factors included the androgen receptor[80, 81]. Finally, for correctness sake, it must be said that this last observation odds with previous published data showing genome wide repression of target genes impressed by androgen receptor through Ezh2 binding[82].

1.5 Polycomb in Brain Tumors

Glioblastomas are aggressive tumors arising from all cells of the central nervous system. Glioblastomas are highly proliferative with a poor prognosis that results in rapid death within 12 months from diagnosis [83]. Several publications reported that BMI1 and EZH2 are highly expressed in Glioblastomas [84-87]. Down-regulation of either EZH2 or BMI1 expression blocked glioblastoma cell proliferation [84, 87]. RNAi mediated down regulation of EZH2 reduced tumor formation *in vivo* consistent with the block of cancer development observed in mice treated with the EZH2 inhibitor DZNep [86, 87]. Importantly, using *Bmi1-/-* mice, the Maarten van Lohuizen laboratory showed that Bmi1 is essential for the development of glioblastomas in a mouse model that involves loss of Ink4A-Arf expression and Egfr mutations [88]. Interestingly, the requirement of Bmi1 in such model highlights Ink4a/Arf independent functions of Bmi1. In glioblastomas, loss of miR-128 expression negatively correlates with Bmi1 levels. Mir-128 directly regulates Bmi1 translation suggesting an important regulatory mechanism for PcG overexpression in brain tumors [85].

The downstream effects to BMI1 over expression are still poorly characterized. BMI1 acts positively on GSK3ß activity, a growth promoting kinase highly expressed in glioblastomas [86]. Another report proposed a role for Bmi1 in regulating p21 expression to

allow neural stem cells (nSC) self-renewal suggesting a potential mechanism to suppress anti-proliferative factors independently of Ink4a/Arf[89]. In addition, it was proposed that BMI1 overexpression is directly regulated by N-MYC and that BMI1 controls the expression of KIF1ß and TSLC1, two potential tumor suppressor genes in neuroblastoma [90]. Moreover, loss of *Bmi1* in *Ink4a/Arf* null nSC, leads to an increased secretion of extracellular matrix and increased adhesion trough the ß1-integrin receptor suggesting that Bmi1 overexpression could induce low matrix production and adhesion favouring motility and invasion [91]. No reports have been presented for other PcG proteins with the exception of an overlapping function of MEL18 with BMI1 in odds with its putative tumor suppressive role in prostate cancer [92]. The possible existence of PRC2 and PRC1 non-histone targets is now a new unexplored fascinating field. This was partially shocked by the recent work from Jürg Muller lab that elegantly showed, in *D. Melanogaster*, how replacement of all histones H3 with H3K27R mutants recapitulate PcG null phenotype in flies, strongly suggesting that, at least in *Drosophila*, PcGs activity goes entirely through its ability to methylate Lysine 27 on histone H3[93]. Nonetheless recently STAT3 has been reported as a PRC2 non-histone substrate in glioblastoma stem-like cells. Ezh2 phosphorylation on serine 21 is required for STAT3 methylation, this methylation in turn enhances STAT3 activity by means of tyrosine phosphorylation increasing its oncogenic ability in glioblastoma cells[94]. Finally a study that combined an RNAi screening with ChIP-seq data revealed an Ink4/Arf independent role for Bmi1 in maintaining malignant glioma-stem cells probably indirectly negatively acting on Atf3 tumor suppressor pathway[95]. Moreover in contrast to its already described oncogenic role, in that study, CBX7 has been reported to act as tumor suppressor[95] adding another layer of complexity to the already complicated PcG-cancer tale. Anyway a tale is never complex enough if there is not at least another point of view from which the reader could be intrigued, and in this case “the other point of view” consists in the histone tail mutations reported in pediatric gliomas[96, 97]. These mutations have been identified in pediatric glioblastoma by two

different groups that showed the presence of a couple of somatic point mutations on the histone genes H3F3A and HIST1H3B causing a lysine to methionine substitution at position 27 (K27M) or a glycine to arginine substitution at position 34 (G34R) in a large number of patient[98-100]. Despite the K27M seems to occur only in one or two of the several histone H3 alleles therefore, most likely, not accounting for an important representation in the chromatin landscape, a couple of very recent works ruled out that, this is sufficient to globally affect the PRC2 activity[101, 102]. Both these works demonstrated indeed that the entire ability of PRC2 to tri- or di- methylate the histone H3 on the lysine 27 was completely abolished in pediatric glioma derived cells presenting the K27M mutation[101, 102]. Moreover, exogenous expression of H3K27M definitely impairs PRC2 activity also in other cell types suggesting a cell type-independent mechanism of action for this mutant histone[101, 102]. Finally, one of the two works strongly suggests, using biochemical approaches, that this mutant can inhibit PRC2 activity by tightly binding to Ezh2 catalytic pocket inhibiting its function[101]. Interestingly enough, from that study emerged that by exogenous expression of the mutant histone in 293T cells, this was found in only the 1% of the chromatin but at the same time inhibits the entire PRC2 catalytic activity thus strongly suggesting its possible *in trans* activity on Ezh2[101]. In conclusion, despite in one hand PcG proteins seem to be pro-oncogenic in glioblastomas, on the other a large fraction of pediatric gliomas presents a mutation on histone H3 that is able to entirely inhibit PRC2 function. Even if the role of the mutated histone in pediatric glioma pathogenesis remains still to be established, its discovery along with its mechanism of action are largely irreconcilable with the well-characterized pro-tumorigenic activity of PcG proteins, contributing to add another mysterious piece to the already complicated puzzling PcG-cancer tale.

1.6 Polycomb in Breast Cancer

Breast tumors are another well-documented cancer type where PcG proteins are found significantly overexpressed. EZH2 is highly expressed in a wide range of breast cancers [59,

[103, 104]. Its high expression is detected in pre-neoplastic mammary lesions suggesting that deregulated PRC2 activity is an early event in the development of breast tumors [105]. Similar to prostate cancer, high EZH2 expression correlates with metastatic sporadic and familial breast tumors and strongly associates with bad prognosis [104, 105]. Analysis of BMI1, MEL18 and HPC2 showed that only BMI1, between the PRC1 group, is found overexpressed in breast cancers correlating with MYC expression [106]. MEL18 expression was instead frequently lost further supporting its tumor suppressive role in epithelial tumors [107]. Both BMI1 and EZH2 show direct oncogenic roles in breast cancer formation. EZH2 overexpression in normal immortalized epithelial cells induces anchorage independent growth and invasive potential [104] while BMI1 overexpression collaborates with H-RAS in transforming MCF10A breast epithelial cells [108]. One report proposed that EZH2 is essential for the proliferation of BRCA1-/- cells and those similar phenotypes are observed with the use of the EZH2 inhibitor DZNep [109]. *In vivo* overexpression of EZH2 is not sufficient to induce breast cancer formation yet induce full penetrant hyperplasia of the mammary epithelia supporting *in vivo* EZH2 oncogenic functions [110]. In addition to *ADRB2* repression [66], no other mechanisms have been proposed in breast cancer. *In vivo* over-expression of EZH2 induces an upregulation of the Wnt/ß-Catenin signaling pathway and association of EZH2 with nuclear ß-Catenin [110]. Despite the attractive transcriptional link, no mechanisms have been proposed for such interaction. Importantly, poorly differentiated breast tumors present an ES cell like signature characterized by the expression of pluripotency factor like NANOG, OCT4, SOX2 and MYC and PcG targets repression. Such signature strongly correlates with high-grade Estrogen Receptor negative tumors and poor clinical outcome [111]. Finally, an exciting publication demonstrated that *HOTAIR*, a Large intervening non coding (Linc) RNA, is overexpressed in primary and metastatic breast tumors and that *HOTAIR* overexpression associates with a poor clinical outcome [112]. *HOTAIR* is transcribed from the *HOXC* locus and through direct association with the PRC2 complex regulates *HOXD* expression in normal skin fibroblasts [113]. Direct

HOTAIR overexpression increases cancer epithelial cells invasiveness in a PRC2 dependent manner while loss of *HOTAIR* expression reduced this potential [112]. Consistent with its ability to bind the PRC2 complex, *HOTAIR* overexpression redirect PRC2 binding to the DNA towards a fibroblast like signature [112]. More recently it has been shown that BRCA1, a well-known TSG in breast and ovarian cancer, is able to inhibit PRC2 binding to *HOTAIR* thus resulting in de-localization of EZH2 on chromatin[114]. Such result not only introduces a new key mechanism of regulation of PcG functions in cancer cells but propose an important role for LincRNAs in epigenome regulation.

1.7 Polycomb in Hematological Malignancies

As mention earlier, BMI1 was first identified as a proto-oncogene that collaborates with c-Myc in inducing B-Cell Lymphomas[57]. EZH2, EED and BMI1 have important functions in normal B-cell development and KO mouse models for these proteins display impairment in proper B-cell differentiation[12, 115, 116]. EZH2 and BMI1 are frequently expressed at high level in different types of B-cell lymphomas[117-120]. BMI1 over-expression correlates with an active B cell phenotype[121] and transgenic mice expressing BMI1 in the lymphoid compartment stimulate lymphoma formation[122]. Even though, historically, BMI1 has been largely studied in lymphoma and hematological malignancies, today, indisputably, the scientific world eye is tightly focused on EZH2. This is largely due to the discovery of recurrent mutations identified in diffused large B-cell lymphomas (DLBCL) that affect EZH2 SET catalytic domain. Initially, a frequent (~7 to 20% of cases) mutation at Tyrosine (T) 641 of EZH2 in B-Cell Lymphomas that, at that time, was considered an inactivating mutation[123]. That interpretation, indeed, was in sharp contrast with the general idea that increased PRC2 activity had oncogenic functions. Moreover that mutation was found only in heterozygosity indicating that a wild type EZH2 allele is required for lymphoma maintenance[123]. At that time the information were very few and poorly characterized to really rule out how an EZH2 heterozygote putatively inactivating mutation could affect lymphomagenesis and the overall PRC2 activity. During the same year, a

biochemical study identified the T641 mutations (T641F, T641N and T641S) has a "super-activating" mutation[124]. That work demonstrated, indeed, how the mutated EZH2 was able to rapidly and processively convert H3K27 di-methylation to H3K27 tri-methylated H3K27 while less efficiently converts mono-methylation to di-methylated H3K27 and shows nearly no activity on unmethylated histone H3 compared to EZH2 wt containing PRC2[124]. These findings were also successively confirmed by another similar work[125]. Therefore, while initially this mutation was erroneously considered inactivating, EZH2 T641 mutations are, on the contrary, increasing the normal EZH2 ability to convert H3K27me2 to H3K27me3. Whether this mutation participated or not to lymphomagenesis is still not fully understood. However, different labs and companies have made strong efforts to develop selective compounds which are able to inhibit the mutated form of EZH2[126]. When lymphoma cells were treated with those compounds, the tumorogenic potential was abolished or strongly impaired both *in vitro* and *in vivo*, thus strongly supporting a pivotal role for mutated EZH2 in the lymphoma pathogenesis[127-129]. However, the inability of the mutated form to efficiently methylate the unmethylated histone H3 or to convert H3K27me1 to H3K27me2/me3 highlights the key role for EZH2 wild-type allele[124]. This mechanism is supported by the lack of homozygous mutations in DLBL derived cells[130]. Indeed, a transgenic mouse carrying an inducible extra copy of the EZH2 allele that harbours the T641N missense mutation was recently generated[131]. When the mutated allele was expressed in the germinal center B-cells, it led to a strong germinal center hyperplasia suggested to be largely caused by the transcriptional repression of the Cdkn1a tumor suppressor locus and by an impairment of differentiation[131]. However, the mutant Ezh2 expression in the germinal center was never compared with its WT counterpart, leaving open the possibility that is the mere EZH2 overexpression to induce hyperplasia. Importantly, a mouse model harbouring an inducible *Ezh2* extra allele in the hematopoietic cells was already available[132] and activation of the extra-copy of *Ezh2* wild-type allele in hematopoietic cells was shown to induce myeloproliferative diseases[132]. An

additional PcG protein involved in Lymphoma development is CBX7. CBX7 is a PRC1 chromo-domain subunit that mediates PRC1-H3K27me3 interaction [43]. CBX7 is expressed in germinal center lymphocytes and in germinal center derived lymphomas in correlation with Myc expression. Ectopic expression of CBX7 in lymphoid progenitors initiates T-cell lymphomas and its co-expression with Myc induces formation of aggressive B-Cell lymphomas [133]. Both PRC2 and PRC1 complexes play an important role in the oncogenic activities of PML-RARα and PLZF-RARα, two fusion proteins that cause Acute Promyelocytic Leukemia [134]. Both fusion proteins induce recruitment of PRCs repressive activities at retinoic acid responsive promoters and depletion of either EZH2 or BMI1 decrease the oncogenic potential of PML-RARα [135] and PLZF-RARα [136] by promoting cellular differentiation. In addition, BMI1 is found frequently over-expressed in patients with either Acute Myeloid Leukemia or Chronic Myeloid Leukemia [137-139]. In the latter case, high BMI1 expression correlates with bad survival [138]. Loss of BMI1 in mice delay the development of primary leukemia and, importantly, it prevents the onset of secondary leukemia possibly by promoting cancer stem cells exhaustion [140]. Interestingly, the use of PRC2 inhibitors such as DNZep reduces the leukemic potential of HL60 cells [141]. In line with the different roles of PRC1 members in solid tumors, the expression of PHC1/RAE28, a member of the PRC1 complex, is lost in some patients with Acute Lymphoid Leukemia suggesting a putative tumor suppressive role [142]. Finally, two works discovered that the *EZH2* locus is frequently targeted by deletions, missense and frame-shift mutations in myeloid disorders [130, 143]. In few cases such mutations are homozygous resulting in global loss of EZH2 enzymatic activity [130]. Finally, the global hematopoietic genetic knockout of *Ezh2* in mice, paradoxically, results in a highly-frequent γδ T-cell acute lymphoid leukemia (T-ALL)[62] in sharp contrast with the myeloproliferative disorders reported when Ezh2 was overexpressed in the same cells[132].

1.8 Polycomb in other tumors

Implications for EZH2 and BMI1 have been proposed in the development of lung tumours. EZH2 expression is low in normal epithelia but is found highly expressed in Squamous Lung Cell Carcinomas (SLCC) and correlates with high BMI1 and Ki67 expression[144]. Like EZH2, BMI1 is frequently overexpressed in SLCC (77% of cases)[145]. Consistent with this, in non-Small Cell Lung Cancer, BMI1 is required *in vivo* for K-RAS induced tumorigenesis with a mechanism that links RAS mutation lung cancer sensitivity with PcG proteins ability to repress the INK4b-ARF-INK4a locus (discussed later) [146]. Interestingly, the exposure of lung carcinoma cell lines to tobacco smokes condensate (TSC) represses the expression of the WNT signaling antagonist DKK1. DKK1 expression is frequently lost in tumor samples and knock down of DKK1 enhance tumor formation similar to TSC exposure. Importantly, TSC exposure triggers PcG proteins recruitment at the DKK1 promoter suggesting that TSC can induces epigenetic reorganizations that favor cancer formation through PcG mediated repression of tumor suppressor genes [147]. Significant increases in EZH2 and BMI1 expression has been reported in several others tumors suggesting that deregulation of PcG activities is a common feature of transformed cells. This includes, Hepatocellular Carcinomas[148, 149], Oral Squamous Cell Carcinomas[150, 151], gastrointestinal cancers[152-155], ostosarcomas[156] and bladder tumors[157-160]. In melanoma, while EZH2 expression increases between benign to melanoma nevi[161], BMI1 expression is lost in aggressive tumors and its high expression correlates with a favorable outcome suggesting a tumor-suppressive role[162]. In contrast, in normal nasopharyngeal epithelial cells, BMI1 over-expression induces epithelial to mesenchymal transition through a mechanism that involves direct repression of *PTEN* expression[163]. In bladder tumors, EZH2 levels are controlled by mir-101 similar to mammary and prostate cells [164]. High EZH2 expression in bladder cancers correlates with repression of the pro-apoptotic protein APAF1 and is associated with tumor stage and invasive potential [165]. In pancreatic carcinomas, BMI1 expression is frequently increased with particular high levels in cancer stem cells [155]. Recently it has been shown that Ezh2 is required for pancreatic cells

proliferation during pancreatic regeneration post-injury[166]. The mechanism through which Ezh2 controls pancreatic regeneration involves its ability to repress the Ink4a/Arf locus, moreover loss of Ezh2, paradoxically, seems to accelerate K-RAS driven pancreatic tumor[166]. In contrast, CBX7 expression is lost with high frequency in pancreatic carcinomas suggesting opposite functions for BMI1 and CBX7 in these tumors[167].

Consistent with this , a genomic region containing the PHC3 locus undergoes frequent loss of heterozygosity in osteosarcomas [168]. PHC3 expression is lost in approximately 65% of tumor samples of which a large proportion contains PHC3 mutations. The putative tumor suppressive function of PHC3 (as well as for other PRC1 proteins) is not clear but in quiescent and differentiated cells PHC3 co-localizes and associates with E2F6 suggesting anti-proliferative proprieties [168]. Finally, in Endometrial Stromal Sarcomas (ESS), the genomic loci of two different PcG proteins (SUZ12, and PHF1) translocate with the *JAZF1* locus [169, 170]. These translocations are found with high frequency in ESS leading to the expression of poorly characterized fusion proteins. Is not clear if the expression of these fusion proteins has oncogenic functions but an mRNA transcript, identical to the *JAZF1-SUZ12* fusion, is expressed as a product of a transplicing event in normal endometrial cells [171]. Such transpliced mRNA is specifically expressed in the proliferative stage of stoma cells during the menstrual cycle suggesting that JAZF1-SUZ12 fusion have growth promoting effects that are transiently required in the normal endometrium. Constitutive expression, due to genes translocation, might instead have oncogenic effects.

1.9 Polycomb recruiting mechanisms

The mechanisms of PcG recruitment to specific DNA sites are still poorly understood. Genome wide studies have shown that PcG proteins bind preferentially CG rich genomic regions but sequence analysis and transcription factor binding sites predictions failed to identify enriched consensus sequences[1]. In Drosophila, several DNA binding transcription factors are required for PcG and TrxG association at Polycomb Responsive Elements (PREs)[172], this allowed the development of an algorithm to determine novel PREs showing

that some predicted elements have PRE proprieties *in vivo*[173]. Despite this, the use of genome wide ChIP-chip approaches showed that predicted elements and PcG binding sites poorly overlap[174]. Moreover, application of such algorithm to mammalians genome fails to predict any potential PRE[173] consistent with the poor conservation of the Drosophila DNA binding factors in mammalian cells. In contrast, recent reports have identified two mammalian genomic regions with putative PRE behavior[175, 176] supporting a mechanistic conservation between flies and mammals. PcG and TrxG proteins seem to compete in metazoan for the same regulatory pathways (binding sites) and, despite the mechanisms of recruitment are poorly understood, deregulation of such equilibrium by either loss or gain of function of specific subunits may reflect in changes in cell identity that could play essential roles in pathogenesis. In mammalian cells, the DNA binding factors Aebp2[13], Jarid1A [22, 27, 177] and Jarid2 [22, 23, 25-27] associates with the PRC2 complex. These factors are required for the repression of specific PRC2 target genes but only Jarid2 is required for genome-wide PRC2 localization at chromatin in mouse ES cells[26]. Despite Jarid2 interaction to PRC2 is not restricted to ES cells, the differences in target genes between cell types suggests tissue specific mechanisms of PcG recruitment[1, 32, 33]. Therefore it is possible that Jarid2 stabilizes PRC2 association with DNA but that combinations with cell type specific transcription factors might specify target genes association. For example, SNAIL1 recruits PRC2 to repress E-CADHERIN expression [178] suggesting a potential role of PRC2 in regulating important cell adhesion molecules that inhibit Epithelial to Mesenchymal Transition (EMT) of metastatic cells. Consistent with this, PRC2 was also reported to interact in breast cancer cells with two critical EMT players, Estrogen Receptor and ß-CATENIN [179]. Several reports have recently shown that PRC complexes interact in the nucleus with non-coding (nc) RNAs. A possibility is that tissue specific ncRNAs determines and or contribute to PcG targets specification and that deregulations of such activities might have important roles in cancer development. So far the PRC2 complex was shown to interact with *Xist*, *Tsix RepA*, (ncRNAs of the X-chromosome inactivating

machinery) and *HOTAIR*. *RepA* mediates PRC2 recruitment to the inactivating X-chromosome (Xi) [180] while *HOTAIR* is required for PcG association and *HOXD* locus repression in primary foreskin fibroblasts [113]. In both cases, RNAi mediated inhibition of *RepA* and *HOTAIR* results in defective PcG recruitment. In addition to PRC2, CBX7 was shown to interact with *ANRIL*, a non-coding antisense transcript of the INK4B-ARF-INK4A locus [181]. Such interaction plays an important role in PcG association at the *INK4A* locus that; together with the high levels of *ANRIL* expression in prostate cancer, identifies a new important component of *INK4A-ARF* repression in cancer cells. A similar mechanism has been presented for *HOTAIR* in breast cancer where high *HOTAIR* expression correlates with an epigenetic reprogramming of PcG binding sites. Importantly, HOTAIR over-expression confers tumorigenic potential to benign cells in a PcG dependent manner[112]. It is still not clear how ncRNAs could regulate PcG binding but a recent report showed that *HOTAIR* can function as a scaffold for simultaneous recruitment of co-repressor complexes[182]. However, only very recently it has been shown that PRC2 can bind RNA in a promiscuous manner thus challenging the current specific ncRNA mediated PRC2 recruitment[183]. For what concerns PRC1 recruitment, for years the general accepted model consisted in a PRC2 dependent recruitment mechanism[184]. Precisely it has been shown that stable components of PRC1 such as the CBX proteins can target the entire PRC1 directly to chromatin through theirs ability to bind the H3K27me3 mark[13, 185]. Indeed it has been demonstrated that the abrogation of the entire H3K27me3 in *Eed* null mouse ES cells affects global Ring1b stability at chromatin but this does not affect the histone H2A lysine 119 mono-ubiquitination (H2a K119ub) levels[186]. These data indicate that, although PRC2 activity is required to stably localize the PRC1 at chromatin, H3K27me3 is generally indispensable to maintain global H2a K119ub levels. Moreover, very recently, different PRC2-independent PRC1 chromatin recruitment have been proposed[186-189] that could explain how global H2a K119ub levels do not change in PRC2 knockout cells.

1.10 Polycomb inhibitors

Due to the frequent deregulation of PcG activities in cancer cells and their role in regulating their proliferative potential, the inhibition of PcG functions is an attractive strategy for therapeutic approaches[126, 190]. To date no inhibitors have been developed for PRC1 while the 3-Deazaadenosine analog 3-Deazaneplanocin A (DZNep) has been shown to inhibit EZH2 activity[191]. 3-Deazaadenosine inhibits S-adenosylhomocysteine (AdoHcy) hydrolases and, by increasing AdoHcy intracellular levels, globally inhibits methyltransferases. DNZep treatment induces a strong degradation of EZH2 leading to loss of H3K27me3. DNZep treatment of cancer cells blocks proliferation induces apoptosis and reactivates PRC2 target genes expression[109, 141, 191, 192]. However, some concerns were raised about DNZep specificity and different reports have shown a more general effect of DNZep in inhibiting several other histone lysine and arginine methylations[191, 193]. Moreover, inhibition of EZH2 activity was reported by treating breast and bladder cancer cells with adenosine dialdehyde, another analog of 3-Deazaadenosine, and with the inhibitor of methyltransferases Sinefungin, an analog of S-adenosyl-methionine [193]. Whether or not these drugs are more specific then DNZep remains unclear. Recently new specific drugs targeting Ezh2 catalytic pocket have been generated[127-129, 131], these aimed preferentially to inhibit the new EZH2 gain-of-function mutations found in lymphoma (discussed earlier) but some of them could be also used to inhibit the wild type form of EZH2. An additional possibility to target PcG functions might reside in the ability of PRC1 and PRC2 complexes to bind directly H3K27me3 [36, 194]. While PRC1 affinity for H3K27me3 is weak and rather unspecific, PRC2 seems to have much stronger affinity and higher specificity [36]. It has been proposed that PRC2 binding to H3K27me3 is important for the maintenance of H3K27me3 during DNA replication [36]. H3K27me3 is directly bound by EED through its WD40 domain [194]. Importantly, mutations of critical EED H3K27me3 binding residues demonstrate that the association of PRC2 to H3K27me3 is essential to rescue both the developmental phenotypes and the global loss of H3K27me3

observed in EED deficient flies [194]. Inhibiting molecules specific for the aromatic methyl lysine-binding cage of EED may serve as an alternative strategy to block PRC2 functions. Only very recently Orkin's lab generated a molecule that is able to uncouple Ezh2:Eed binding thus inhibiting Ezh2 catalytic activity and stability[195].

1.11 Ink4b-Arf-InK4a locus and Polycomb control

One of the best-characterized PcG target in mammalian cells is the *INK4b-ARF-INK4a* locus [196-198]. This locus codifies for $p15^{INK4b}$, $p19^{ARF}$ ($p14^{ARF}$ in humans) and $p16^{INK4a}$, three important negative regulator of cell cycle that play important oncosuppressive roles in human tumors [199]. While $p16^{INK4a}$ and $p15^{INK4b}$ binds to Cyclin/CDK complexes and inhibit cell cycle by blocking CDK mediated phosphorylation of the Retinoblastoma protein pRB, $p14^{ARF}$ binds to MDM2 and blocks its ability to degrade p53. Stabilization of p53 has anti-proliferative and pro-apoptotic effects in part through the transcriptional activation of the Cyclin/CDK inhibitor p21 [199]. Loss of function of any of these proteins has growth-promoting effects and prevents cells to undergo replicative and or oxidative induced senescence [199]. In proliferating cells, PcG proteins associate to the *INK4b-ARF-INK4a* locus to maintain its repression. Both PRC1 and PRC2 components associate specifically at the $p16^{INK4a}$ promoter [196, 197]. Several reports have shown that loss of PcG functions induce cellular senescence and correlates with activation of *INK4b-ARF-INK4a* expression [196-198, 200]. BMI-1deficient mouse embryonic fibroblasts (MEF) undergo a dramatic block of proliferation and a strong activation of $p15^{INK4b}$, $p19^{ARF}$ and $p16^{INK4a}$ [198]. Consistent with this, BMI1 cooperates with C-MYC in lymphomagenesis by repressing *INK4b-ARF-INK4a* thus decreasing C-MYC induced apoptosis [201]. Similar to BMI1, other PRC1 subunits such as CBX7, CBX8 and MEL18 as well as PRC2 subunits like EZH2 have been implicated in *INK4A-ARF* regulation Forced expression of CBX7, CBX8 and EZH2 allows escaping senescence in mouse and human primary cells [59, 196, 197, 200] while loss of function of CBX7, CBX8, MEL18, EZH2 and SUZ12 induce premature senescence in mouse and human cells [19, 59, 69, 197, 200]. However, MEF derived from Cbx7 null mice

showed growth rate comparable to wild-type MEF[202]. The physiological relevance for such regulation has been demonstrated in different genetic mouse models. For example, the developmental defects of Bmi1-/- mice can be partially rescued by *Ink4a-Arf* inactivation[203] while the embryonic lethality of Ring1b-/- mice can be rescued from E9.5 to E11.5[11]. Inactivation of *Ink4a-Arf* fully rescues the development of diabetes mellitus induced by ß-cells specific inactivation of *Ezh2* [204]. On the same line Bmi1 controls ß-cells proliferation during their regeneration ad aging counteracting MLL1 recruitment and activation of Ink4a/p16 transcription[205]. Moreover, very recently, it has been demonstrated that a combination of trithorax depletion and ectopic Ezh2 expression in β-pancreatic cells leads to rejuvenation of those cells by means of transcriptional repression of the Ink4a/Arf locus[206]. In addition, conditional *Ezh2* depletion in proliferating epidermis progenitors induce skin defects with premature differentiation of basal layer cells that correlate with a strong activation of *Ink4b-Arf-Ink4a* expression[207]. Ezh1, the Ezh2 homolog, depletion in mouse hematopoietic stem cells (mHSCs) impairs their self-renewal and proliferation potential, these defects can be completely reverted by the concomitantly deletion of the Ink4a/Arf locus[208]. In rodent incisor stem cells, Bmi1 ensure their proliferation by repressing the Ink4/Arf locus and the Hox genes[209]. Such results stress the importance of *Ink4a-Arf* repression but also suggest *Ink4a-Arf* independent functions for PcG proteins. In support to this, thymocytes differentiation and growth defects of *Bmi1* KO mice can be rescue by genetic inactivation of a downstream kinase of the DNA damage response, Chk2 [210]. Such phenotype has been attributed to a Bmi1 dependent deregulation of mitochondrial functions that leads to aberrant production of free radicals triggering a DNA damage response. *Ink4a/Arf* loss cannot rescue such defects and *Chk2* KO mediated rescue of Bmi1 phenotypes occurs independently of *Ink4a-Arf* repression[210]. In line with these findings, there is not a clear correlation between overexpression of PcG proteins and *INK4b-ARF-INK4a* repression in human tumors. For example, no correlation between BMI1 and $p16^{INK4a}$ expression was found in different hematological malignancies[121], while a negative

correlation between BMI1, $p16^{INK4a}$ and $p14^{ARF}$ was reported in non-small cell lung cancers[211]. In contrast, half of BMI1 positive Hodgkin lymphomas had a positive correlation with $p16^{INK4a}$ expression [212]. Importantly, in a mouse model of EGFR-driven glioma, Bmi1 is essential for *in vivo* tumor formation independently of Ink4-Arf[88]. Moreover, hepatocellular carcinomas and transformation of MCF10A mammary epithelial cells by co-expression of RAS and BMI1 have no effect on Ink4a-Arf expression [108] while in a lung cancer mouse model BMI1 play a role in repressing the *INK4A-ARF* locus during $K\text{-}RAS^{G12D}$ driven transformation[213]. In Oral Squamous Cell Carcinoma, BMI1 is essential for cancer cell proliferation independently of INK4A-ARF [150] and the oncogenic effects of BMI1 in an Ewing Sarcoma's tissue culture model show no dependency on *INK4A-ARF* expression[214]. All together these evidences demonstrate the importance of PcG mediated *INK4A-ARF* repression but also highlight the existence of additional regulatory pathways that play essential roles in development and carcinogenesis.

1.12 Preface

Uncontrolled proliferation is one of the hallmarks of cancer that is required for tumour growth and spreading [215]. The normal cell cycle progression is tightly controlled by a variety of molecular checkpoints that supervise the biological processes that take place in the different phases of the cell cycle [216]. Notably, the cell cycle checkpoint that involves the Ink4a/Arf-p53-pRb axis has been regarded and described as the principle barrier for the initiation and maintenance of neoplastic transformation[217-220]. The cross talk among the proteins active in these pathways and the epigenetic control of Ink4a/Arf expression has been largely investigated to characterize the role of proto-oncogenes that negatively affect this molecular checkpoint[221, 222]. Among these, PcGs exert a fundamental role in controlling Ink4a/Arf transcriptional repression to promote cell cycle progression in physiological and pathological conditions[199]. PcGs pro-proliferative and oncogenic activity have been tightly linked with the transcriptional control of this locus, suggesting that PcG-dependent control of proliferation mainly depends on the ability to repress Ink4a/Arf

expression [72, 133, 166, 196-198, 200, 201, 203-205, 223-225]. Moreover, the PcG proteins Ring1b and Bmi1 can also directly regulate the stability of p53, further stressing their role in regulating cellular proliferation and tumorigenesis by negatively acting on the pRb-p53 pathway[226-228]. In contrast, few studies have also highlighted that the proto-oncogene Bmi1 can control proliferation independently of Ink4a/Arf expression[88, 214, 229]. Although the overall role of PRC1 and PRC2 activities remains completely uncharacterized, this finding suggests the existence of additional mechanisms by which PcGs can regulate cellular proliferation. Several components of PRC1 and PRC2 are frequently overexpressed in human tumours correlating with negative prognosis and poor survival [56]. Considering that the majority of tumours are also characterized by mutations in the Ink4a/Arf-p53-pRb axis [230], we speculate that PcGs can control cellular proliferation through additional mechanisms that acquire a particular significance during oncogenesis and represent a potential therapeutic value[127-129].

CHAPTER 2: Results

2.1 PcG proteins are required for fibroblast proliferation at low oxygen tension

To study the relationship between PcG proteins and cell-cycle checkpoints in regulating cellular proliferation, we analysed the role of PRC1 and PRC2 activity in the proliferation of mouse embryonic fibroblasts (MEFs) grown at low oxygen tension (3% O_2). Differently from normoxia (21%O_2), MEFs cultured at 3% oxygen levels (hypoxia) did not undergo stress-induced senescence, crisis and spontaneous immortalization and grew indefinitely maintaining functional checkpoints[231]. However, MEFs cultured at 3% O_2 accumulated p16 and p19/Arf levels to a similar extent of senescent cells without undergoing a cell cycle arrest[231] (Figure 1a and 1b).

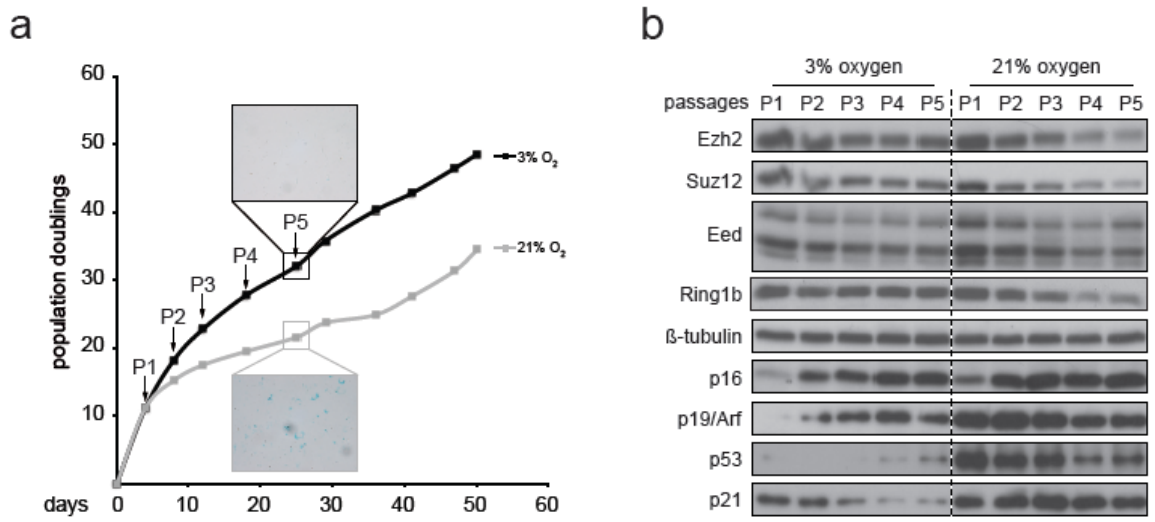

Figure 1. MEF proliferation and PcG proteins accumulation. a,Cumulative population doublings of MEF grown at 3% or 21% O_2. Insets show a representative picture of the MEF stained for senescence-associated β-galactosidase activity (SA-β-gal) at passage 5. **b,** Immunoblots using the indicated antibodies with protein extracts obtained from MEF grown at 3% and 21% O_2 at the indicated passages. β-tubulin served as loading control.

The expression of PRC2 and PRC1 components such as Ezh2, Suz12, Eed and Ring1b remained stable during the passages of MEFs in 3%O_2. Differently, PcGs levels were reduced in MEFs cultured at 21% oxygen levels in parallel to the appearance of markers of cellular senescence (Figure 1a and 1b). In contrast, strong differences in p53 activation were observed between normoxia and hypoxia, a result that is consistent with previous reports [231]. The increased expression of p16 and p19/Arf further suggests that loss of PcG activity at 3%O_2 is likely to have minor effects on Ink4a/Arf expression, potentially highlighting Ink4a/Arf-independent PcGs activities in normal cells.

To test this possibility, we generated *Ezh2* conditional knockout (cKO) MEFs (*Ezh2 fx/fx*) [116] from mice that carried a 4-hydroxytamoxifen (OHT) inducible estrogen receptor fused to CRE recombinase (*CRE-ER*^{T2}) that is constitutively expressed by the Rosa26 locus (R26) [232]. After one week of OHT exposure, growth curves and BrdU incorporation assays showed that the proliferation of *Ezh2* KO MEFs was strongly impaired (Figure 2a-c).

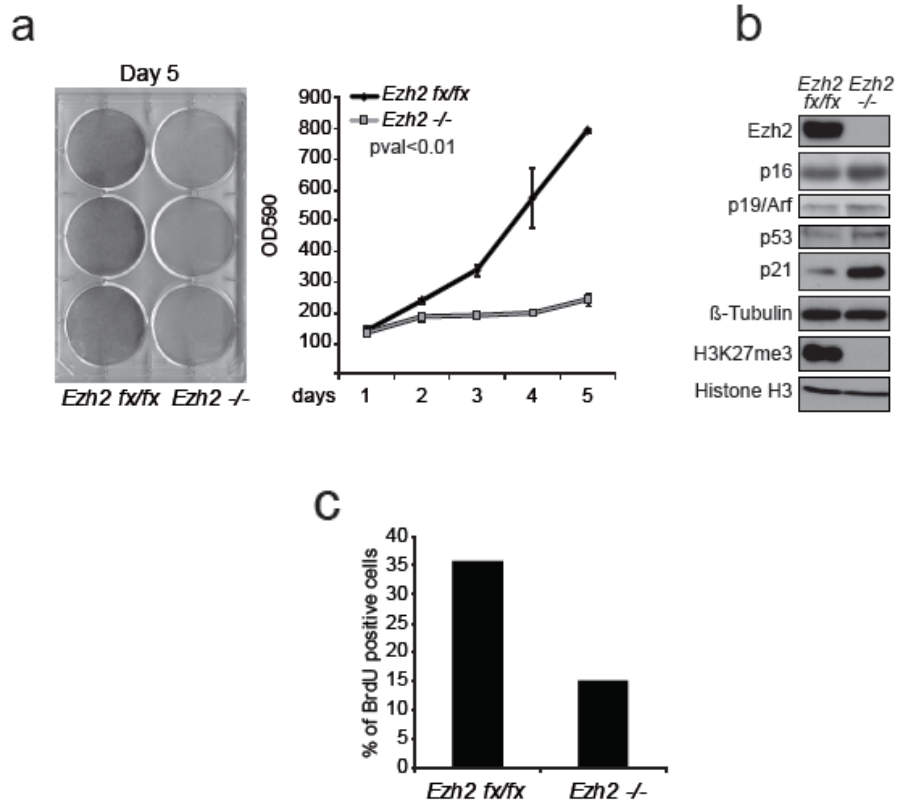

Figure 2. *Ezh2* knockout in low oxygen grown MEF. a, Growth curves of *Ezh2 fx/fx* and *Ezh2 -/- CreERT*^{2} MEFs grown at 3% O_2. Left panel shows crystal violet staining of cells at day 5 of growth curve. The graph represent the quantification of crystal violet absorbance at λ=590nm at the indicated time points. Error bars indicate SD, n=3. **b**, Immunoblots using the indicated antibodies with protein extracts prepared from *Ezh2 fx/fx* and *Ezh2 -/-* MEFs at day 5 of the growth curves. β-tubulin and total Histone H3 served as loading controls. **c**, Bar plot shows the percentage of BrdU incorporation measured by FACS analysis between *Ezh2 fx/fx* and *Ezh2 -/-* MEFs.

Similarly, the knockdown of Suz12 and Eed, (two essential PRC2 components[41, 233]) using stable expression of specific short-hairpin RNAs (shRNAs), blocked the proliferation of MEFs in 3%O_2 and reduced their BrdU incorporation levels (Figure 3a-c and Figure 4a-c).

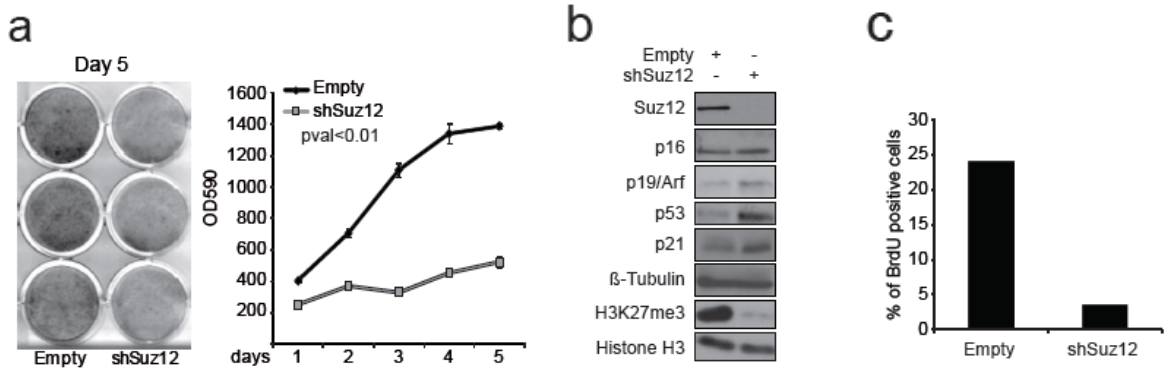

Figure 3. Suz12 knockdown in low oxygen grown MEF. Growth curves of MEFs infected with Empty or shSuz12 expressing lentivirus grown at 3% O_2. Left panel shows crystal violet staining of cells at day 5 of growth curve. The graph represent the quantification of crystal violet absorbance at λ=590nm at the indicated time points. Error bars indicate SD, n=3. **b**, Immunoblots using the indicated antibodies with protein extracts prepared from Empty or shSuz12 MEFs at day 5 of the growth curves. β-tubulin and total Histone H3 served as loading controls. **c**, Bar plot shows the percentage of BrdU incorporation measured by FACS analysis between Empty or shSuz12 MEFs.

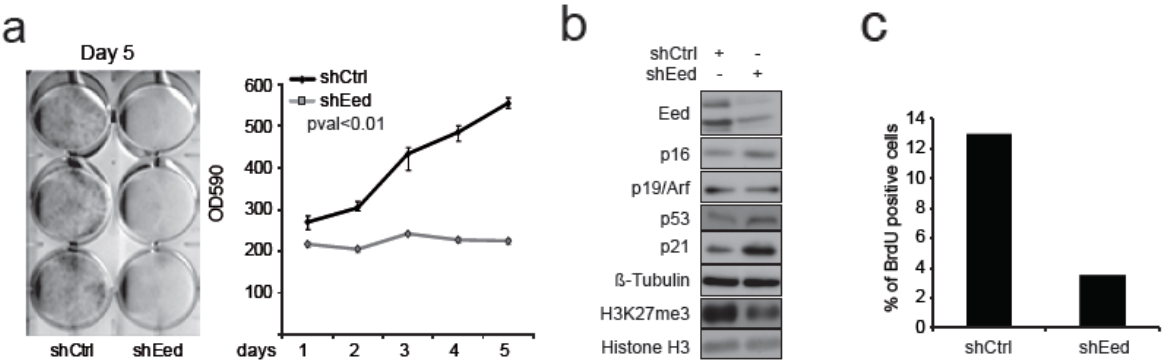

Figure 4. Eed knockdown in low oxygen grown MEF. Growth curves of MEFs infected with shCtrl or shEed expressing lentivirus grown at 3% O_2. Left panel shows crystal violet staining of cells at day 5 of growth curve. The graph represent the quantification of crystal violet absorbance at λ=590nm at the indicated time points. Error bars indicate SD, n=3. **b**, Immunoblots using the indicated antibodies with protein extracts prepared from shCtrl or shEed MEFs at day 5 of the growth curves. β-tubulin and total Histone H3 served as loading controls. **c**, Bar plot shows the percentage of BrdU incorporation measured by FACS analysis between shCtrl or shEed MEFs.

Importantly, loss of PRC2 activity only led to a very modest increase of p16 and p19/ARF levels, to a slight increase in p53 levels and to p21 up-regulation (Figure 2-4). Although these results suggest independency from Ink4a/Arf expression, they cannot exclude a role of pRb and p53 in PRC2-dependent proliferation defects.

2.2 The PRC2 complex regulates proliferation and development independently of Ink4a/Arf-p53-pRb axis

To test if PcG-dependent proliferation defects rely on p16 and p19/Arf expression, we crossed the R26CreER^{T2}-*Ezh2 fx/fx* mice with an *Ink4a/Arf* -/- strain[219] and generated MEFs at low oxygen tension (Figure 5).

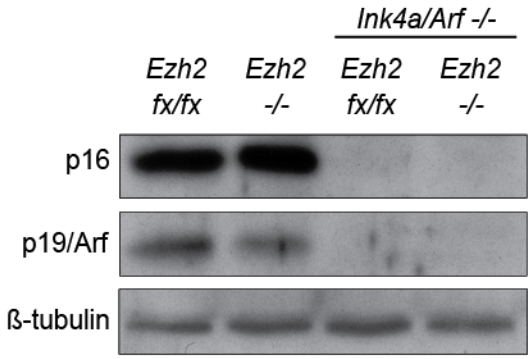

Figure 5. Immuoblot in MEF wt or *Ink4a/Arf* -/-. Immunoblots using p16 and p19/Arf specific antibodies with protein extracts prepared from *Ezh2 fx/fx* and *Ezh2* -/- MEFs with an *Ink4a/Arf* wild type or *Ink4a/Arf* -/- background. β-tubulin served as loading control.

After 7 days of OHT exposure, loss of Ezh2 activity induced strong proliferation defects in absence of a functional p16 and p19/Arf response (Figure 6).

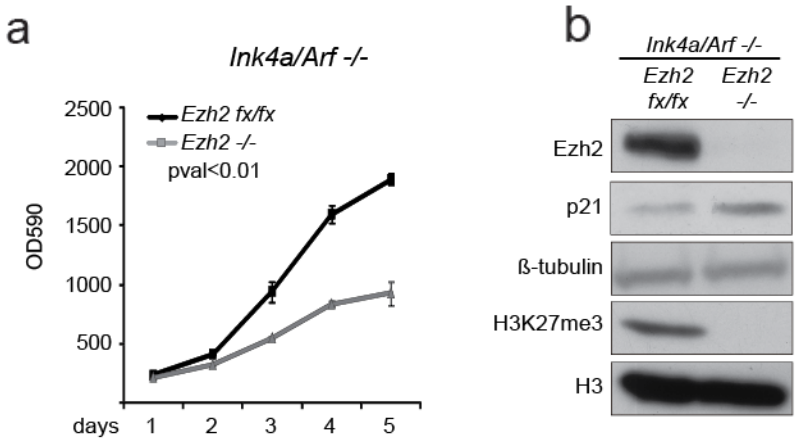

Figure 6. ***Ezh2*** **knockout in** ***Ink4/Arf*** **-/- MEF. a**, Growth curve measured with crystal violet (λ=590nm) of *Ezh2 fx/fx* and *Ezh2 -/- Ink4a/Arf -/-, Cre-ER*^{T2} MEFs. Error bars indicate SD, n=3 **b**, Western blot analysis of protein extracts from *Ezh2 fx/fx* and *Ezh2 -/- Ink4a/Arf -/-, Cre-ER*^{T2} MEFs using the indicated antibodies. β-tubulin and total Histone H3 served as loading controls.

Similarly, the proliferation of tip-tail fibroblasts (TTF) derived from the same strain, also displayed a compromised proliferation upon deletion of Ezh2 activity (Figure7).

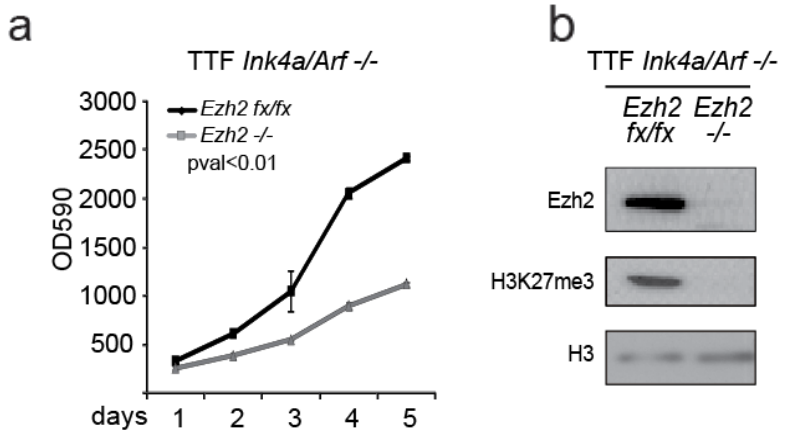

Figure 7. ***Ezh2*** **knockout in** ***Ink4/Arf*** **-/- TTF. a**, Growth curve measured with crystal violet (λ=590nm) of *Ezh2 fx/fx* and *Ezh2 -/- Ink4a/Arf -/-, Cre-ER*^{T2} MEFs. Error bars indicate SD, n=3 **b**, Western blot analysis of protein extracts from *Ezh2 fx/fx* and *Ezh2 -/- Ink4a/Arf -/-, Cre-ER*^{T2} MEFs using the indicated antibodies. H3 served as loading controls.

Consistent with this, the acute knockdown of Suz12 and Eed in *Ink4a/Arf* -/- MEFs further demonstrated that PRC2 controls proliferation independently of Ink4a/Arf expression (Figure 8 and Figure 9).

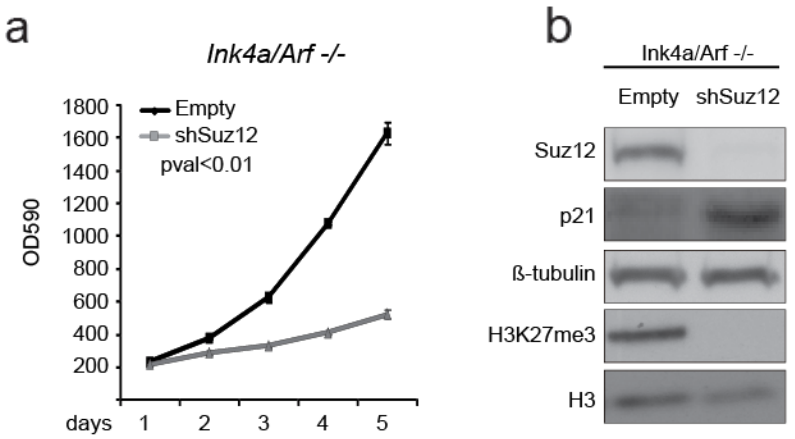

Figure 8. Suz12 knockdown in *Ink4/Arf* -/- MEF. a, Growth curve measured with crystal violet (λ=590nm) of *Ink4a/Arf* -/- MEFs infected with Empty or shSuz12 expressing lentivirus. Error bars indicate SD, n=3 **b**, Western blot analysis of protein extracts from *Ink4a/Arf* -/- MEFs infected with Empty or shSuz12 expressing lentivirus using the indicated antibodies. β-tubulin and total Histone H3 served as loading controls.

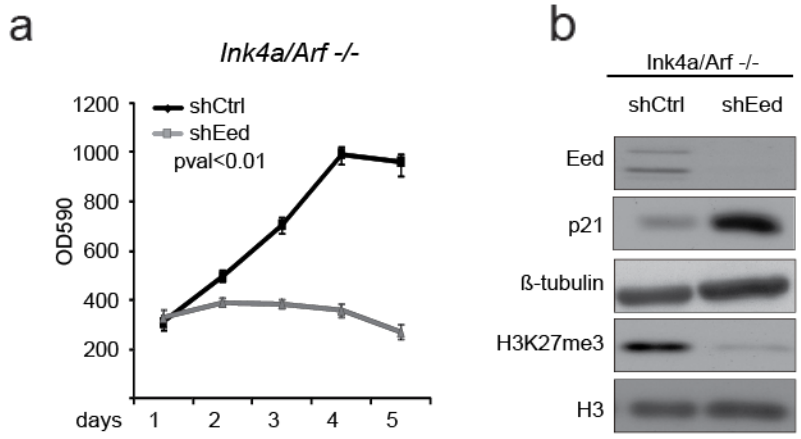

Figure 9. Eed knockdown in *Ink4/Arf* -/- MEF. a, Growth curve measured with crystal violet (λ=590nm) of *Ink4a/Arf* -/- MEFs infected with shCtrl or shEed expressing lentivirus. Error bars indicate SD, n=3 **b**, Western blot analysis of protein extracts from *Ink4a/Arf* -/- MEFs infected with Empty or shEed expressing lentivirus using the indicated antibodies. β-tubulin and total Histone H3 served as loading controls

To gain *in vivo* insights for these observations, we took advantage of the *Suz12* KO mouse model that we previously generated[233]. *Suz12* -/- embryos are blocked in embryonic development and die around 8.5 days *post coitum* (dpc) with strong proliferation defects[233]. We crossed *Suz12* +/- mice into an *Ink4a/Arf* -/- background and tested whether loss of *Ink4a/Arf* expression could rescue its developmental and proliferative defects. Consistent with the results obtained with MEFs, the embryonic development of *Suz12-Ink4a/Arf*

double KO embryos remained impaired showing a complete size block at 8.5 dpc (Figure 10).

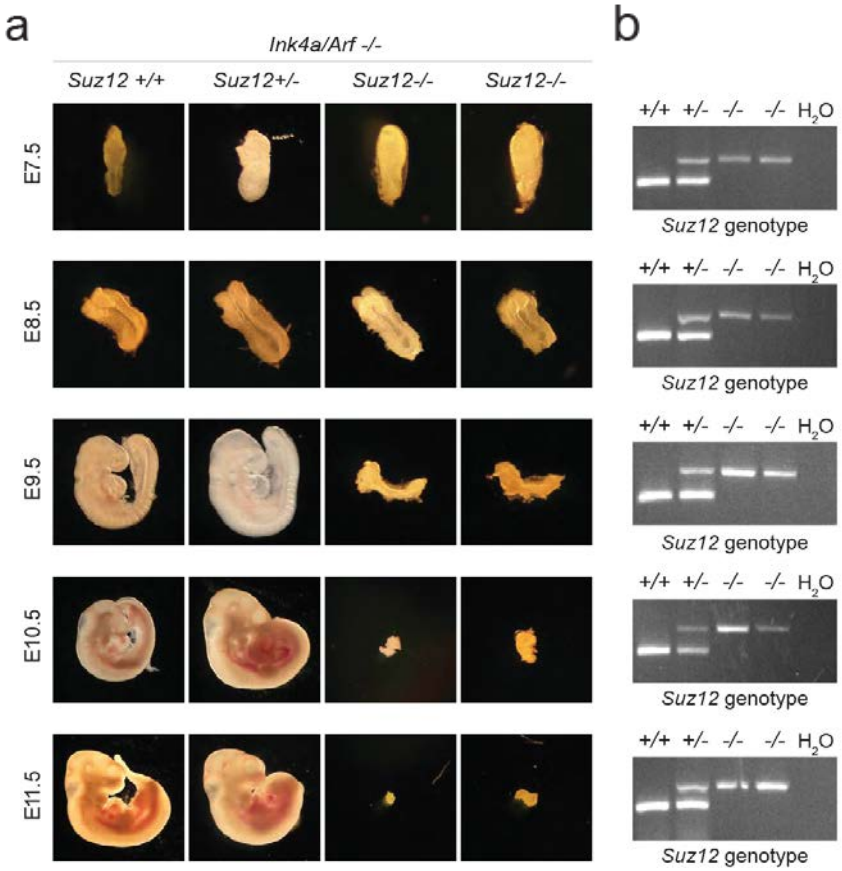

c

Ink4a/Arf -/-;Suz12 +/- intercrosses

	Suz12	Percent	Normal	Retarded	Total
E 7.5	+/+	20	100	0	8
	+/-	55	95.5	4.5	22
	-/-	17.5	71.4	28.6	7
	resorpted	7.5			3
					40
E 8.5	+/+	26.3	93.3	6.7	15
	+/-	38.6	95.5	4.5	22
	-/-	12.3	100	0	7
	resorpted	22.8			13
					57
E 9.5	+/+	27.9	100	0	12
	+/-	30.2	76.9	23.1	13
	-/-	34.9	0	100	15
	resorpted	7.0			3
					43
E 10.5	+/+	20	90	10	10
	+/-	48	95.8	4.2	24
	-/-	24	0	100	12
	resorpted	8			4
					50
E 10.5	+/+	12.5	100	0	3
	+/-	54.2	100	0	13
	-/-	8.3	0	100	2
	resorpted	25			6
					24

Ink4a/Arf +/+;Suz12 +/- intercrosses

	Suz12	Percent	Normal	Retarded	Total
E 7.5	+/+	14.3	100	0	4
	+/-	60.7	100	0	17
	-/-	17.9	100	0	5
	resorpted	7.1			2
					28
E 8.5-9	+/+	26.1	100	0	6
	+/-	52.2	75	25	12
	-/-	17.4	0	100	4
	resorpted	4.3			1
					23

Figure 10. ***Suz12-/-; Ink4a/Arf-/-*** **mouse embryogenesis. a,** Pictures of embryos derived from *Suz12 +/-*, *Ink4a/Arf -/-* mating at the indicated developmental stages. **b,** PCR genotypes of the single embryos at each developmental stage are presented in **a**. **c,** Table summerizing all the statistics on the analysed embryos.

Although we cannot discern the contribution between proliferation and differentiation defects, this result highlights *in vivo* the Ink4a-Arf independent proprieties of PRC2 activity and suggests that defective proliferation could play a role in the PRC2-dependent developmental defects.

To further investigate the role of pRb and p53 pathways in PcG-dependent proliferation control, we took advantage of p53 (*p53-/-*) or pRb (*pRb-/-*) deficient MEFs (Figure 11 and Figure 12).

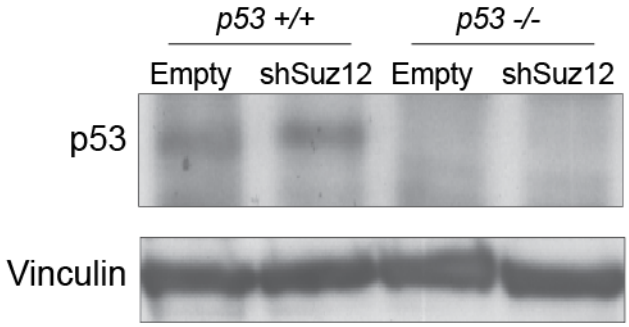

Figure 11. p53 Immunoblot in wt and *p53* -/- MEF. p53 immunoblot in wild type and *p53-/-* MEF infected with Empty or shSuz12 expressing lentivirus. Vinculin served as loading control.

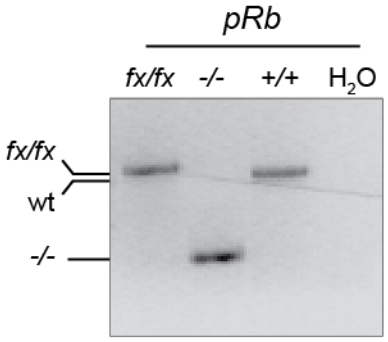

Figure 12. PCR Genotypes of the *pRb* alleles . Agarose gel of samples coming from *pRb fx/fx*, pRb -/- and wt MEF. Water is used as negative control

Knocking down Suz12 in both *p53 -/-* or *pRb -/-* MEF demonstrated that loss of PRC2 activity induced proliferative defects also in the absence of either pRb or p53 functional responses (Figure 13 and Figure 14).

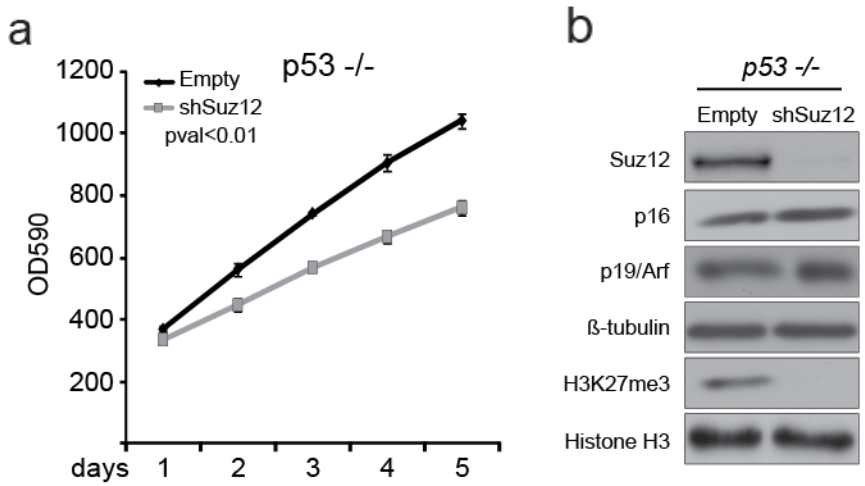

Figure 13. Suz12 knockdown in *p53-/-* MEF. a, Growth curve measured with crystal violet (λ=590nm, top panels) in *p53-/-* MEFs infected with Suz12 specific shRNA expressing or empty lentiviral vectors. Error bars indicate SD, n=3 **b,** immunoblots of protein extracts using the indicated antibodies in *p53-/-* MEFs infected with Suz12 specific shRNA expressing or empty lentiviral vectors. β-tubulin and total Histone H3 served as loading controls.

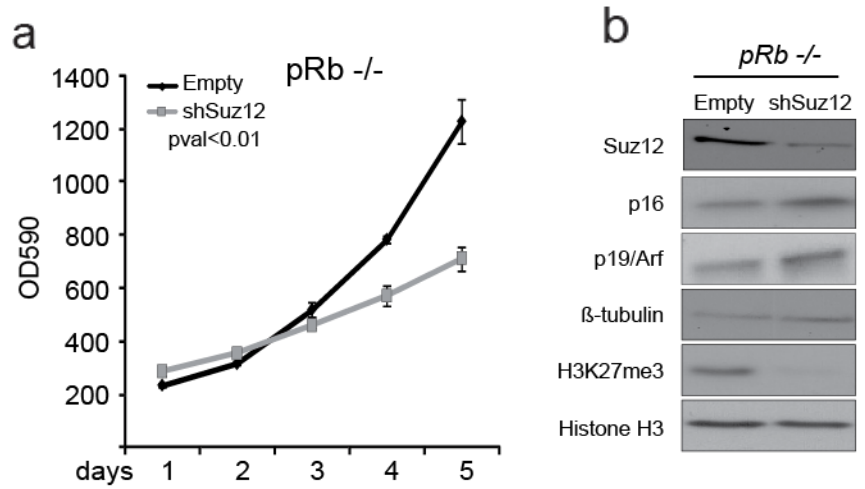

Figure 14. knockdown in *pRb-/-* MEF. a, Growth curve measured with crystal violet (λ=590nm, top panels) in *pRb-/-* MEFs infected with Suz12 specific shRNA expressing or empty lentiviral vectors. Error bars indicate SD, n=3 **b,** immunoblots of protein extracts using the indicated antibodies in *p53-/-* MEFs infected with Suz12 specific shRNA expressing or empty lentiviral vectors. β-tubulin and total Histone H3 served as loading controls.

Moreover, to exclude that the two "arms" of the pathway could generate compensatory effects, we simultaneously inactivated p53 and pRb functions by expressing the Large T (LT) oncoprotein encoded by the simian virus 40 early region (SV40ER) in *Ezh2* cKO MEFs[217] (Figure 15). Also in this case, OHT-mediated deletion of the *Ezh2* locus induced proliferation defects (Figure 16).

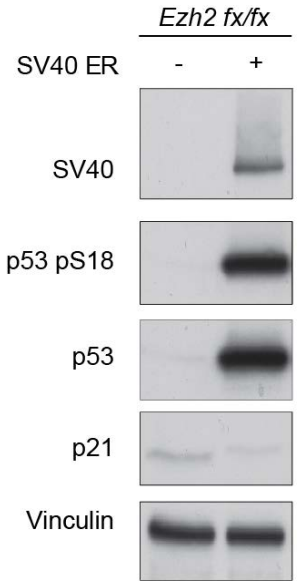

Figure 15. Immunoblot in *Ezh2 fx/fx* SV40 immortalized and wt MEF. Western blot with the indicated antibodies in SV40 immortalized or wt MEF *Ezh2 fx/fx; Cre-ER^{T2}*. Vinculin served as loading control.

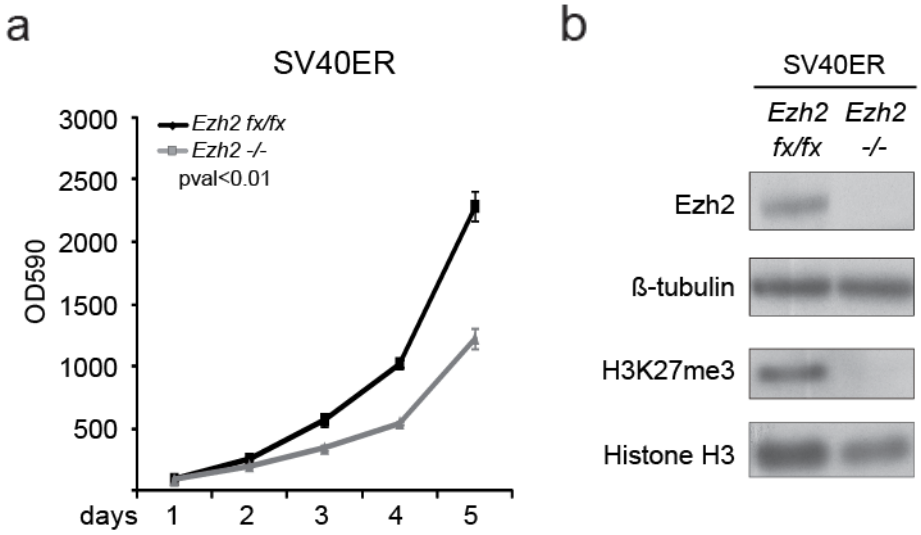

Figure 16. *Ezh2* knockout in SV40 immortalized MEF. a, Growth curve measured with crystal violet (λ=590nm) of *Ezh2 fx/fx* and *Ezh2 -/-* SV40, *Cre-ER^{T2}* MEFs. Error bars indicate SD, n=3 **b,** Western blot with the indicated antibodies in *Ezh2 fx/fx* and *Ezh2 -/-* SV40, *Cre-ER^{T2}* MEFs. β-tubulin and total Histone H3 served as loading controls.

Differently from cells with proficient cell cycle checkpoints, loss of Ezh2 activity did not induce a cell cycle arrest but a constant reduction in the proliferation rate of the MEFs and an overall impairment on colony formation ability (Figure 17 and Figure 18). Overall, these data demonstrate that PRC2 can control cellular proliferation independently from the Ink4a/Arf-pRb-p53 axis.

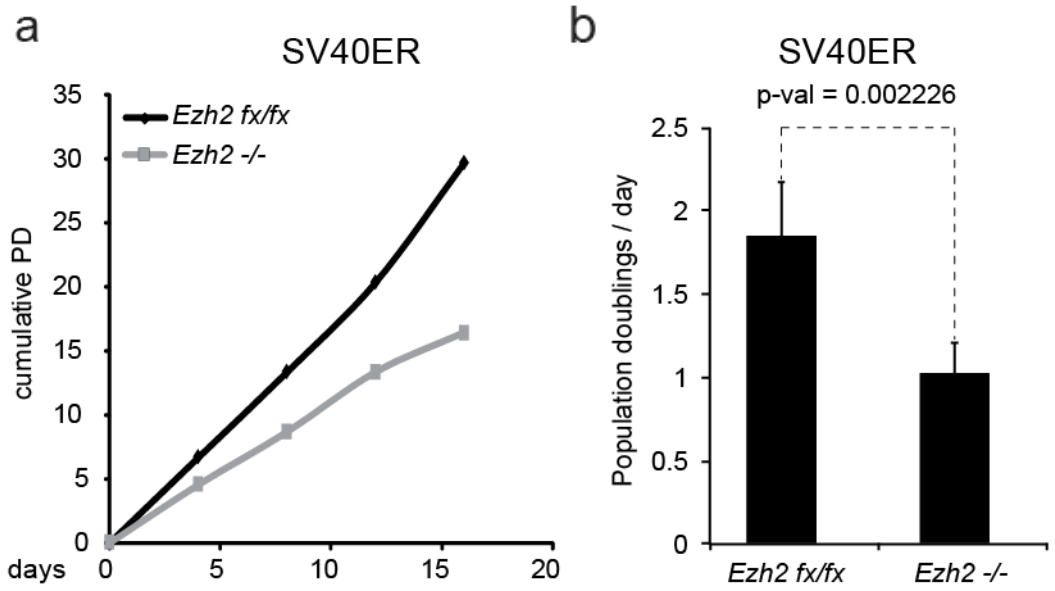

Figure 17. 3T3 like growth curve of Ezh2 fx/fx and Ezh2 -/- SV40 *Cre-ERT2*. a, 3T3-like assay performed with *Ezh2 fx/fx* and *Ezh2 -/-* SV40 *Cre-ERT2* MEF. 10^6 cells per 10 cm dish were plated every 4 days and counted over a time of 16 days. **b**, Average population doublings for each day in *Ezh2 fx/fx* and *Ezh2 -/-* SV40 *Cre-ERT2* MEF . Error bars indicate SD, n=3.

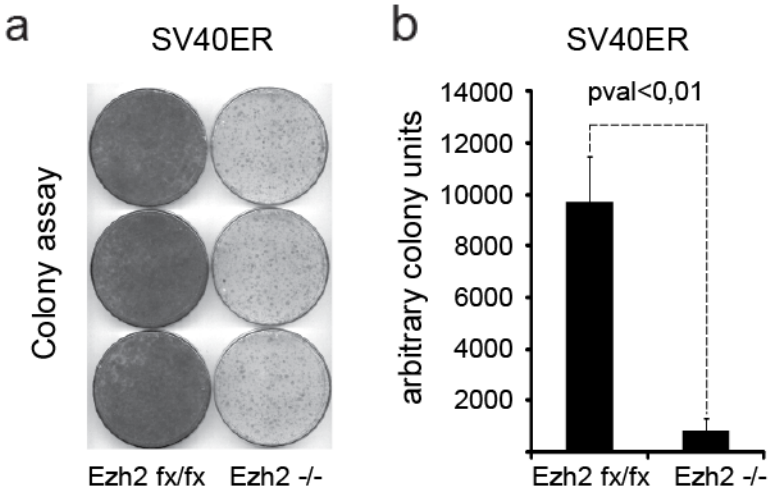

Figure 18. Colony assay in *Ezh2 fx/fx* and *Ezh2 -/-* SV40 immortalized MEF. a, Colonigenic assays stained with crystal violet of *Ezh2 fx/fx* and *Ezh2 -/-* SV40 immortalized MEFs. **b**, Colonies quantification determined using ImageJ. Error bars indicate SD, n=3.

2.3 PRC2 controls cellular transformation in p53-pRb independent manner

PRC2 components are frequently found highly expressed in human tumours[56] and this can be mirrored in cell culture using cellular immortalization and transformation protocols (Figure 19).

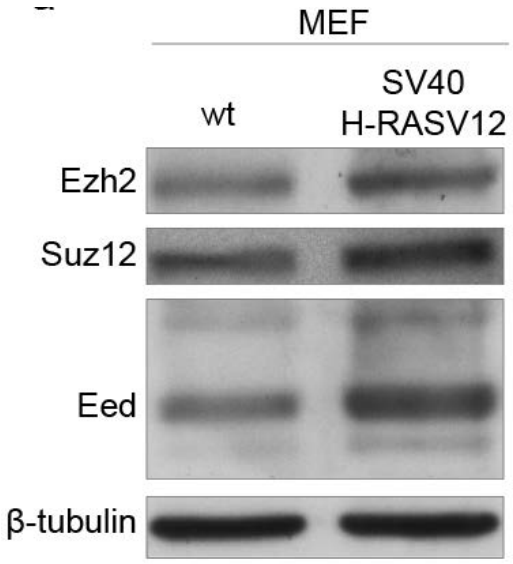

Figure 19. PRC2 components levels in wt or transformed MEF. Immunoblots with the indicated antibodies of wild type and SV40ER H-RASV12 expressing MEFs protein extracts. β-tubulin served as loading control.

To assess whether PRC2 ability to control proliferation in a p53-pRb independent manner could be a determinant for cellular transformation, we expressed independently the H-RASV12 and c-MYC oncogenes in R26CreERT2, *Ezh2* cKO MEFs that were previously immortalized by SV40ER expression. First, we assayed the requirement of Ezh2 for the transformation of MEFs by expressing H-RASV12 in SV40ER immortalized *Ezh2*-/- MEFs (condition defined as PRE, Figure 20a). Then, we evaluated the requirement of Ezh2 for the maintenance of the transformed phenotype by knocking it out in MEFs that were already transformed by H-RASV12 expression (condition defined as POST, Figure 20b). By performing colony and foci formation assays in cell culture, we demonstrated that loss of Ezh2 activity both prevented (PRE condition) and impaired (POST condition) cellular transformation in SV40 H-RASV12 transformed MEF (Figure 21).

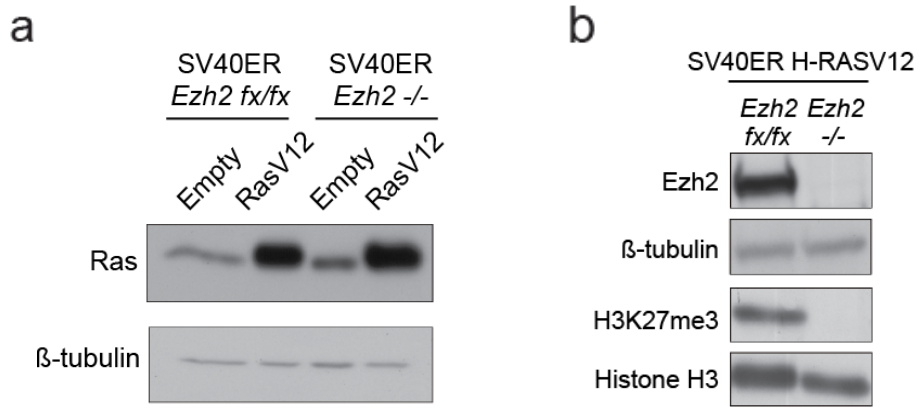

Figure 20. H-RASV12 and Ezh2 expression in MEF SV40 H-RASV12 in PRE and POST conditions. a, (PRE condition) H-RASV12 expression in SV40 immortalized *Ezh2 fx/fx* or *Ezh2 -/-* MEF. β-tubulin served as loading control. **b,** (POST condition) Ezh2 and H3K27me3 levels in SV40 H-RASV12 transformed *Ezh2 fx/fx* or *Ezh2 -/-* MEF. β-tubulin and histone H3 served as loading control.

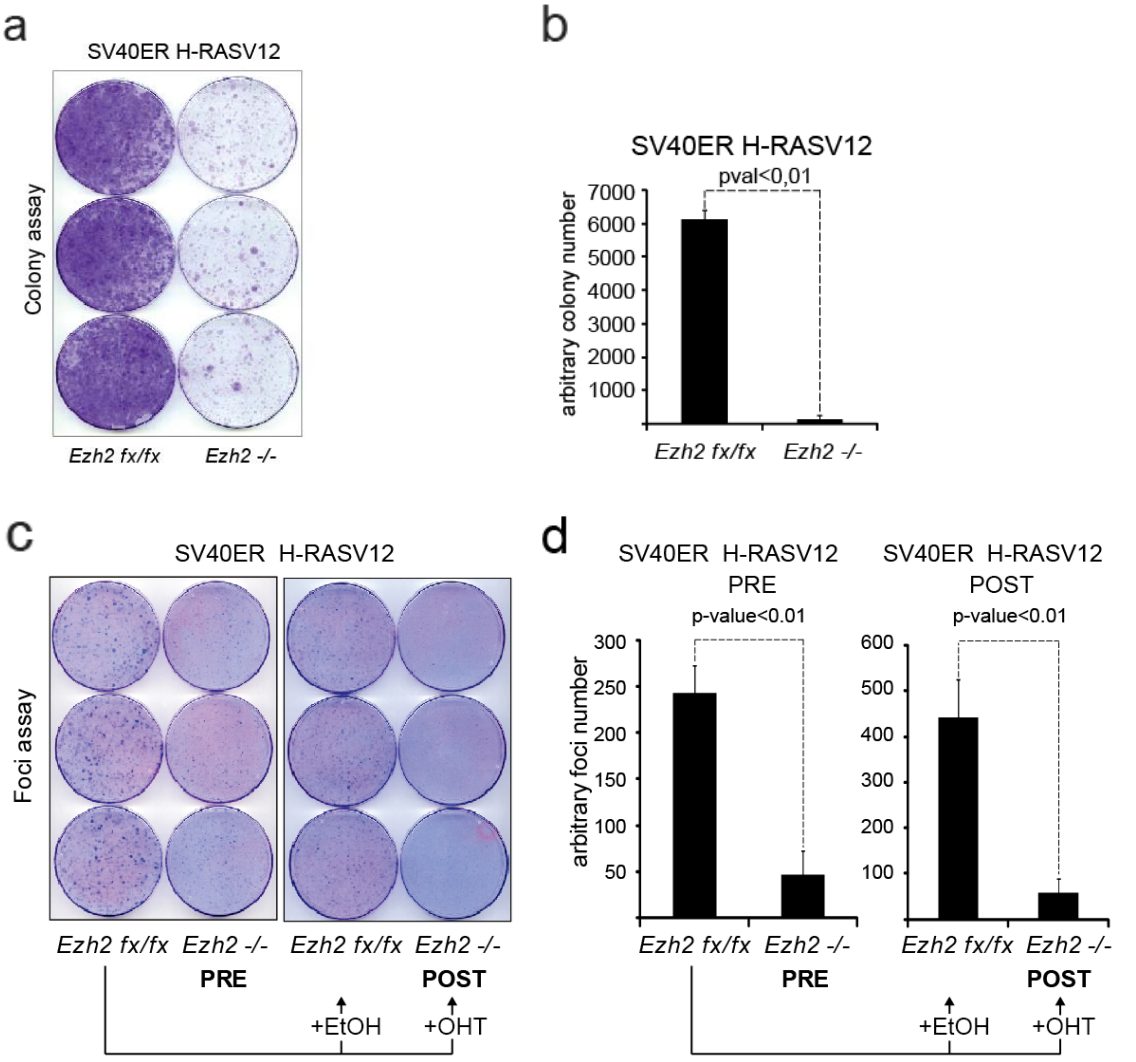

Figure 21. Colony and Foci assay in *Ezh2* knockout SV40 H-RASV12 transformed cells. a, Colonigenic assay stained with crystal violet of SV40ER H-RASV12 transformed *Ezh2 fx/fx* or *Ezh2 -/- CreERT*^{2} MEFs. **b,** Colonies in **a** were quantified using ImageJ. Error bars indicate SD, n=3. **c,** Foci formation assay stained with Giemsa of SV40ER immortalized *Ezh2 fx/fx* or *Ezh2 -/- CreERT*^{2} MEFs that stably expressed H-RASV12. PRE indicates that SV40ER immortalized *Ezh2 fx/fx, CreERT*^{2} MEFs were exposed to OHT treatment before H-RASV12 expression. The POST condition indicates that H-RASV12 was expressed in SV40ER immortalized, *CreERT*^{2} Ezh2 fx/fx MEFs before OHT treatment. **d,** Foci in **c** were and quantified using ImageJ. Error bars indicate SD, n=3.

We then explore the possibility that these findings could be recapitulated also *in vivo*. To address this issue we took both MEF *Ezh2 fx/fx* and *Ezh2 -/-* SV40 H-RASV12 transformed MEF coming from the PRE or the POST condition and we inoculated them in immunocompromised mice. As shown by the tumour volume, the masses formed with *Ezh2-/-* MEF are dramatically reduced or sometimes absent compared to those generated by *Ezh2 fx/fx* MEF in both PRE and POST conditions (Figure 22).

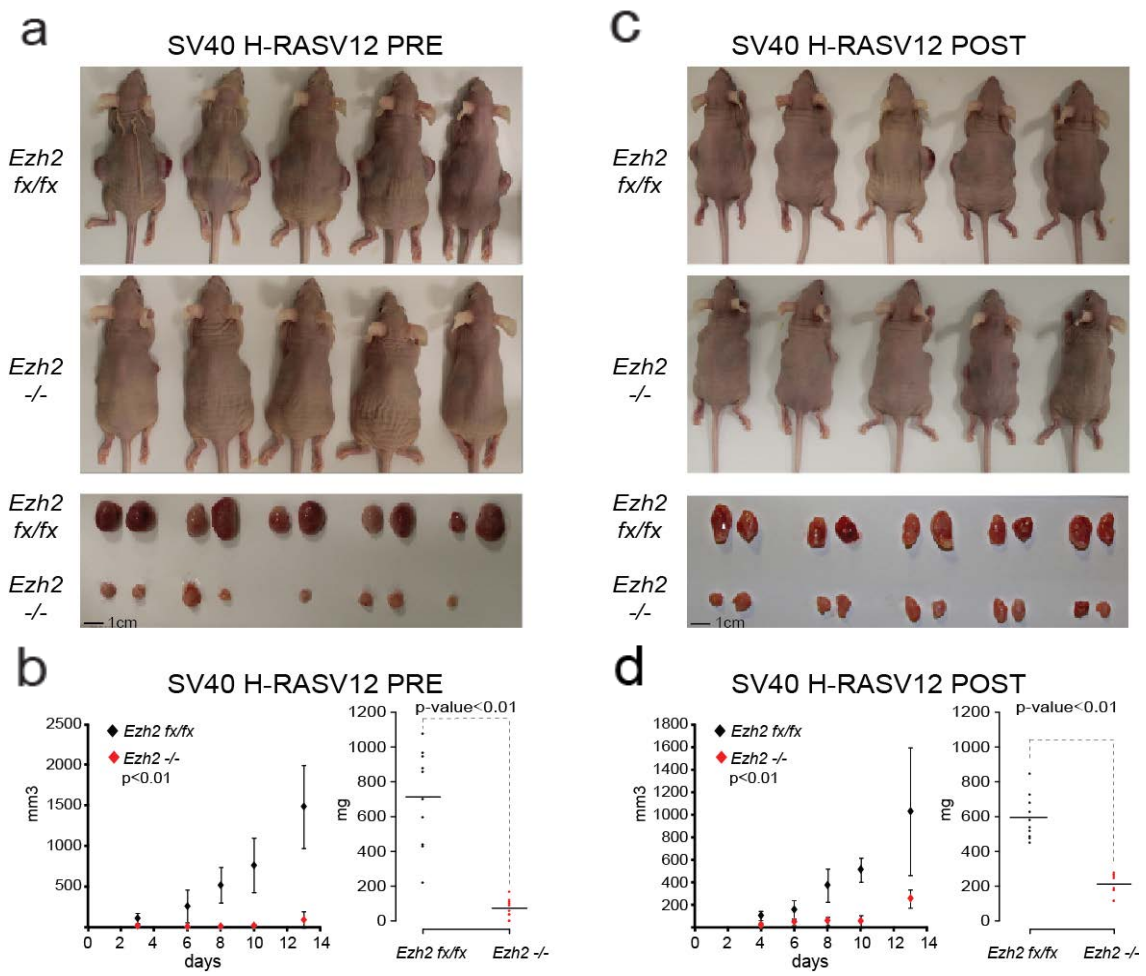

Figure 22. Injection of *Ezh2 fx/fx* and *Ezh2 -/-* SV40 H-RASV12 transformed MEF in nude mice. a, Pictures of nude mice and isolated tumour masses at 14 days post-injection of *Ezh2 fx/fx* and *Ezh2 -/-* SV40 H-RASV12 transformed MEF (PRE condition). **b,** Average increase of tumour size (volume) at the indicated time (left) and the weights of the tumour masses (right) shown in **a**. Error bars indicate SD, n=10. **c,** Same outline of **a** injecting cells of the POST condition. **d,** same as **b** referred to **c.**

Consistent with these observations we were able to obtain similar results using another well-known oncogene such as C-MYC to transform SV40 immortalized *Ezh2* cKO MEF (Figure 23). Together, these results demonstrate that Ezh2 is required for the

transformation and maintenance of tumour growth even though the p53 and pRb pathways are inactivated.

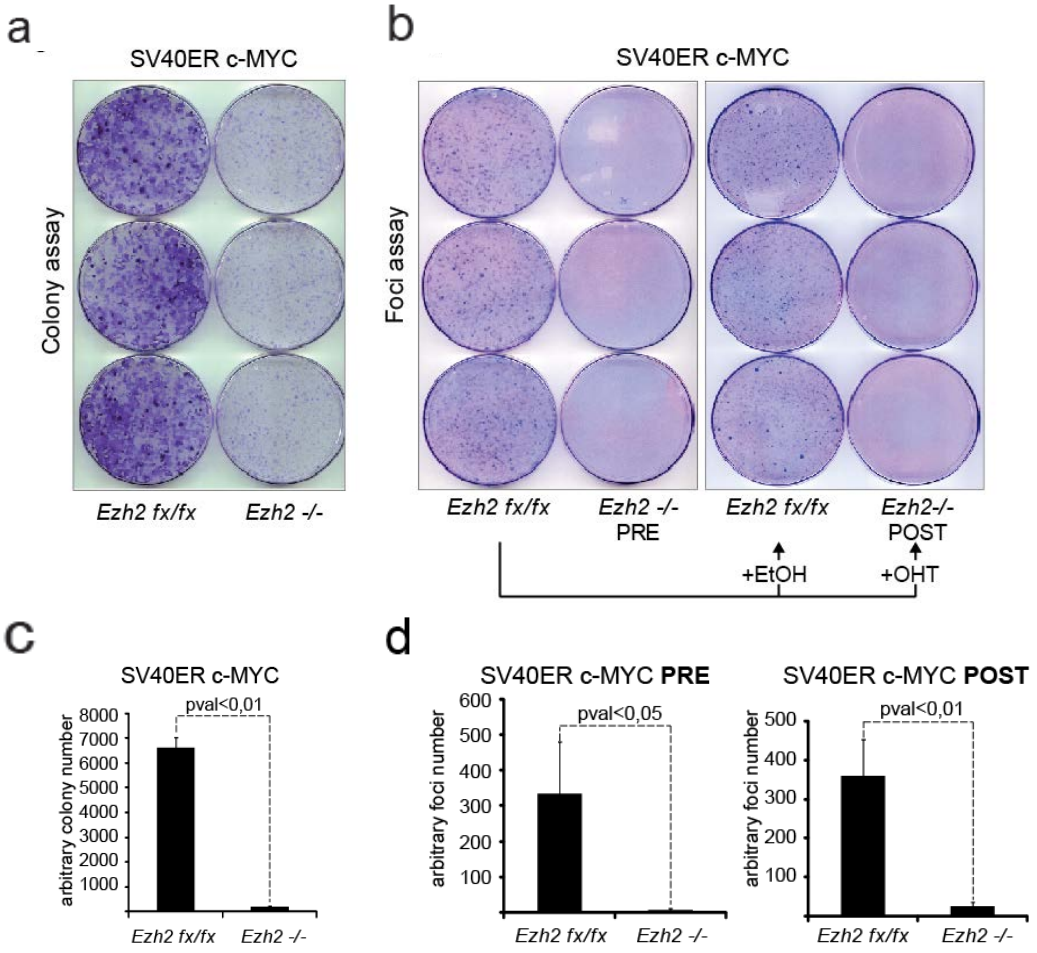

Figure 23. Colony and Foci assay in *Ezh2* knockout SV40 c-myc transformed cells. a, Colonigenic assay stained with crystal violet of SV40ER immortalized *Ezh2 fx/fx* or *Ezh2 -/- CreERT*^{2} MEFs expressing c-myc. **b,** Colonies in **a** were quantified using ImageJ. Error bars indicate SD, n=3. **c,** Foci formation assay stained with Giemsa of SV40ER immortalized *Ezh2 fx/fx* or *Ezh2 -/- CreERT*^{2} MEFs that stably expressed c-myc. PRE indicates that SV40ER immortalized *Ezh2 fx/fx, CreERT*^{2} MEFs were exposed to OHT treatment before H-RASV12 expression. The POST condition indicates that c-myc was expressed in SV40ER immortalized, *CreERT*^{2} Ezh2 fx/fx MEFs before OHT treatment. **d,** Foci in **c** were and quantified using ImageJ. Error bars indicate SD, n=3.

2.4 Redundant role of PRC1 in cells proliferation and transformation control

PRC1 shares several functions with PRC2 including the control of cell proliferation. Despite PRC2-independent recruitment of PRC1 sub-complexes was extensively described[184], PRC1 and PRC2 retain a large part of common regulatory pathways[234]. Similar to PRC2, the expression of Ring1b (the central catalytic subunit for all forms of PRC1) is maintained during culture of MEFs under hypoxic conditions (Figure 1b).

To extend our observations regarding the Ink4a/Arf, pRb and p53 independent role of PRC2 in regulating cell proliferation and transformation, we generated R26CreER^{T2} mice that carry a constitutively deleted allele for *Ring1a* (*Ring1a -/-*, Figure 24) and a Cre-dependent conditional allele for *Ring1b* (*Ring1b* fx/fx)[235].

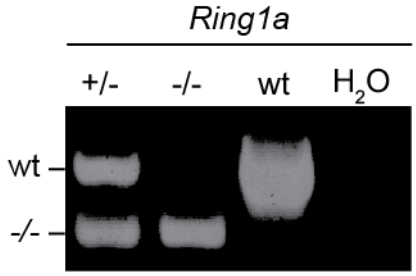

Figure 24. Ring1a PCR genotype. Agarose gel representing wt and KO *Ring1a* alleles PCR products . *Ring1a* heterozigote (+/-), knockout (-/-) and wt MEF DNA amplified with specific primers. Water is used as negative control.

MEFs generated at 3%O_2 from these mice and exposed to OHT treatment for one week, displayed a rapid cell cycle arrest (Figure 25). Compared to PRC2, loss of PRC1 activity induced a significant activation of p16 and p19/Arf expression that correlated with p53 stabilization and activation (Figure 25b). This result suggests that PRC1 repression of *Ink4a/Arf* may be largely independent on PRC2 activity and that the increased levels of p16 and p19/Arf could still induce a cell cycle arrest in *Ring1a/b* KO hypoxic cultures.

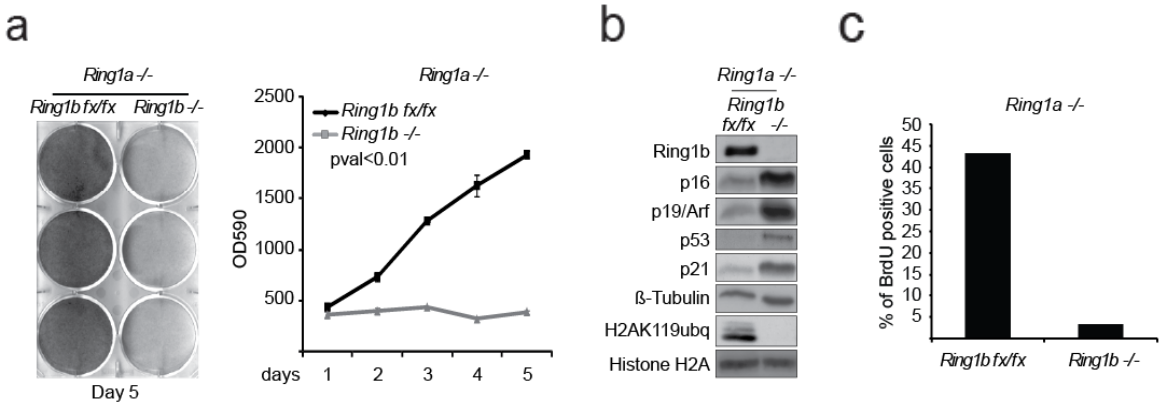

Figure 25. Ring1b and Ring1a depletion in low oxygen grown MEF. a, Growth curves of *Ring1b fx/fx* and *Ring1b -/- Ring1a -/- CreERT*^{2} MEFs grown at 3% O_2. Left panel show crystal violet staining of cells at day 5 of growth curve. The graph represent the quantification of crystal violet absorbance at λ=590nm at the indicated time points. Error bars indicate SD, n=3. **b**, Immunoblots using the indicated antibodies with protein extracts prepared from *Ring1b -/- Ring1a -/- CreERT*^{2} MEFs at day 5 of the growth curves. β-tubulin and total Histone H2a served as loading controls. **c**, Bar plot shows the percentage of BrdU incorporation measured by FACS analysis between *Ring1b -/- Ring1a -/- CreERT*^{2} MEFs.

Thus, we crossed these mice with an *Ink4a/Arf -/-* strain and tested if PRC1 activity was required for the proliferation of MEFs that cannot express p16 and p19/Arf (Figure 26).

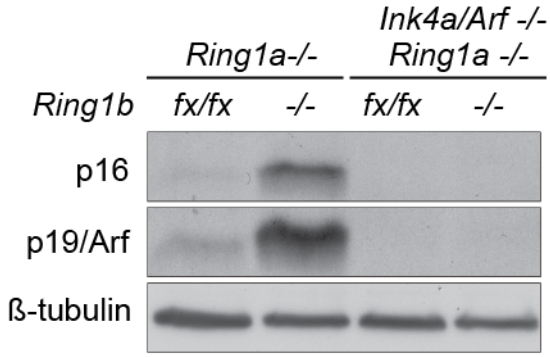

Figure 26. Immuoblot in *Ring1a -/- Ring1b fx/fx* MEF or *Ring1a -/- Ring1b fx/fx Ink4a/Arf -/-* MEF. Immunoblots using p16 and p19/Arf specific antibodies with protein extracts prepared from *Ring1b fx/fx Ring1a -/-* and *Ring1b -/- Ring1a -/-* MEFs with an *Ink4a/Arf* wild type or *Ink4a/Arf -/-* background. β-tubulin served as loading control.

Consistent with our previous results, loss of PRC1 activity in *Ink4a/Arf -/-* MEFs impaired cellular proliferation under hypoxia conditions (Figure 27).

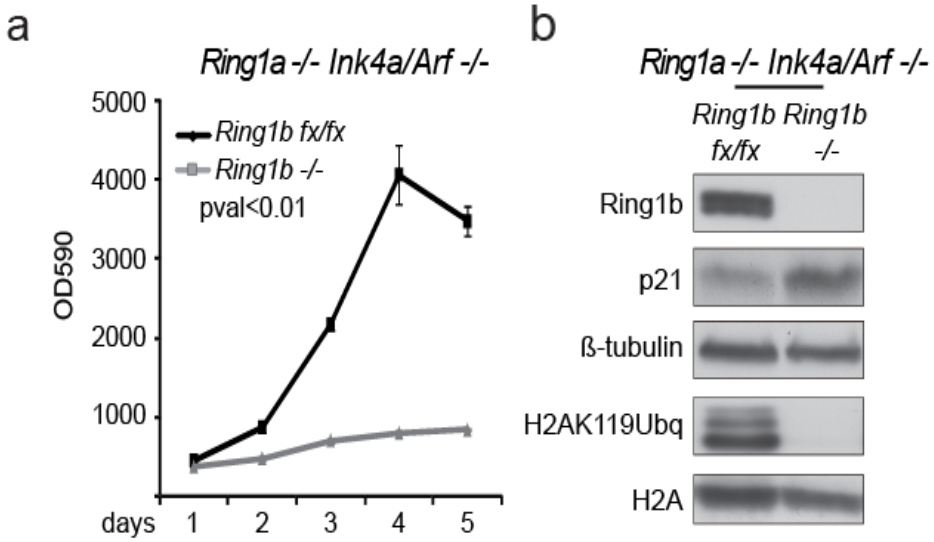

Figure 27. *Ring1a-/-* and *Ring1b* knockout in *Ink4/Arf -/-* MEF. a, Growth curve measured with crystal violet (λ=590nm) of *Ring1b fx/fx* and *Ring1b -/- Ring1a -/- Ink4a/Arf -/-, Cre-ER^{T2}* MEFs. Error bars indicate SD, n=3 **b**, Western blot analysis of protein extracts from of *Ring1b fx/fx* and *Ring1b -/- Ring1a -/- Ink4a/Arf -/-, Cre-ER^{T2}* MEFs using the indicated antibodies. β-tubulin and total Histone H2a served as loading controls.

To further exclude that pRb and p53 activation could still mediate a cell cycle arrest, we inhibited their activity by expressing SV40ER in *Ring1a -/-, Ring1b fx/fx* R26CreER^{T2} MEFs (Figure 28).

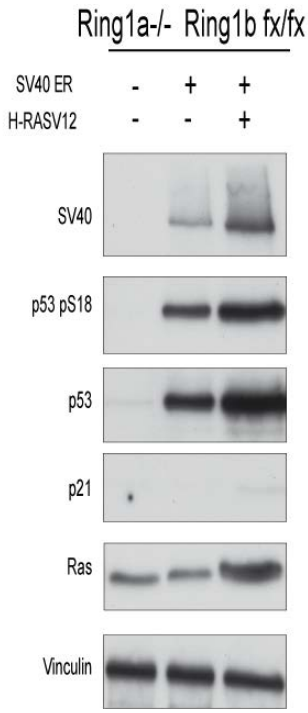

Figure 28. Immunoblot in *Ring1b fx/fx Ring1a -/-* SV40 and SV40 H-RASV12 MEF. Western blot with the indicated antibodies in SV40 immortalized or SV40 H-RASV12 transformed MEF *Ring1a -/-, Ring1b fx/fx Cre-ER^{T2}*. Vinculin served as loading control

As for *Ezh2* KO MEFs, the genetic inactivation of the PRC1 activity strongly inhibited cellular proliferation and colonigenic potential in the absence of a functional pRb and p53 pathway (Figure 29 and Figure 30).

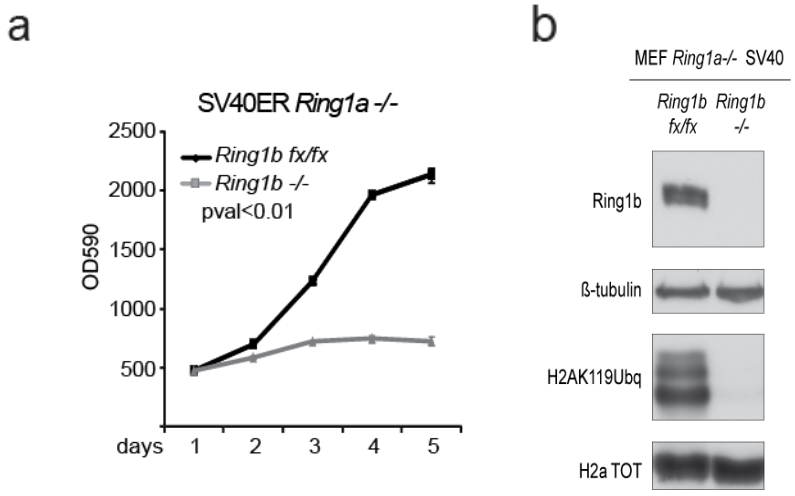

Figure 29. PRC1 knockout in SV40 immortalized MEF. a, Growth curve measured with crystal violet (λ=590nm) of *Ring1b fx/fx* and *Ring1b -/- Ring1a -/-*, SV40, *Cre-ER^{T2}* MEFs. Error bars indicate SD, n=3 **b,** Western blot with the indicated antibodies in *Ring1b fx/fx* and *Ring1b -/- Ring1a -/-*, SV40, *Cre-ER^{T2}* MEFs. β-tubulin and total Histone H2a served as loading controls.

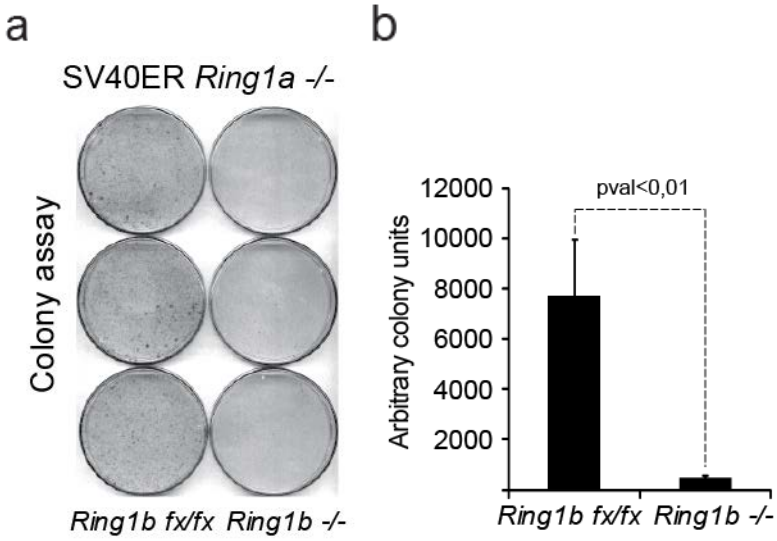

Figure 30. Colony assay in PRC1 knockout in SV40 immortalized MEF SV40 immortalized MEF. a, Colonigenic assays stained with crystal violet of *Ring1b fx/fx* and *Ring1b -/- Ring1a -/-*, SV40, *Cre-ER*^{T2} MEFs.**b**, Colonies quantification determined using ImageJ. Error bars indicate SD, n=3.

To further test whether PRC1 activity is required for the transformation of MEFs and tumour growth, we inactivated *Ring1b* before or after H-RASV12 ectopic expression in *Ring1a -/-* SV40 immortalized MEF (respectively PRE and POST, Figure 30).

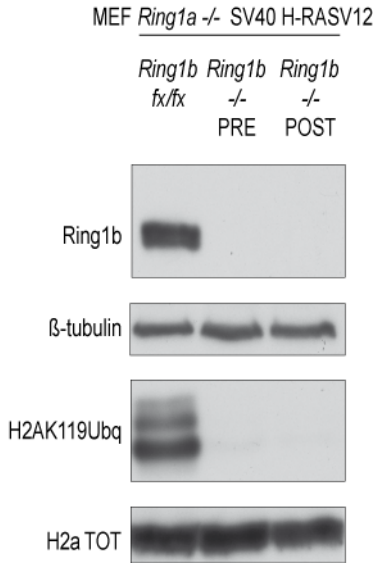

Figure 31. *Ring1a-/-* and *Ring1b* knockout in SV40 H-RASV12 transformed MEF. a, Western blot with the indicated antibodies in *Ring1b fx/fx* and *Ring1b -/- Ring1a -/-*, SV40, H-RASV12 *Cre-ER*^{T2} transformed MEFs. β-tubulin and total Histone H2a served as loading controls.

Like it happens for the PRC2 depletion, loss of *Ring1a* and *Ring1b* functions strongly affects colonies and foci formation as well as *in vivo* tumour growth in nude mice, thus demonstrating that PRC1 is essential for the acquisition (PRE) and the maintenance (POST) of oncogenic potential in a pRb-p53 independent manner (Figure 32-33).

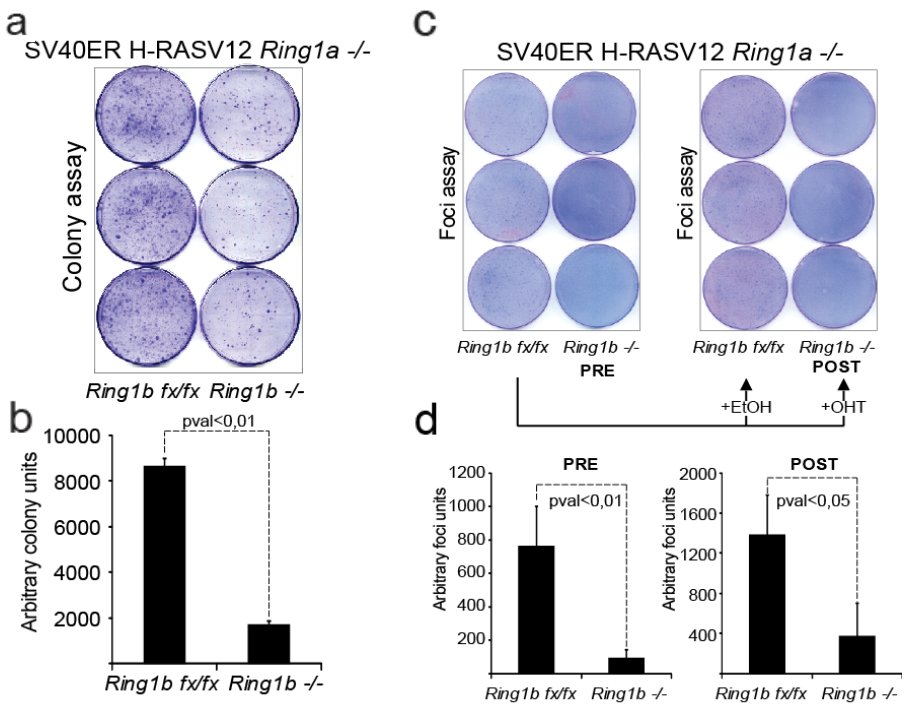

Figure 32. Colony and Foci assay in *Ring1b* and *Ring1a* knockout SV40 H-RASV12 transformed cells. a, Colonigenic assay stained with crystal violet of *Ring1b fx/fx* and *Ring1b -/- Ring1a -/-*, SV40, H-RASV12 *Cre-ER*^{T2} transformed MEFs. **b,** Colonies in **a** were quantified using ImageJ. Error bars indicate SD, n=3. **c,** Foci formation assay stained with Giemsa of *Ring1b fx/fx* and *Ring1b -/- Ring1a -/-*, SV40, H-RASV12 *Cre-ER*^{T2} MEFs. PRE indicates that SV40ER immortalized *Ring1b fx/fx* and *Ring1b -/- Ring1a -/- CreERT*^{2} MEFs were exposed to OHT treatment before H-RASV12 expression. The POST condition indicates that H-RASV12 was expressed in SV40ER immortalized, *Ring1b fx/fx Ring1a -/- CreERT*^{2} before OHT treatment. **d,** Foci in **c** were and quantified using ImageJ. Error bars indicate SD, n=3.

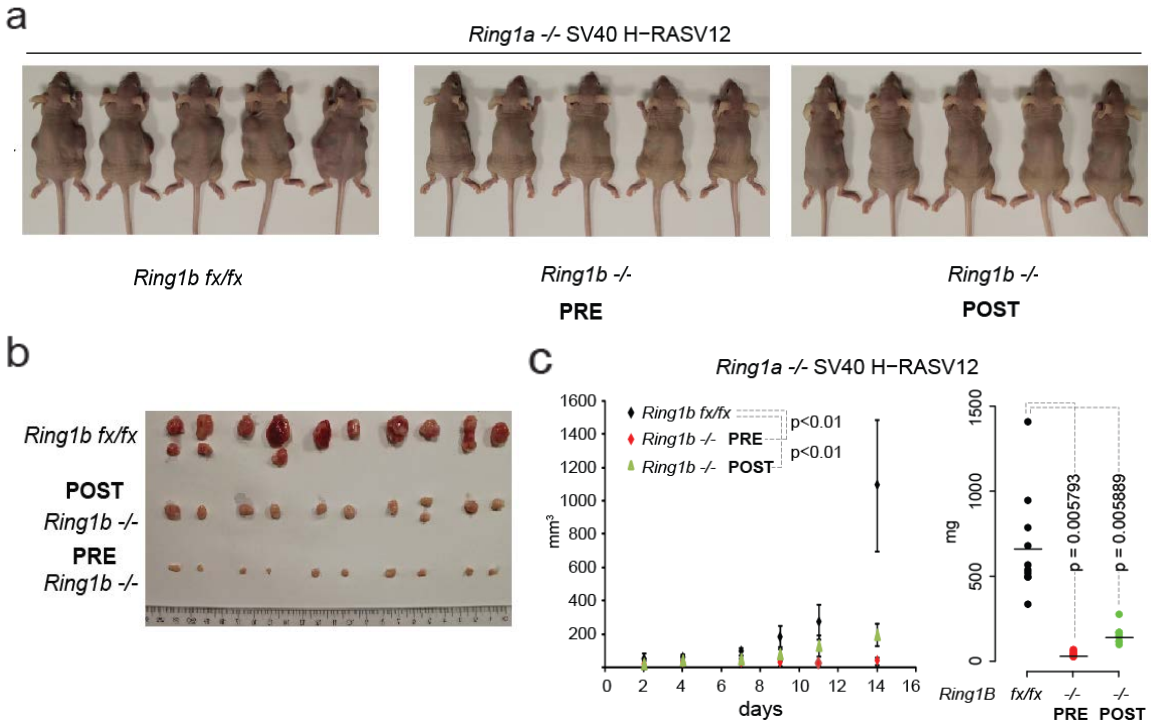

Figure 33. Injection of *Ring1b* and *Ring1a* knockout SV40 H-RASV12 transformed MEF in nude mice. a, Pictures of nude mice and isolated tumour masses at 14 days post-injection of *Ring1b fx/fx* and *Ring1b -/- Ring1a -/-*, SV40, H-RASV12 *Cre-ER*^{T2} transformed MEFs. **b,** Tumor masses isolated from mice show in **a. c,** Average increase of tumour size (volume) at the indicated time (left) and the weights of the tumour masses (right) shown in **b**. Error bars indicate SD, n=10

These results were further supported by the rapid exhaustion of the self-renewing potential of normal and MYC-transformed hematopoietic stem cells upon inactivation of PRC1 activity (Figure 34). Together, these results suggest the existence of alternative mechanisms of PcG-dependent proliferation control that could be in common among different cell types.

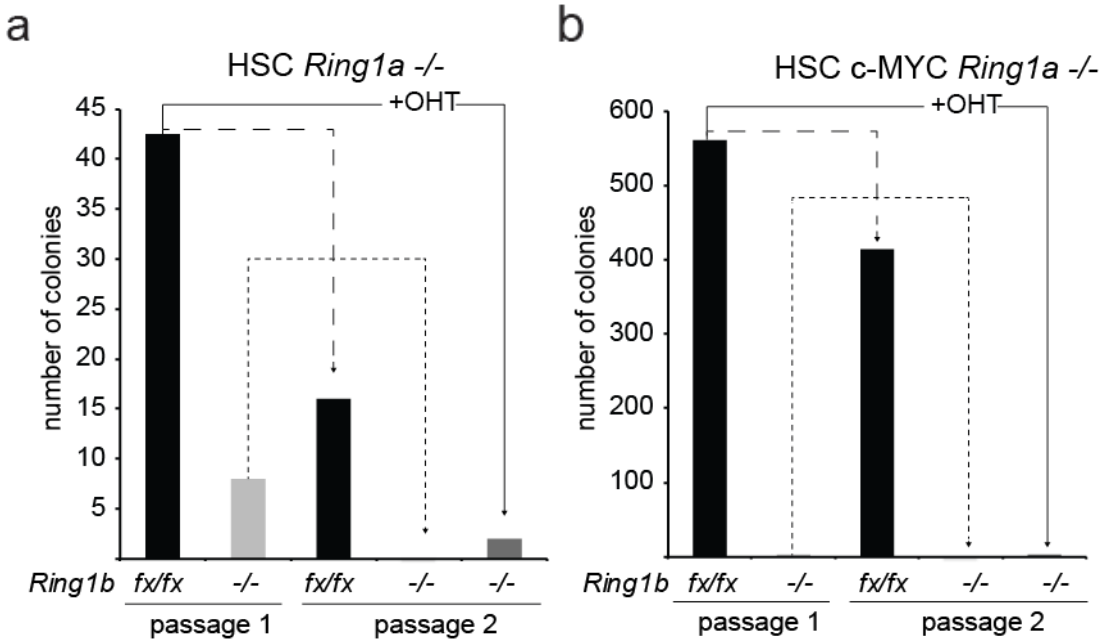

Figure 34. PRC1 activity depletion in hematopoietic stem cells. Hematopoietic stem cells self-renewal assay (methylcellulose assay) performed with lineage negative (lin-) bone marrow purified cells from *Ring1a -/-, Ring1b fx/fx Cre-ER*^{T2} mice in absence (**a**) or presence (**b**) of c-MYC ectopic lentiviral-driven expression and treated with EtOH or OHT. Bar plots indicates the number of colonies formed on methylcellulose matrix 7 days after each plating. An equal amount of *Ring1a -/-, Ring1b fx/fx Cre-ER*^{T2} cells isolated from the first passage were also re-plated in the presence of OHT to allow conditional alleles deletion (passage 2, +OHT treatment).

2.5 PcG proteins control S-phase entry and DNA replication

Since PcGs repressive activity is not exclusively recruited at the ink4a-Arf locus but potentially regulates the expression of more than 2500 genes in MEFs (Figure 35b), we hypothesised that additional transcriptional pathways could be under the direct transcriptional control of PcG proteins. To our surprise, despite the strong proliferation impairment (Figure 6), expression analyses performed in *Ink4a/Arf -/- Ezh2 -/-* MEF identified only 46 genes that were significantly up regulated upon loss of Ezh2 activity (Figure 35a). Differently, expression analyses performed in *Ink4a/Arf +/+ Ezh2 -/-* MEF identified 792 genes that were up regulated compared to *Ezh2 fx/fx* MEF of which only 31

were found commonly regulated between Ink4-Arf proficient and KO MEFs (Figure 35a). Moreover, a few proportion of H3K27me3 enriched genes[1] was transcriptionally up-regulated upon inactivation of Ezh2 activity in both WT and *Ink4a-Arf-/-* MEFs (respectively ~7% and ~0.4%) of WT and *Ink4a-Arf-/-* MEFs (Figure 35b), suggesting indirect transcriptional regulations that are prevalently dependent on the activation of cell-cycle restriction checkpoints in *Ink4a-Arf* proficient MEFs (Figure 35b). Together, these data point towards a transcriptional-independent mechanism by which PcGs can control cellular proliferation.

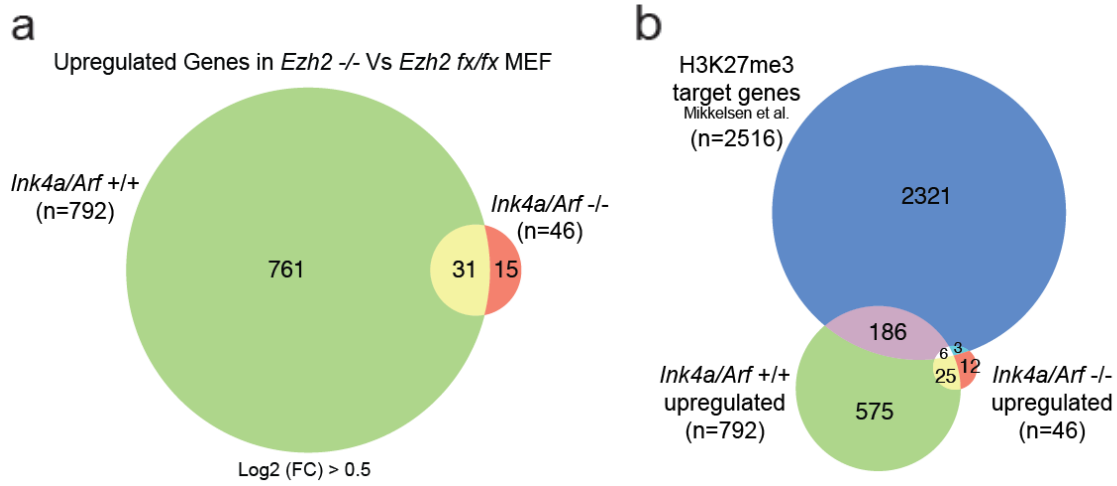

Figure 35. Transcriptional changes in *Ezh2 -/-* MEF. a. Venn diagrams representing the overlap of genes up-regulated in either *Ezh2 fx/fx* or *Ink4a/Arf -/- Ezh2 fx/fx* MEF treated with OHT (*Ezh2 -/-*) respect to EtOH (*Ezh2 fx/fx*) with a minimal fold difference of 1.5. b,The diagrams represent the same overlap of **a** respect to previously characterized[1] H3K27me3 enriched promoters in WT MEFs.

Loss of Suz12 expression from serum starved quiescent human fibroblasts impairs the cell cycle re-entry measured by incorporation of BrdU[233]. This result suggests that loss of PRC2 activity could affect the progression of G1 or S-phase. The finding that PcG proteins can remain associated with chromatin during DNA synthesis[236], together with the localization of PRC2 subunits at sites of ongoing DNA replication[237], potentially suggests a direct link between PcG activities and DNA replication. To test this, we synchronized *Ezh2 fx/fx* and *Ezh2-/-* MEFs at the G1/S boundary with a double-thymidine block, allowed S-phase re-entry for 30 minutes in the presence of BrdU, and measured DNA synthesis by flow cytometric analyses (FACS) with a BdrU specific antibody. Due to the polyploidy of

RASV12 or MYC-transformed MEFs[238, 239] (Figure 35 and Figure 36), we restricted BrdU measurements to the 2C population to avoid cross-contaminations of G1/S boundaries. This analysis highlighted a reduced number of cells that synthesized DNA in *Ezh2* -/- MEFs, suggesting direct defects of DNA replication in the absence of PRC2 activity (Figure 36 and Figure 37).

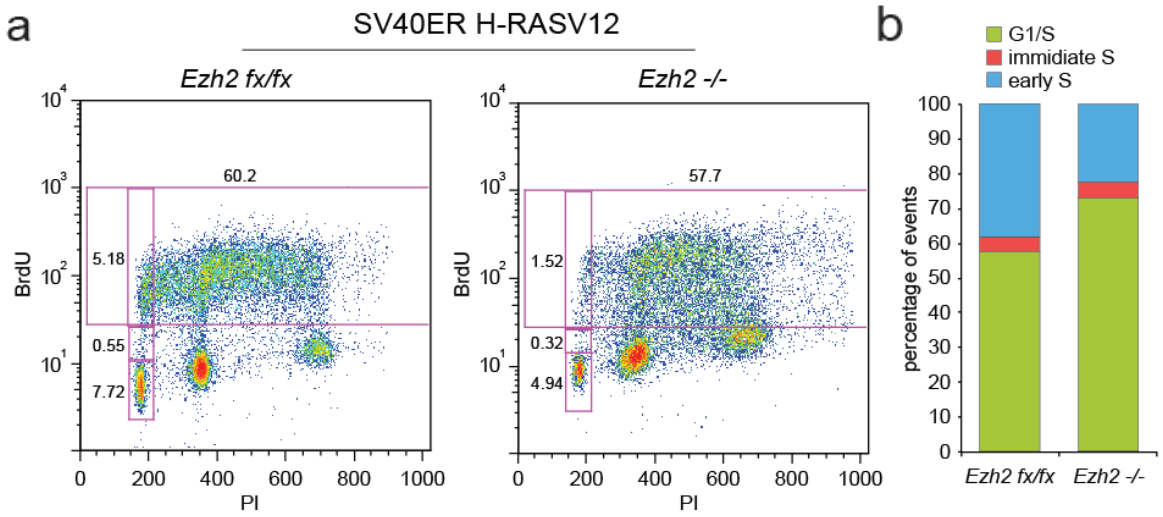

Figure 36. FACS plot of SV40 H-RASV12 *Ezh2fx/fx* and *Ezh2* -/- MEF re-entry in S-phase. a, FACS dot plot of SV40 H-RASV12 *Cre-ER*^{T2} transformed Ezh2 fx/fx MEFs 7 days after EtOH (Ezh2 fx/fx) and OHT (Ezh2 -/-) treatment fixed 30 minutes after release from a double-thymidine G1/S block in the presence of BrdU. The numbers near the boxes indicated the relative cell percentage present in each box. **b,**The bar plots represent the relative percentage of cells with 2C DNA content present in the highlighted boxes in **a**(BrdU negative, intermediate and BrdU positive).

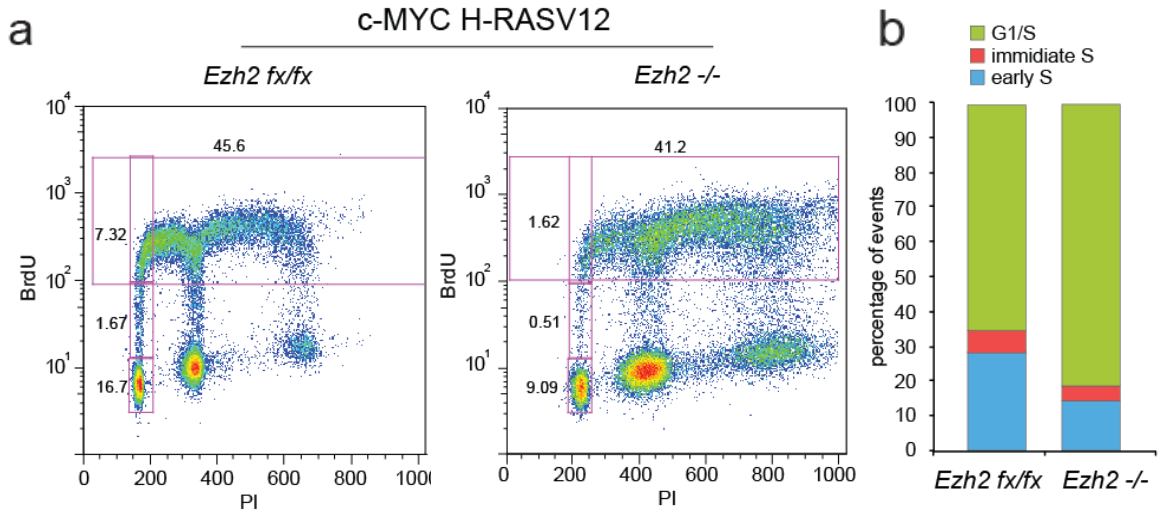

Figure 37. FACS plot of SV40 c-MYC *Ezh2fx/fx* and *Ezh2* -/- MEF re-entry in S-phase. FACS dot plot of SV40 c-MYC *Cre-ER*^{T2} transformed Ezh2 fx/fx MEFs 7 days after EtOH (Ezh2 fx/fx) and OHT (Ezh2 -/-) treatment fixed 30 minutes after release from a double-thymidine G1/S block in the presence of BrdU. The numbers near the boxes indicated the relative cell percentage present in each box. **b,**The bar plots represent the relative percentage of cells with 2C DNA content present in the highlighted boxes in **a**(BrdU negative, intermediate and BrdU positive).

Consistent with this, Ezh2 proficient cells displayed a high degree of overlap between core PRC2 (Suz12) and PRC1 (Ring1b) subunits with sites of BrdU incorporation during S-phase (Figure 38). Loss of *Ezh2* strongly reduced Suz12 levels and severely affects its association to BrdU signal. Furthermore *Ezh2* strongly impairs Ring1b association with newly synthesized DNA (Figure 38) and suggested a hierarchical recruitment at replication sites between PRC2 and PRC1 as described for several target genes[184].

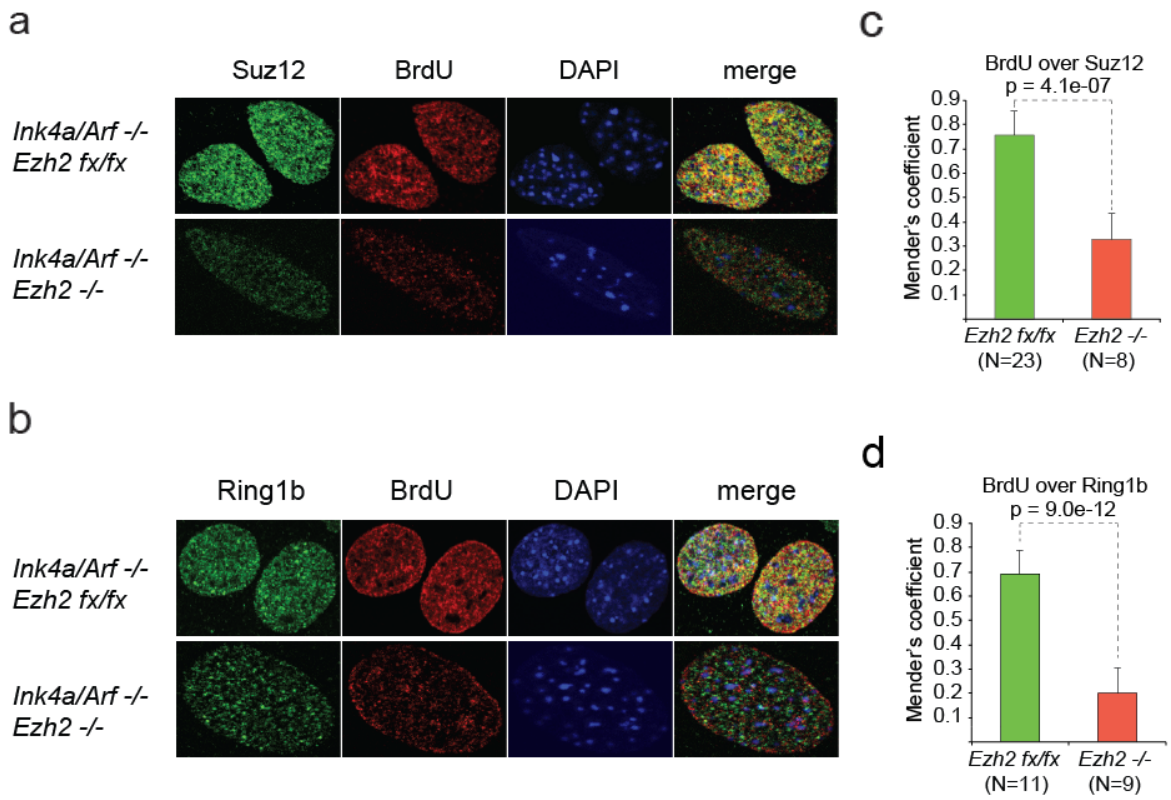

Figure 38. PcGs and BrdU localization in S-phase in *Ezh2 fx/fx* and *Ezh2 -/- Ink4a/Arf -/-* MEFs. a and **b,** Confocal immunofluorescence images of *Ink4a/Arf -/-; Ezh2 fx/fx* and *Ink4a/Arf -/- Ezh2 -/-* MEFs 2 hours after release from double-thymidine G1/S block in the presence of BrdU stained with the indicated antibodies. **c** and **d,** Bar plots indicates the average Mender's co-localization coefficient among all images Z-stacks for each cell stained as in **a**. Error bars indicate SD. n is indicated in the figure.

To test whether PcG deficiency could affect DNA replication, we performed DNA molecular combing experiments, which allow the quantitative study of individual DNA replication events[240]. *Ezh2 fx/fx* and *Ezh2 KO* MEFs initially pulse-labelled with IdU for 20 minutes and then immediately pulse-labelled with CldU for other 20 minutes. These two pulses allow to label active replicating forks with 2 different thymidine analogues. Pulse labelling cells with two analogues allows the analysis of more replication parameters

than in the case of labelling with a single analogue. Indeed, double labelling allows the precise evaluation of for the symmetry of fork progression, inter-origin distances, which can only be inferred in case of single labelling. Labelled cells were included into agarose plugs then the DNA was extracted and slowly (300µm/s or 2 Kb/s) combed on hydrophobic glass slides. Then IdU and CIdU incorporated on DNA fibres combed on glass slides were detected by fluorescent staining, together with anti-single-strand DNA antibody (to identify fibres). First, we measured the overall velocity of replication forks by dividing the length of the signal coming from analogues staining (in kb) by the analogue pulsing time (in minutes), also considering that each µm of signal correspond to 2 kb[240]. When this was measured in our *Ezh2* cKO MEF, while Ezh2 proficient MEFs displayed a unimodal fork speed distribution (centred around a mean fork velocity of 2.02 Kb/min), *Ezh2 -/-* cells displayed an overall slower velocity (mean velocity 1.79 kb/min) and a bimodal distribution highlighting the presence of a DNA replication fork population significantly slower (Figure 39).

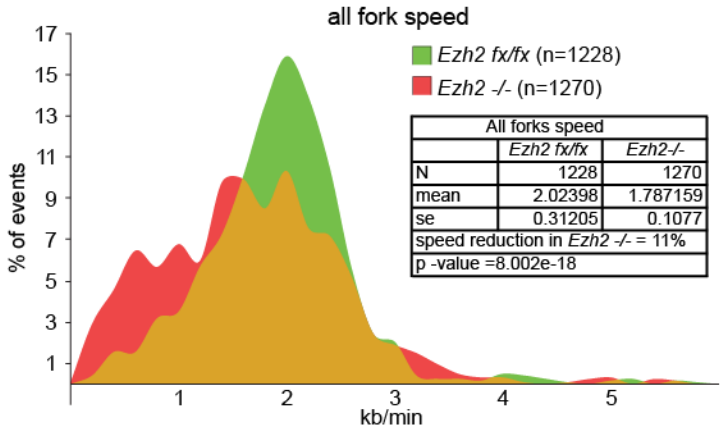

Figure 39. Distribution of fork speed values in *Ezh2 fx/fx* and *Ezh2 -/-* SV40 H-RASV12 transformed MEFs. Distribution of the replication speed for all forks between SV40 immortalized *Ezh2 fx/fx MEFs* that stably expressed H-RASV12, 7 days after EtOH (*Ezh2 fx/fx*) and OHT (*Ezh2 -/-*) treatment. N, mean and standard error are indicated in the figure. p-value was determined by Chi-squared test.

Next, we determined the replication symmetry by measuring the length of newly synthesized DNA and comparing the fork progression of the left and right arms of the DNA replication bubble departing in opposite directions from the same DNA replication

origin. To analyse the replication forks symmetry we firstly identify replication origins that consist in fibre zones with no signal flanked by IdU staining (first pulse marked in red). After origin localization we consider arbitrary left and right forks of which we measured respectively the length of the signal coming from the two different nucleotide analogues.

We observed three main patterns of DNA replication: “symmetric fork progression” in which DNA replication fork progression is comparable between left and right forks (IdU and CldU left/right ratio less than 30% difference, Figure 40 top panel), “asymmetric fork progression”, in which the difference between the two DNA replication forks is more than 30%, (IdU and CldU left/right ratio > 30% difference, Figure 40 middle panel) and ”unidirectional fork progression” in which only one DNA replication fork depart from one origin (Idu signal absent in one of the two direction, Figure 40 bottom panel). Following this classification, the analysis of *Ezh2 fx/fx* and *Ezh2 KO* replicating DNA demonstrated that *Ezh2* -/- MEFs accumulated a greater number of asymmetric and unidirectional DNA replication forks (Figure 41).

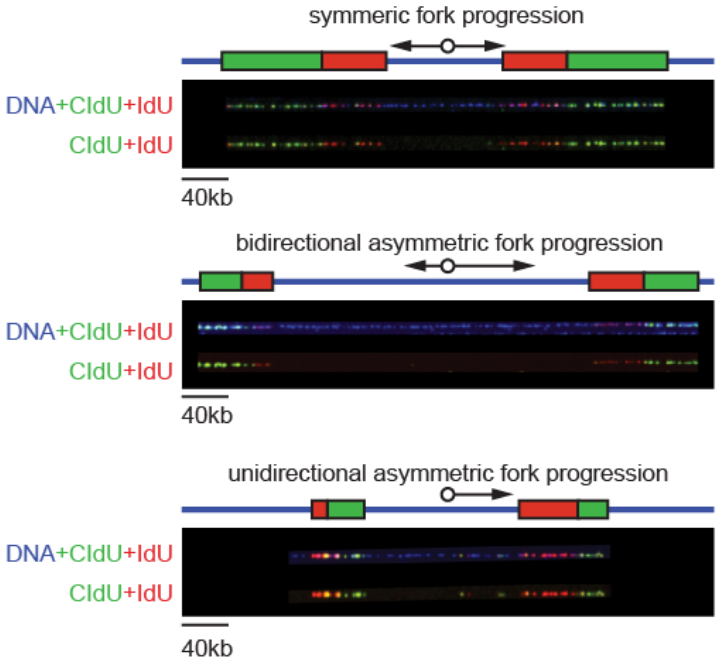

Figure 40. Replication forks symmetry classification. Representative spinning disk confocal microscopy images of DNA combing performed in the cells presented in Figure 38 and stained with specific antibodies against nucleotide analogues indicated in the figure. DNA fibres were visualized using ssDNA specific antibody (marked as DNA in the figure).

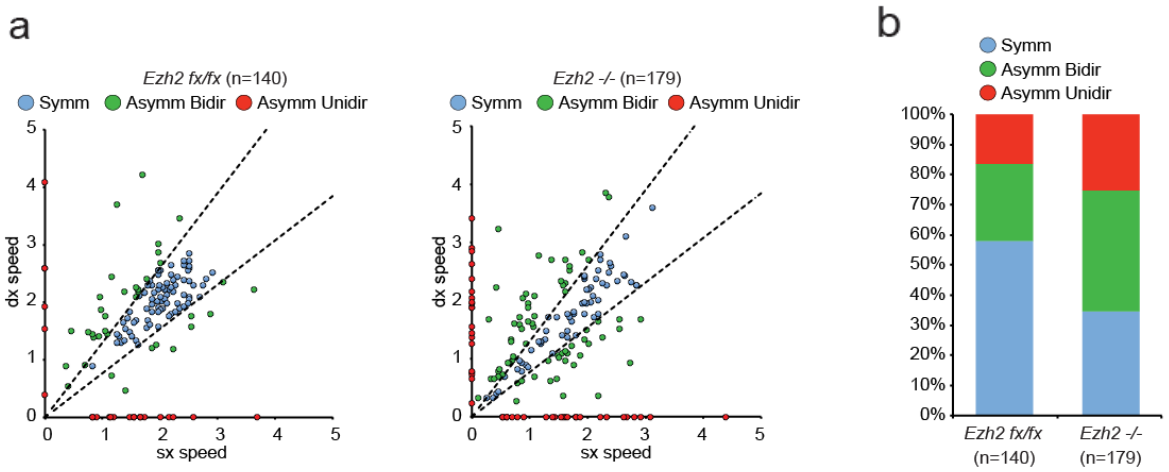

Figure 41. Symmetry based distribution of replication forks in *Ezh2 fx/fx* and *Ezh2 -/-* SV40 H-RASV12 transformed MEFs. a, dot plot colour coded representing symmetric (light blue) asymmetric bidirectional (green) and asymmetric unidirectional (red) replication forks in SV40 immortalized *Ezh2 fx/fx MEFs* that stably expressed H-RASV12, 7 days after EtOH (*Ezh2 fx/fx*) and OHT (*Ezh2 -/-*) treatment. Dotted lines indicate the 30% ratio tolerance applied to define symmetric fork progression N is mentioned in the figure. **b,** bar plot quantification of **a**

To test whether the fork speed reduction was associated with asymmetric fork progression within individual replicons, we selected only the fork speed values deriving from replicons, regardless their levels of symmetry (all fork speed in replicons, Figure 42).

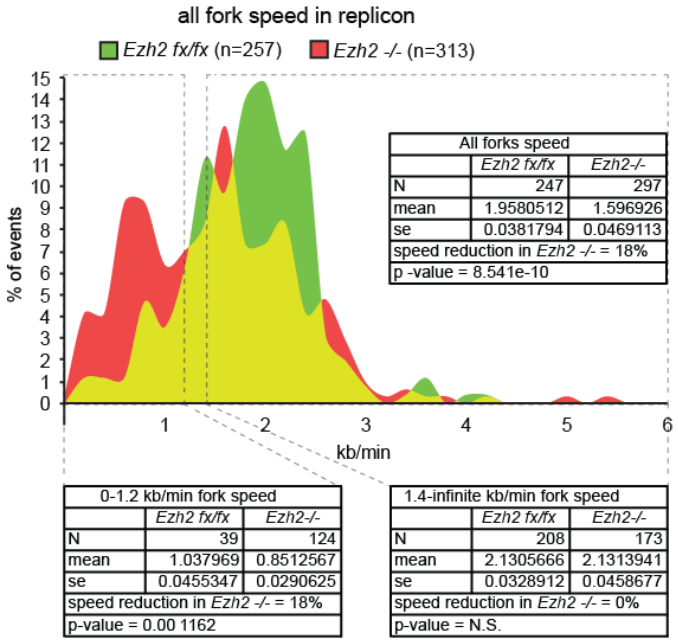

Figure 42. Distribution of fork speed values in replicons. Distribution of the replication forks speed in replicons between SV40 immortalized *Ezh2 fx/fx MEFs* that stably expressed H-RASV12, 7 days after EtOH (*Ezh2 fx/fx*) and OHT (*Ezh2 -/-*) treatment. N, mean and standard error are indicated in the figure. p-value was determined by Chi-squared test.

Next, we analysed fork speed only in symmetric DNA replication operons, thus excluding asymmetric ones, and found a consistent reduction in fork speed in *Ezh2* -/- MEFs compared to wild-type MEFs (symmetric fork speed in replicons, Figure 43).

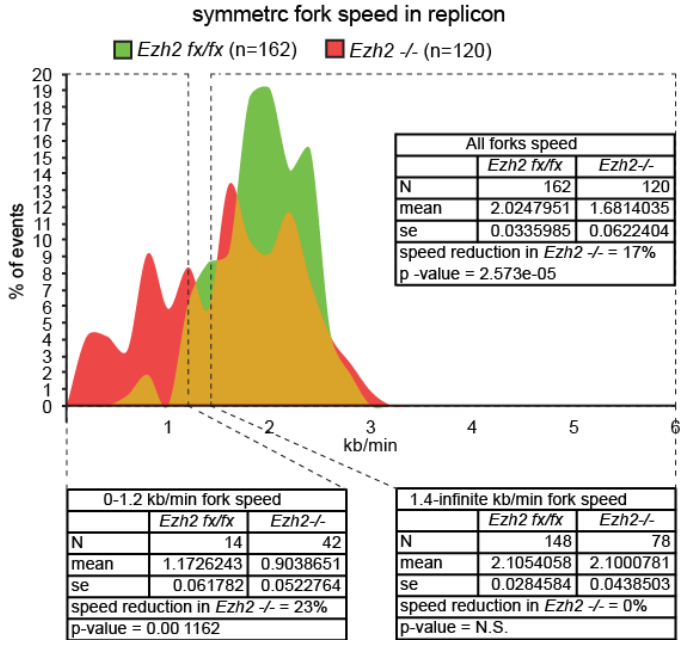

Figure 43. Distribution of symmetric fork speed values in replicons. Distribution of the symmetric replication forks speed in replicons between SV40 immortalized *Ezh2 fx/fx MEFs* that stably expressed H-RASV12, 7 days after EtOH (*Ezh2 fx/fx*) and OHT (*Ezh2* -/-) treatment. N, mean and standard error are indicated in the figure. p-value was determined by Chi-squared test.

Overall these results show that lack of Ezh2 increases the rate of DNA replication fork stalling, as demonstrated by increased levels of asymmetric and unidirectional forks. In addition, Ezh2 inactivation also reduces DNA replication fork speed, but, surprisingly, this is not a peculiarity only of stalled (asymmetric) DNA replication forks.

In yeasts, increased DNA replication fork stalling can trigger firing of dormant origins[241]. To test this possibility, we analysed the impact that loss of Ezh2 expression have on DNA replication origin firing. Accordingly to an increased impairment in DNA replication, *Ezh2 KO* cells showed an increased number of active replication origins as inferred by the decreased inter-origin distances (IODs) of *Ezh2* -/- respect to *Ezh2 fx/fx* cells (Figure 44). These differences are maintained also when the IOD was analysed on DNA fibres longer than three times the average of fibres length[242] (Figure 44b).

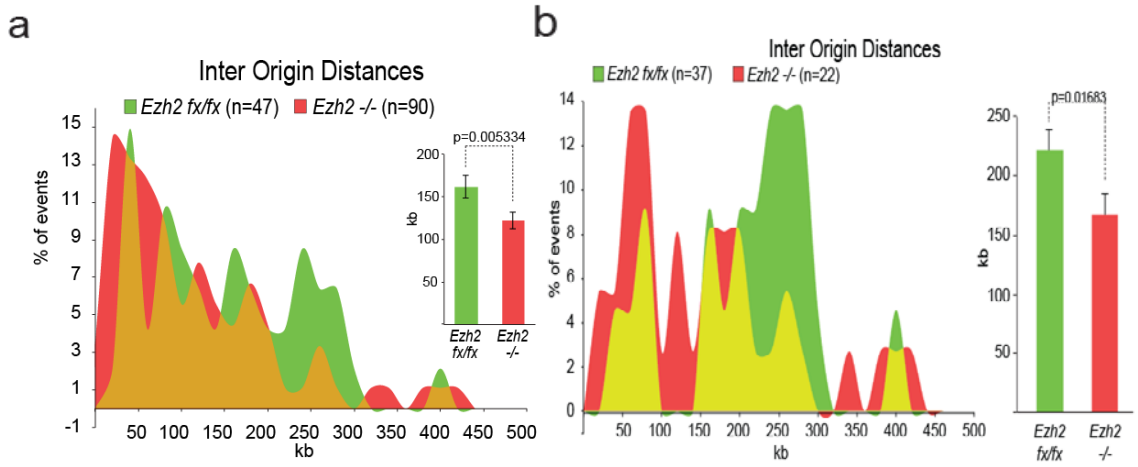

Figure 44. Inter Origin Distances (IODs) in *Ezh2 fx/fx* and *Ezh2 -/-* SV40 H-RASV12 transformed MEFs. a, Distribution of inter-origin distances (IOD) measured for all DNA fibres between *Ezh2 fx/fx* and *Ezh2-/-* cells described in Figure 38. Bar plots show the average IODs of *Ezh2 fx/fx* and *Ezh2-/-* cells. Error bars indicate SD. n is indicated in the figure. p-value was determined by Chi-squared test. **b,** same as in **a** calculating only IODs coming from DNA fibres 3 times longer than the average of fibres length.

Furthermore these results are not a consequence of increased DNA fibres fragmentation of *Ezh2 KO* samples as both *Ezh2 fx/fx* and *Ezh2 -/-* DNA preparations displayed overlapping DNA lengths distribution (Figure 45).

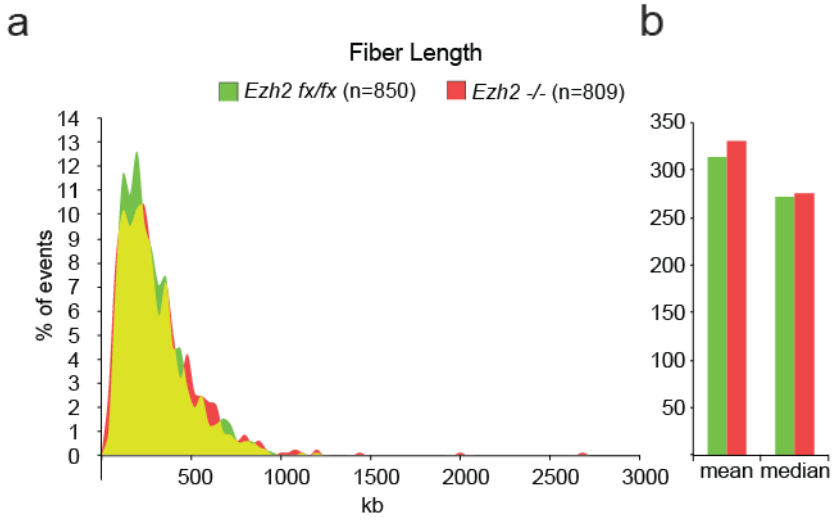

Figure 45. Distribution of fiber lengths in DNA combing analyses a, Distribution of the fibres length used in DNA combing analyses (Figure 38-42). **b,** Bar plots of mean and median values of fibres length referred to **a**

Finally, since altered DNA replication parameters, and in particular DNA replication stalling events, may trigger DNA damage response (DDR) activation, we monitored DDR signalling at the single-cell level, by the study of 53BP1 foci formation in S-phase[243].

Ezh2 deficient MEFs present an increased number of 53BP1 foci respect to WT cells (Figure 46). Overall, these data demonstrate that PcG activity localizes at sites of DNA synthesis and plays an important role in regulating the normal progression of DNA replication.

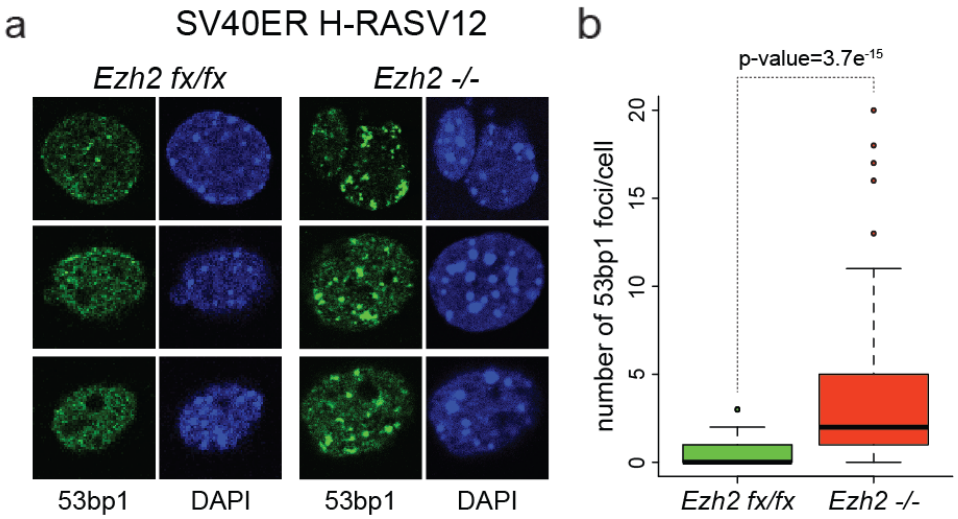

Figure 46. 53bp1 staining in *Ezh2 fx/fx* and *Ezh2* -/- SV40 H-RASV12 transformed MEFs. a, Confocal immunofluorescence images of SV40ER immortalized *Ezh2 fx/fx MEFs* that stably expressed H-RASV12 7 days after EtOH (*Ezh2 fx/fx*) and OHT (*Ezh2* -/-) treatment, 30 minutes after release from a double-thymidine G1/S block stained with 53BP1 specific antibody. **b,** Box plot represents the number of 53bp1 foci in each cell. Foci number was quantified using ImageJ. n is indicated in the figure. p-value was determined with paired t-test.

Discussion

In the present thesis, we provided genetic proofs for the role of PRC2 and PRC1 in controlling normal and neoplastic cells proliferation independently of Ink4a/Arf-p53-pRb cell cycle regulation. This finding has a particular relevance in the context of tumour development where loss of *Ink4a/Arf*, *pRb* and/or *p53* response is a hallmark for all type of human tumours[215].

Ezh2 enzymatic activity has become an appealing pharmacological target to hamper tumour spreading[127-129] and our data genetically supports the effectiveness of PcG inhibition for cancer treatment. For example, it has been recently demonstrated that diffuse large B cell lymphomas (DLBCL) that carry hyper-activating mutations of EZH2 (DLBCLs frequently present defective p53 response[244, 245]), can be efficiently treated with EZH2 selective compounds[127].

Here we demonstrated the tumorigenic cells dependency on both PRC1 and PRC2 activity. Precisely we were able to show that the two complexes are definitely required for the initial acquisition of the transformed phenotype. This notion is of particular importance, because this is one of the few evidences, so far reported, that PRC1 or PRC2 abrogation in immortalized cells prevents the acquisition of transformed phenotype upon expression of a strong oncogene such as H-RASV12 or C-MYC. Furthermore the importance of this issue consists in supporting a potential strategy to target PcGs also in low aggressive tumours in which severe tumorigenic features, such as metastatic potential, have not been acquired yet.

Our findings suggest a scenario where PcG proteins exert a parallel control over DNA replication and Ink4a/Arf transcription. Loss of PcG activities in normal cells, will affect at the same time cellular proliferation, by favouring the efficient replication of the DNA, and cell cycle checkpoints, by regulating the transcription of Ink4a/Arf (Figure 45). While loss

of Ink4a/Arf repression can activate cell cycle checkpoints, a defective DNA replication will trigger a parallel stress response to potentiate Ink4a/Arf, pRb and p53 dependent cell cycle arrest in a positive feedback loop (Figure 47). In absence of functional checkpoints, cells will not undergo a cell cycle arrest but their proliferation will still result dependent on PcG activity (Figure 47). An additional layer of complexity could come from PcG-dependent transcriptional regulation of additional targets. This could involve the de-repression of lineage specific genes, which would result essential for the maintenance of cellular identity; or the activation of a common set of targets genes with anti-proliferative function in all cell types. Although we cannot exclude these contributions, genome-wide transcription analysis, performed in *Ink4a/Arf* -/- MEFs, before and after *Ezh2* deletion, did not show any relevant transcriptional effects in the presence of compromised cellular proliferation (Figure 6 and Figure 35) as also showed by a recent study in SUZ12 knockdown cells[183].

Tumour cells are exposed to continuous replication stresses imposed by the activity of oncogenic signals. Common examples are the constitutive activation of RAS signalling or the overexpression of the MYC proto-oncogene [246, 247]. When replication stress is coupled to defective cell cycle checkpoints, it results in the escape from cellular senescence. At the same time, this prolonged replicative stress promotes the instability of cancer cell genomes [248]. This could suggest that the direct role in regulating DNA replication processes could render cancer cells more sensitive to PcG inhibition. The finding that PcG proteins co-localize and favour the progression of DNA replication suggests a direct implication of PcG activity with the replication of the DNA. PcGs could either play a role in origin firing, as depict by the decreased inter-origin distance of *Ezh2* -/- MEFs, or they could be involved in chromatin dynamics during the progression of the replication forks. Alternatively, PcGs could play a role in regulating the collision between RNA transcription and DNA replication, for example through their ability to bind and disassemble the RNA

polymerase II complex[249]. This last hypothesis is currently under investigation due to new very recent and preliminary results we obtained from the purification of both PRC1 and PRC2 during S-phase (see Appendix).

Together, our data provide evidences for a novel role of PcG proteins in regulating cellular proliferation that further explains the requirement of PcG activity for the growth of normal and cancer cells paving the way for the understanding of novel mechanisms of proliferation control.

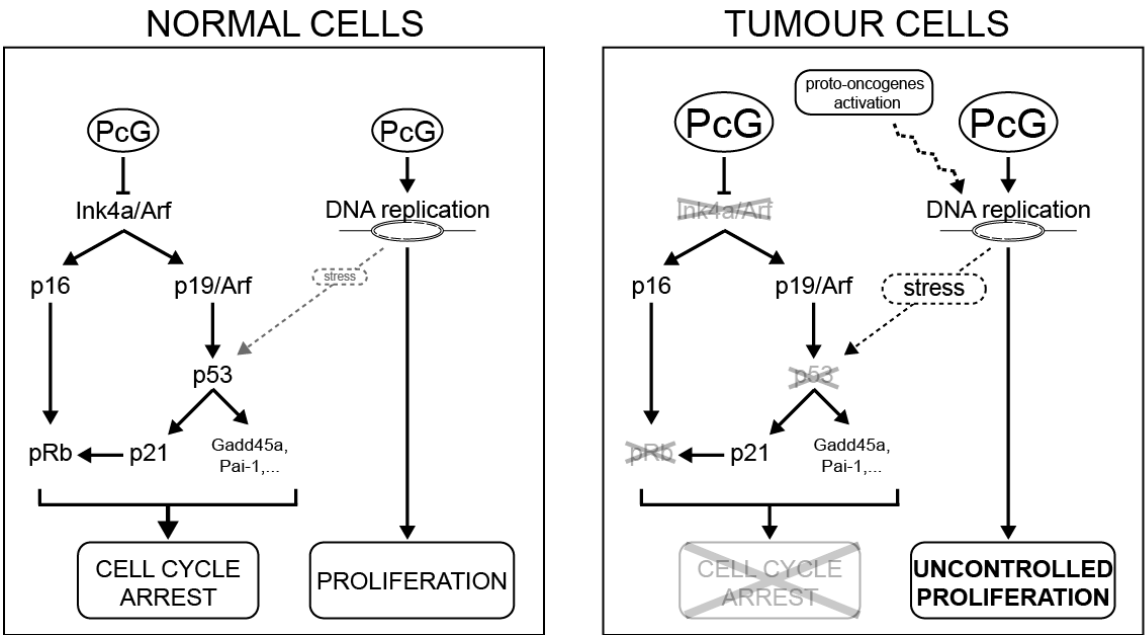

Figure 47. Inter Origin Distances (IODs) in *Ezh2 fx/fx* and *Ezh2 -/-* SV40 H-RASV12 transformed MEFs. a, Distribution of inter-origin distances (IOD) measured for all DNA fibres between *Ezh2 fx/fx* and *Ezh2-/-* cells described in Figure 38. Bar plots show the average IODs of *Ezh2 fx/fx* and *Ezh2-/-* cells. Error bars indicate SD. n is indicated in the figure. p-value was determined by Chi-squared test. **b,** same as in **a** calculating only IODs coming from DNA fibres 3 times longer than the average of fibres length.

CHAPTER 4: Appendix

To understand whether PRC1 and PRC2 associate with new partners in S phase we recently generated two MEF *BirA* lines: one stably expressing a Flag-Avi-Ring1b protein and the other expressing a Flag-Avi-Eed protein. These two MEF cell lines were synchronized at the G1/S boundary by a double thymidine block and then they were allowed to enter S phase for 1 hour. At that time we performed a double step purification for tagged Ring1b and Eed proteins coupled to mass spectrometry analyses to identify new PRC1 and PRC2 interactors in S-phase. The preliminary results indicate that several DNA/RNA helicases and RNA binding proteins also involved in RNA splicing interact with both PRC1 and PRC2 (Figure 48 and Figure 49). In the light of our results on PRC1 and PRC2 involvement in DNA replication we speculate that their interaction with DNA/RNA helicases could play a direct role in the process. We hypothesize that these helicases may solve R-loops facilitating DNA replication when this collides with the transcriptional machinery[250]. We also speculate that, in concert, the role for PcG proteins in this context could consist in a transient local transcriptional repression that allows the replication of the DNA. We are currently investigating these hypotheses to better understand the molecular mechanism the underlies PcG control on DNA replication.

Gene names	Peptides Ring1b	Peptides Empty	Sequence coverage Ring1b [%]	Sequence coverage Empty [%]	iBAQ Ring1b	iBAQ Empty
Ring1b	**20**	**3**	**58,6**	**9,8**	**2,23E+07**	**2,57E+04**
Ywhaz	8	0	33,5	0	5,56E+05	0,00E+00
Srsf1	11	0	37,2	0	4,09E+05	0,00E+00
Srsf7	6	0	22,1	0	1,98E+05	0,00E+00
Pabpc1;Pabpc6	19	0	28,6	0	1,44E+05	0,00E+00
Ywhaq	6	0	24,5	0	1,37E+05	0,00E+00
Srsf6	7	1	19,5	2,7	1,16E+05	1,05E+03
Ywhag	6	0	24,7	0	9,34E+04	0,00E+00
Tra2b	4	0	17,7	0	8,03E+04	0,00E+00
Ddx5	7	1	11,7	1,3	5,58E+04	3,95E+03
Ywhae	4	0	16,1	0	5,28E+04	0,00E+00
Sfn	4	0	14,9	0	5,08E+04	0,00E+00
Ell	7	1	12,1	1,7	3,40E+04	2,72E+03
Hnrnpc	4	1	12,5	4,2	3,30E+04	3,10E+03
Magoh; Magoh-rs1;Magohb	3	0	18,5	0	3,22E+04	0,00E+00
Srrm2	21	0	9,4	0	2,96E+04	0,00E+00
Pabpc4;Gm10110	8	1	12,9	1,7	2,57E+04	4,15E+03
Prmt5	4	0	6,6	0	2,15E+04	0,00E+00
Ruvbl2	5	0	11,9	0	1,94E+04	0,00E+00
Hnrnpk;Gm7964	4	0	10,6	0	1,82E+04	0,00E+00
Hnrnph1;Hnrnph2	4	0	13,3	0	1,56E+04	0,00E+00
Ywhah	3	0	11	0	9,16E+03	0,00E+00
Ddx3x;D1Pas1;Ddx3y	7	0	11,5	0	7,96E+03	0,00E+00
Ddx17	8	1	13,7	1,2	7,78E+03	0,00E+00
Ruvbl1	3	0	8,1	0	6,85E+03	0,00E+00
Ddx1	3	0	3,9	0	6,19E+03	0,00E+00

Figure 48. PRC1 partners in S-phase. MEF *BirA* Flag-Avi-Ring1b have been synchronized by double thymidine block and released in S-Phase for 1 hour. Nuclear extracts have undergone double step purification and the eluate analysed by mass spectrometry. In the table are listed a selection of proteins identified. Peptides Ring1b are the unique peptides of proteins listed retrieved in Flag-Avi-Ring1b IP. Peptides Empty are the unique peptides of the proteins listed retrieved in mock IP. Proteins sequence coverage and iBAQ index are also presented for each protein identified

Gene names	Peptides Eed	Peptides Empty	Sequence coverage Eed [%]	Sequence coverage Empty [%]	iBAQ Eed	iBAQ Empty
Eed	**31**	**6**	**63,3**	**15,2**	**3,89E+07**	**29985**
Setx	23	0	9,3	0	2,30E+04	0
Ddx21	12	3	14,8	3,2	7,45E+04	1783,3
Dhx15	12	4	15,3	4,7	4,14E+04	1975,4
Prpf3	8	1	12,4	1,8	3,30E+04	0
Cpsf1	7	1	5,3	0,8	1,21E+04	0
Sf3b2	6	1	8,8	1,4	3,74E+04	1482,5
Srsf10	6	4	26	15,3	2,20E+05	51269
Upf1	6	0	6,3	0	1,79E+04	0
Larp7	5	0	10,2	0	4,85E+04	0
Prpf4	5	1	10,2	1,5	2,48E+04	0
Cpsf2	4	0	5	0	1,46E+04	0
Taf4a	4	0	4,2	0	1,05E+04	0
U2surp	4	1	3,4	0,7	2,58E+03	1822,5
Rbm15	4	0	3,7	0	1,65E+03	0
Ncbp1	3	1	4,2	1,5	1,60E+04	1116,9
Rbm10	3	0	3,9	0	2,47E+03	0
Mov10	3	0	2,8	0	1,91E+03	0
Fmr1	3	1	5,9	1,3	8,49E+02	0
Prpf40a	2	0	2,3	0	1,74E+05	0
Sfpq	2	0	3,1	0	4,35E+03	0
Ddx20	2	0	2,3	0	2,42E+03	0
Cpsf3	2	0	2,9	0	1,78E+03	0
Pura	2	0	5,9	0	0,00E+00	0
Pnn	2	0	2,5	0	1,88E+03	0
Sltm	2	0	1,8	0	1,16E+03	0
Rbm5	1	0	1,5	0	3,23E+03	0
Rbm39	1	0	2,1	0	2,61E+03	0
Ddx23	1	0	1,3	0	1,79E+03	0
Taf6	1	0	1,8	0	1,74E+03	0
Rbfox2;Rbfox1;Rbfox3	1	0	2,2	0	0,00E+00	0
Polr1e	1	0	2,5	0	0,00E+00	0
Taf11	1	0	5,7	0	0,00E+00	0
Sf3b14	1	0	11,2	0	1,38E+04	0
Tcof1	1	0	0,7	0	7,22E+02	0

Figure 49. PRC2 partners in S-phase. MEF *BirA* Flag-Avi-Eed have been synchronized by double thymidine block and released in S-Phase for 1 hour. Nuclear extracts have undergone double step purification and the eluate analysed by mass spectrometry. In the table are listed a selection of proteins identified. Peptides Eed are the unique peptides of proteins listed retrieved in Flag-Avi-Ring1b IP. Peptides Empty are the unique peptides of the proteins listed retrieved in mock IP. Proteins sequence coverage and iBAQ index are also presented for each protein identified

CHAPTER 5: Material & Methods

5.1 Ethic statements

All mouse work has been conducted in accordance with the Italian and international legislations.

5.2 MEF generation and grow conditions

Mouse Embryonic Fibroblasts (MEFs) are primary cells derived from mice embryos. These cells are commonly used as proliferating differentiated cells to study a broad range of biological process such as cellular proliferation, cellular senescence, DNA damage response, etc... Conditional alleles are commonly used for inducible knock-out, allowing alleles deletion after cells derivation from the animal (in this case from the embryos). CRE recombinase is the enzyme required to delete the conditional allele, this enzyme could be fused with a mutated ligand binding site of the Estrogen Receptor (ER ^{T2}), this leads the Cre recombinase inactive (because is retained in the cytoplasm) until the ligand (4-hydroxytamoxifen) is provided. The expression of the Cre recombinase could be targeted in different cell types by expressing it under a cell type specific promoter or it could be stably expressed in virtually all cell types by expressing it under a house-keeping promoter.

Thymidine G1/S synchronization is achieved by the feedback inhibition of CMP (5'-cytosine mono-phosphate) to dCTP (5'-deoxycytosine triphosphate) conversion leading to low/absent dCTP for DNA synthesis in S-phase. Double Thymidine G1/S synchronization is performed to allow cells that were already in S-phase during the first synchronization (therefore blocked in that phase) to finish the S-phase and to be synchronized in the second thymidine synchronization. This procedure allows having virtually all the cells at the very initial stage of the S-phase.

All MEFs have been derived from 13.5 dpc embryos. Rosa26 CRE-ER^{T2}, *Ezh2* knockout, *Ink4a/Arf* knockout, *Suz12* knockout, *p53* knockout, *pRb* knockout *Ring1a* knockout, *Ring1b* knockout and Rosa26 BirA genes used in this work have been described elsewhere [116, 218, 219, 235, 251, 252]. In all the experiments, low passages MEFs have been grown in DMEM medium supplemented with 10% fetal bovine serum (Euroclone), non-essential amino acids (Gibco), sodium pyruvate (Gibco) and 1% penicillin/streptomycin (Gibco), in

a CO_2 incubator (5% CO_2) with reduced oxygen tension (3% oxygen) if not differently specified. MEFs were passaged every 3-4 days. To induce CRE-ER^{T2} nuclear translocation, cells were treated with 500 nM of 4-hydroxytamoxifen (4-OHT, Sigma) dissolved in absolute ethanol (Panreac).

For G1/S synchronization using a double thymidine block, sub-confluent asynchronous MEFs were treated with 2mM thymidine (Sigma) for 12 hours, release with normal medium for 8 hours and treated again with 2mM thymidine for additional 12 hours.

5.3 Beta-galactosidase staining

Beta-galactosidase activity is considered one of the hallmarks of senescent cells due to the enhanced expression of the lysosomal protein GLB1, even though it does not seem to participate to the senescent phenotype induction. This activity is generally defined SA-βGal (Senescent associated β-galactosidase activity.

10^5 MEFs grown at 3 % oxygen or 21% oxygen (5% CO_2) have been plated at passage 5 (~20 days from derivation) on 0.1% gelatine-coated slide chambers and analysed for beta-galactosidase positivity using the Senescence β-Galactosidase Staining Kit (Cell Signaling).

5.4 Growth curves, colony and foci formation assays

Growth curve are the most useful tools to measure cellular proliferation. We used an unbiased method consisting in plating the entire curve in the same moment and collecting the plates day by day detecting the number of cells by staining (Crystal violet). This allows you to physically detect the cells (and their growth) also by eyes at the end of the curve, and to easily quantify the growth by spectrophotometer detection of the cell-bound crystal violet (that is proportional to the number of cells) resuspended in a fix volume of acetic acid.

Colony assays are standard assay used to measure the ability of the cells to growth when they are extremely diluted in the dish. This ability is peculiarity of immortalized and transformed cells that are largely insensitive to the absence of cell to cell contacts (which in wild type MEFs is fundamental for proper proliferation) and can growth in a clonal like manner.

Foci formation assay is one of the gold-standard methods to test the transformed phenotype of the cells that, in the case of MEFs and other cell types, consists in the ability to growth in an anchorage-independent manner forming so called foci. Historically this methodology was applied to test the transformation ability of pieces of DNA transfected in NIH/3T3 immortalized MEF. Oncogenic DNA were then analysed to find new putative oncogenes. This method is quite low efficient, firstly because is based on transient transfection, and secondly because the DNA oncogenic potential was unknown. In our study we stably expressed well-known potent oncogenes to transform our MEF (H-RASV12 and c-myc) therefore virtually all the cells are stably transformed. Then we had to adapt that method using a mixed population of immortalized and transformed MEF that allowed us to discriminate individual foci that otherwise would have not been distinguishable.

All growth curves have been generated by plating $5x10^4$ cells/well in a 6 wells plate or $3x10^4$ cells/well in a 12 wells plate in triplicate for each day of the growth curve. Each day of the growth curve, cells have been fixed using cold (+4°C) 4% formaldehyde buffered at pH 6,9 (Panreac) for 10 minutes at RT, washed twice with distilled water and air-dried. At the end of each curve single wells were stained with a 0,1% w/v solution of crystal violet (Sigma) for 30 minutes at RT. Plates were washed 4 times in water and dried O/N. Crystal violet was solubilized using 10% acetic acid (Carlo Erba) and the absorbance measured at λ=590nm. All growth curves were plated 1 week after OHT administration for the conditional KO MEFs and 2 days after antibiotic selection for the lentiviral infected cells. All the growth curves presented are representative of at least 3 independent experiments.

Colony formation assays were performed with triplicate plating of 10^4 cells in a 10 cm dish. After 12-14 days cells were fixed and stained with crystal violet as described for the growth curves.

Foci formation was obtained by plating $4x10^6$ SV40ER-immortalized MEFs with $2x10^5$ SV40ER H-RASV12 transformed MEFs in a 10 cm dish. After 15-20 days cells have been fixed with 10% formaldehyde for 30 minutes at RT, stained with a 4% Giemsa (Sigma) solution in 1XPBS for 2 hours at RT, washed 4 times in water and air dried O/N. All the foci formation assays presented are representative of at least 2 independent experiments.

Colonies and foci counting have been performed with imageJ counting particles tools. Equal threshold settings and other parameters have been applied to all images.

5.5 Immunoblots

This is a standard procedure that allows detecting the abundance levels of proteins or proteins PTM from a cell lysate.

Immunoblots have been performed as described elsewhere[253]. All blots including conditional knockout or infected MEFs have been carried out with protein lysates prepared 7-8 days after 4-OHT administration or after two days from antibiotic selection for the infected cells. A list of antibodies is available in Table 1.

5.6 BrdU FACS analysis

This is a standard procedure that allows locating the cells in a phase of the cell cycle.

Cells grown in the presence of 33µM BrdU for the indicated time were fixed with 75% ethanol (Panreac), permeabilized with 2N HCl (Panreac) for 30 minutes at RT and the pH equilibrated using 0,1M BORAX (Sigma) for 2 minutes. Cells were incubated with a mouse anti-BrdU antibody (BD) in 1% BSA/1X PBS for 1h at room temperature, washed and stained with a donkey anti-mouse FITC-conjugated antibody (Jackson). Stained cells were treated with RNAse A (Sigma) followed by DNA staining with 2,5 ug/ul propidium iodide (Sigma) O/N at 4ºC. BrdU intensities have been were acquired on FACS Calibur and analyzed using the FLOW JO software. Antibodies details are available in Table 1.

5.7 Viral transductions

Retro and Lentiviral transductions are very useful tools to stably express a protein in the cell

Lentiviral transduction has been carried out by infection with a VSV-G pseudotyped lentivirus. Viral particles were produced by calcium-phosphate transfection of 10^6 293T cells in a 10 cm dish using 10ug of viral delivery vector, 3 µg of VSV-G and 6µg of Δ8.2 packaging vectors per dish. 36 hours post transfection, the supernatant containing viral

particles was collected, 0.45µm filtered and added to $5x10^5$ MEFs that were plated the day before on a 10cm dish. 2 rounds of infection (~8 hours per day) were carried out for each plate in the presence of 5ug/mL of polybrene (Sigma) followed by selection with the appropriate antibiotic selection.

Retrovarial transductions were carried out by transfecting 10ug of the viral vector in 10^6 Phoenix-Eco cells plated on a 10 cm dish. Infections were carried out as for lentiviruses with the introduction of two additional round of infection (two per day) without polybrene. A list of the vectors used for infections is available in Table 2.

5.8 Embryos development

Mouse embryo development is a high complex physiological process that requires and involves several and different biological functions among which, one of the most important is certainly cellular proliferation. However it's very difficult to correlate embryos defects to a precise problem in a biological process involved. Therefore this analysis generally results in correlations between the phenotype/s observed and the biological processes altered.

To obtain *Suz12 -/-, Ink4a/Arf -/-* double KO embryos, *Suz12 +/-, Ink4a/Arf -/-* have been mated and embryos analysed at the indicated time from the detection of vaginal plugs (referred as 0.5 dpc). Each embryo's morphology was recorded with a stereomicroscope and genotyped as previously described[251].

5.9 Nude mice tumours formation

Nude mice tumours formation is the gold standard methodology that formally proves the oncogenic ability of the cells. Moreover it can be used as a surrogate in vivo tumour development system that allows monitoring a certain number of parameters such as tumour growth rate.

10^6 cells subcutaneously injected in each flank of 6 weeks-old nude athymic mice (*nu/nu*) (Charles River laboratories) in 100µl of 1XPBS. Masses growth was measured every 2-3 days from the injection using an electronic calliper. Mice were sacrificed after 14-15 days from injection; the tumour masses isolated and weighted using an electronic scale.

5.10 Immunofluorescence

This is a standard technique that allows to spatially locating in single cells the antigens you are interested in (such as proteins or nucleotide analogue in genomic DNA in our case). Moreover using the confocal microscope it is possible to test the colocalization of 2 or more antigens on the same focal plane with a resolution of 200-400nm.

Indicated MEFs were seeded on 0.1% gelatinized glass coverslips and treated as indicated. To prepare nuclei on coverslips, cells were treated with cold pre-extraction buffer (10mM Tris HCl pH 7,6, 100mM NaCl, 2mM $MgCl_2$, 0,3M sucrose and 0,25% Igepal) for 10 minutes at +4°C.Nuclei were fixed at -20°C with 100% methanol (Panreac) for 10 minutes. Nuclei were further incubated with 20mU/µl of DNAseI (NEB) for 30 minutes at 37°C to unmask incorporated BrdU. Fixed nuclei were incubated with primary antibodies diluted in 0.1% tween-TBS for 1h at RT, washed and incubated with secondary antibodies conjugated with different fluorophores. Nuclei were counterstained with DAPI and embedded in anti-fade containing glycerol (DABCO).

Images were acquired using a Leica SP2 confocal microscopy. Mender's co-localization coefficient was calculated on the entire images Z-stacks using the jacop tool of the Image J software.

The list of antibodies and reagents is available in Table 1.

5.11 Microarray expression analyses

Microarray analysis on cDNA is commonly used to look at transcriptome variations among different biological samples. It is limited by the probes present in the array.

RNA from two independent OHT or EtOH treatments of *Ezh2fx/fx Ink4/Arf-/-* MEF and the RNA from one OHT or EtOH treatment in MEF *Ezh2fx/fx* were hybridized independently to Mouse Gene 1.0 ST Affymetrix Arrays. Signals were RMA normalized and analyzed using Affy and limma bioconductor packages in R. Affy IDs were annotated using mogene10sttranscriptcluster.db package. Probeset with a Log2 (FC)>0.5 expression

difference and a p-value less than 0.05 were considered as differentially expressed. The microarray data have been deposited at the GEO database (GSE48520).

5.12 DNA combing

DNA combing is a high specialized technique allowing you to directly visualize replication forks. This technique supplies one of the deepest (together with few other techniques like electron microscopy) way to finely analyse replication forks on different points of view. With this methodology it is possible to measure the replication forks speed, their symmetry degree in respect of an origin of replication, furthermore it is possible to stimate inter-origin distances and indirectly the number of origins of replication.

DNA combing has been performed as previously described elsewhere[240, 254]. Briefly, cells were sequentially labelled for 20 min. with 25 μM IdU followed by 20 min. of 200 μM CldU incubation in the cell culture medium. Labelled cells were embedded in agarose plugs, proteinase K-treated, DNA extracted and combed on silanised coverslips. DNA fibres were incubated with a mouse anti-ssDNA antibody (MAB3034, Chemicon) followed by anti-mouse IgG2a Alexa 546 coupled secondary antibody staining (Molecular Probes). Incorporation of halogenated nucleotides was detected with specific antibodies (IdU: mouse anti-BrdU, Becton Dickinson; CldU: rat anti-BrdU, Abcam) and visualized with appropriate secondary antibodies (goat anti-mouse IgG1-Alexa Fluor 647, Molecular Probes; goat anti-rat- Alexa Fluor 488, Molecular Probes). Images have been acquired automatically with a spinning disk confocal microscope and the individual labelled DNA molecules manually measured with ImageJ. The list of antibody used in the analyses is available in Table 1.

5.13 Hematopoietic stem cells and methylcellulose assay

Methylcellulose assay is a gold standard technique that allows measuring the self-renewal capability of stem cells or progentiors cells (like in this case HSCs or progenitor cells). It is possible to measure the number of colonies and the number of cells per colony (colony size). Transformed HSCs (cancer HSCs) will result in the formation of higher number of colonies and larger size compare to normal HSCs.

Bone marrow cells collected from the femur and tibia of *Ring1a-/-; Ring1b fx/fx* R26CRE-ER^{T2} mice have been subject to lineage negative (Lin-) enrichment using Hematopoietic Progenitor Enrichment Kit (StemCell Technologies) to remove cells expressing differentiation antigens. Lin- cells have been put in culture in DMEM (Lonza) complemented with 10% FBS for mouse myeloid colony forming cell (scFBS StemCell Technologies), 100ng/ml SCF (Peprotech), 20ng/ml recombinant IL3 (Peprotech), 20ng/ml IL6 (Peprotech), and infected using a lentiviral expressing vector EF1a-cMYC. After two rounds of spin-infection using RetroNectin-coated plates and three days of 2ug/mL puromycin selection, $5x10^3$ Lin- cells were plated in each 35mm dish mixed to 1,2ml of Metho cult GF M3434 (StemCell Technologies) in the presence of either 500nM OHT (Sigma) or ethanol (Panreac) as control. After 7 days, colonies were counted and $5x10^3$ cells derived from the colonies were re-plated two additional times in methylcellulose.

5.14 Tip tail fibroblasts

Tip tail fibroblasts are regarded as adult mice derived fibroblasts. Their characteristics (morphology, growth rate, etc.) are globally very similar to MEF ones.

Mice *Ink4a/Arf -/-; Ezh2 fx/fx* have been sacrificed and 4-5 cm of the tail has been cut and collected in cold 1XPBS (Lonza). After sterilization (with ethanol), the tail has been accurately dried off and incised with a razor for skin removal. The tail has been diced in little pieces then plated in 6 well- 0.1% gelatin-coated plates in the same medium described for MEFs.

5.15 Tandem affinity purification

This type of protein purification is used to improve the quality and the clearness of single step tag-protein purification. The FLAG tag is a commonly used to identify and isolate overexpressed proteins. The Avi tag consists in a peptidic sequence that could be identify by a bacterial enzyme called Bir-A that specifically biotinylate a lysine residue of the Avi peptidic sequence. This allows the efficient biotynilation of your Avi-

tagged protein in cells that express the BirA enzyme. Furthermore, performing the second purification step using streptavidin coated beads eliminate antibodies chains which are usually responsible of the noise in later analyses (i.e. mass spectrometry).

To identify protein complexes interacting with proteins of interest, tandem (double-step) affinity purifications were performed with Flag-Avi-Ring1b and Flag-Avi-Eed BirA MEF cell lines, as well as with Flag-Avi-empty BirA MEF, that served as negative control in both cases. All protein purifications were carried out on nuclei of the correspondent cell lines, prepared by 20 min swelling in nuclear prep buffer (10mM Tris, 100mM NaCl, 2mM MgCl2, 0.3 M Sucrose, 0.25 % v/v Igepal) at 4 °C. Nuclei were lysed in high salt buffer (50mM Tris–HCl pH 7.5, 300mM NaCl, 10% glycerol, 0.25% Igepal) with fresh addition of a protease inhibitor cocktail (Roche). The tandem affinity purifications were performed by incubating about 20 mg of nuclear protein extracts with 200 µl of packed agarose beads covalently linked with anti-Flag antibody (anti-Flag agarose beads, Sigma-Aldrich, cat. A2220) over night (ON) at 4 °C on a rotating platform. Beads were washed six times in minimum ten beads volumes of high salt buffer at 4°C and protein complexes eluted for 30 min with 0.5 mg/ml of Flag peptide (DYKDDDDK) in high salt buffer at 20°C four times. Eluates were pulled and further precipitated with 100 µl of streptavidin magnetic beads (Invitrogen, cat. 656-01) ON at 4 °C. Streptavidin beads were washed six times as before at 4°C and protein complexes eluted with Laemmli sample buffer (Invitrogen).

5.16 Proteomic analysis

Analysis of proteins isolated from tandem purifications was done by mass spectrometry (MS). MS is an analytical technique used not only in proteomic studies that produces spectra of the masses of the atoms or molecules present in a sample of material. A mass spectrometer is constituted by three fundamental instruments, corresponding to three specific functions: an ion source, a mass analyzer and a detector. Thus, the sample is first ionized, then correspondent ions are separated according to mass/charge ratio, and finally the detector converts signals received in spectra of the relative abundance of ions as a function of the mass-to-charge ratio. The atoms or molecules can be identified by correlating known masses to the identified

masses. In addition, two steps of mass analyzing can be done to refine the results, and in this case it is called tandem mass spectrometry or MS/MS. In our proteomic approach, briefly, proteins were separated by gel electrophoresis and enzymatically in gel-digested, producing a peptides mixture then separated by liquid chromatography before injecting into the mass spectrometer.

Protein digestion produces peptides earning each one a typical spectrum; in addition, some peptides are produced uniquely by digestion of specific proteins, therefore indicating without any doubt the presence of such proteins in the sample. Combining these features with computational tools, we were able to match peptide spectra with the proteins to which they belong.

Hence, eluted proteins obtained by tandem purifications were separated by 1D SDS–PAGE, using 4–12% NuPAGE Novex Bis–Tris gels (Invitrogen, cat. NP0321BOX) and NuPAGE® MES SDS running buffer (Invitrogen, cat. NP0002) according to manufacturer's instructions. In order to check purification efficiency, 10% of the whole eluate was separated on a gel and stained using SilverQuest staining kit (Invitrogen, cat. LC6070). The remaining part of the purification was separated on an independent gel and stained with Coomassie Blue using a Colloidal Blue Staining Kit (Invitrogen, Cat. LC6025). Samples were digested with trypsin (Promega). Briefly, the gel bands were cut and then washed four times with 50mM ammonium bicarbonate, 50% ethanol and incubated with 10mM DTT in 50mM ammonium bicarbonate for 1 h at 56°C for protein reduction. Alkylation step was performed incubating the sample with 55mM iodoacetamide in 50mM ammonium bicarbonate for 1 h at 25°C in the dark. Gel pieces were washed two times with a 50mM ammonium bicarbonate, 50% acetonitrile solution, dehydrated with 100% ethanol and dried in a vacuum concentrator. Digestion was performed using 12.5 ng/ml trypsin in 50mM ammonium bicarbonate and incubated for 16 h at 37°C for protein digestion. Supernatant was transferred to fresh tube, and the remaining peptides were extracted by incubating gel pieces two times with 30% acetonitrile (MeCN) in 3% trifluoroacetic acid (TFA), followed by dehydration with 100%

acetonitrile. The extracts were combined, reduced in volume in a vacuum concentrator, desalted and concentrated using RP-C18 StageTip columns and the eluted peptides used for mass spectrometric analysis.

Peptide mixtures were separated by nano-LC/MSMS using an Agilent 1100 Series nanoflow LC system (Agilent Technologies), interfaced to a 7-Tesla LTQ-FT-Ultra mass spectrometer (ThermoFisher Scientific, Bremen, Germany). The nanoliter flow LC was operated in one column set-up with a 15-cm analytical column (75 mm inner diameter, 350 mm outer diameter) packed with C18 resin (ReproSil, Pur C18AQ 3 mm, Dr Maisch, Germany). Solvent A was 0.1% FA and 5% ACN in ddH2 O and Solvent B was 95% CAN with 0.1% FA. Samples were injected in an aqueous 0.1% TFA solution at a flow rate of 500 nl/min. Peptides were separated with a gradient of 0–40% Solvent B over 90 min followed by a gradient of 40–60% for 10 min and 60–80% over 5 min at a flow rate of 250 nl/min. The mass spectrometer was operated in a data-dependent mode to automatically switch between MS and MS/MS acquisition. In the LTQ-FT full scan MS spectra were acquired in a range of m/z 300–1700 by FTICR with resolution r =100 000 at m/z 400 with a target value of 1 000 000. The five most intense ions were isolated for fragmentation in the linear ion trap at a target value of 5000. The nanoelectrospray ion source (Proxeon, Odense, Denmark) was used with a spray voltage of 2.4 kV. For the purification carried out on Flag-Avi-empty, Flag-Avi-Ring1b and Flag-Avi-Eed cells, collision gas pressure was 1.3 millitorrs and normalized collision energy using wide band activation mode was 35%. Ion selection threshold was 250 counts with an activation q=0.25. The activation time of 30 ms was applied in MS2 acquisitions. With Flag-Avi-empty Flag-Avi-Ring1b and Flag-Avi-Eed cells purifications, no sheath and auxiliary gases were used and capillary temperature was set to 180ºC. The activation time of 30 ms was applied in MS/MS acquisitions.

5.17 Protein identification

This bioinformatic methodology allows retrieving information on the identities of the proteins that were interacting with your protein of interest using specific algorithm and protein databases.

Data analysis and assigning sequences were done using MASCOT to identify proteins belonging to purifications from Flag-Avi-empty Flag-Avi-Ring1b and Flag-Avi-Eed cells. The raw data from LTQ-FT Ultra were converted to mgf files using Raw2MSM software[255]. The MS/MS peak lists were filtered to contain at most six peaks per 100 Dalton intervals and searched by Daemon (version 2.2.2, Matrix Science) against a concatenated forward and reversed version of IPI mouse database (version 6.63) (56 073 sequences; 25 214 299 residues)[256]. This database was complimented with frequently observed contaminants (porcine trypsin and human keratins) and their reversed sequences as well. Search parameters were: an initial MS tolerance of 7 ppm, a MS/MS mass tolerance at 0.5 Da and full trypsin cleavage specificity, allowing for up to two missed cleavages. Carbamidomethylation of cysteine was set as a fixed modification and variable modifications included oxidation on methionine and acetylation on N-terminus of proteins. We accepted peptides and proteins with a false discovery rate (FDR) of <1%, estimated based on the number of accepted reverse hits[257].

Differently, protein identification was performed using Andromeda search engine for purifications done with Flag-Avi-empty and Flag-Avi-Ring1b and Flag-Avi-Eed cells. The raw data from LTQ-FT Ultra were converted to mgf files using Raw2MSM software[255]. Raw data files were analyzed using MaxQuant software (version 1.3.0.1) as described[255]. Parent ion and MSMS spectra were searched against a database containing 87,061 protein sequences obtained from the human IPI protein database version 3.68 and 248 protein sequences of commonly observed contaminants using Andromeda search engine[258]. Spectra were searched with a mass tolerance of 7 ppm in MS mode and 0.5 Da in MS/MS mode, strict trypsin specificity and allowing up to two missed cleavage sites. Cysteine

carbamidomethylation was searched as a fixed modification, whereas N-terminal protein acetylation, methionine oxidation were searched as variable modifications. We accepted peptides and proteins with a false discovery rate (FDR) of <1%, estimated based on the number of accepted reverse hits[258]. Intensity based absolute quantification score (iBAQ) intensity values as calculated by MaxQuant were used to estimate relative abundance of proteins in each experiment[259].

5.18 Statistical analyses

Statistical analyses were carried out with R packages. p-values for growth curves and *in vivo* tumour growth were determined by computing the area under curve (AUC) using kulife package applied for student's t-test between AUC's of two samples or groups. p-Values for colonies and foci counts have been generated using a paired t-test. p-values for tumour masses weights were generated using a Mann-Whitney test. All p-Values obtained for DNA combing analyses have been determined with a chi-squared test.

5.19 Table 1

Reagent	Company	Catalogue #	Working dilution IB	Working dilution IF	Working dilution FACS
anti-p16	Santa Cruz	sc-1207 (M-156)	1:2000		
anti-p19/Arf	abcam	ab80	1:1000		
anti-β-tubulin	Santa cruz	sc-9104 (H-235)	1:1000		
anti-p21	DakoCytomation	M7202 (SX118)	1:1000		
anti-p53	home made	hybridoma	1:5		
anti-p53 phospho-S18	Cell Signaling	9284S	1:500		
anti-Ezh2	home made	hybridoma (BD43)	1:5		
anti-Suz12	Santa Cruz	sc-46264 (P-15)	1:1000		
anti-Eed	home made	hybridoma (AA19)	1:5		
anti-H-RAS	Santa Cruz	sc-520 (C20)	1:1000		
anti-SV40 T Ag	Santa Cruz	sc-148 (Pab 108)	1:1000		
anti-H3K27me3	Cell Signaling	9733S	1:500		
anti-H3	abcam	ab1791	1:10000		
anti-Ring1b	MBL	D139-3 (3-3)	1:1000		1:100
anti-H2AK119ubq	Cell Signaling	8240S	1:2000		
anti-H2A	Cell Signaling	12349	1:5000		
anti-Vinculin	home made	purified	1:50000		
anti-BrdU	BD	347580		1:5	1:5
anti-Suz12	Cell Signaling	3737S		1:50	
anti-53bp1	Millipore	NB 100-304		1:500	
DAPI	Sigma	D9542		0.5ug/mL	
Propidium iodide	Sigma	P4170			50ug/mL
anti-ssDNA	Chemicon	MAB3034		1:100	
anti-CldU	abcam	ab6326		1:200	
HRP-goat-anti-rabbit	Dako	P0448	1:5000		
HRP-goat-anti-mouse	Dako	P0447	1:5000		
HRP-rabbit-anti-goat	Dako	P0449	1:2000		
Alexa fluor 488 conjugated donkey-anti-rabbit	Invitrogen	A21206		1:100	
Dylight 649 conjugated donkey-anti-mouse	Jackson Immunoresearch	715495151		1:500	
FITC conjugated donkey-anti-mouse	Jackson Immunoresearch	715095150			1:50

5.20 Table 2

Vector name	***viral type***	***hairpin sequence***
H1P-UbqC-HYGROGFP Empty	lentiviral	
H1P-UbqC-HYGROGFP shSzu12	lenitiviral	AAGCTGTTACCAAGCTCCGTG
LKO shLuc puromycin	lentiviral	CCGGCGCTGAGTACTTCGAAATGTCCTCGAGGACATTTCGAAGTACTCAGCGTTTTTG
LKO shEed puromycin	lenitiviral	CCGGTCTTGCTAGTAAGGGCACATACTCGAGTATGTGCCCTTACTAGCAAGATTTTTG
EF1α-c-MYC puromycin	lentiviral	
pWZL SV40 ER neomycin	retroviral	
pBabe Empty puromycin	retroviral	
pBabe H-RASV12 puromycin	retroviral	
EF1α-Avi-Flag-Ring1b puromycin	lentiviral	
EF1α-Avi-Flag-Eed puromycin	lentiviral	

Acknowledgment

I thank Alexader Tarakhovsky for providing the *Ezh2* cKO mice, Miguel Vidal for *Ring1a* and *Ring1b* KO mice, Bruno Amati for the *p53* and *pRb* KO MEF and for his co-supervision during my PhD course, Elena Signaroldi and Federica Alberghini for help with mice and genotypes. I want to acknowledge Aurora Cerutti that performed the DNA combing and Mareike Albert that performed the embryo development experiment. Furthermore I want to thank the entire Pasini's lab for support and in particular Alessandra Rossi, Sriganesh Jammula, Andrea Scelfo and Laura Cedrone that partocopated directly to this project. A big thank to Pietro Vella that started with me the PhD course and shard with me a lot of unforgettable moments. I also thank FIRC (Fondazione italiana per la ricerca sul cancro) to have funded my fellowship for the last 2 years.

Finally 2 special thanks: the first goes to my girlfriend Giulia that shares with me the everyday life in and out the lab. She is the best colleague and girlfriend that anyone could have in his own life. The second goes to my Boss aka "il Capo" for always supporting me and my work in the best way possible and for his everyday (and every hour) availability to discuss both lab and not lab related problems and ideas.

References

1. Mikkelsen, T.S. *et al.* Genome-wide maps of chromatin state in pluripotent and lineage-committed cells. *Nature* **448**, 553-560 (2007).
2. Simon, J.A. & Kingston, R.E. Mechanisms of polycomb gene silencing: knowns and unknowns. *Nat Rev Mol Cell Biol* **10**, 697-708 (2009).
3. Simon, J. Locking in stable states of gene expression: transcriptional control during Drosophila development. *Curr Opin Cell Biol* **7**, 376-385 (1995).
4. Schwartz, Y.B. & Pirrotta, V. Polycomb complexes and epigenetic states. *Curr Opin Cell Biol* **20**, 266-273 (2008).
5. Orlando, V. & Paro, R. Chromatin multiprotein complexes involved in the maintenance of transcription patterns. *Curr Opin Genet Dev* **5**, 174-179 (1995).
6. Kennison, J.A. The Polycomb and trithorax group proteins of Drosophila: trans-regulators of homeotic gene function. *Annu Rev Genet* **29**, 289-303 (1995).
7. Morey, L. & Helin, K. Polycomb group protein-mediated repression of transcription. *Trends Biochem Sci* **35**, 323-332 (2010).
8. Francis, N.J., Saurin, A.J., Shao, Z. & Kingston, R.E. Reconstitution of a functional core polycomb repressive complex. *Mol Cell* **8**, 545-556 (2001).
9. King, I.F., Francis, N.J. & Kingston, R.E. Native and recombinant polycomb group complexes establish a selective block to template accessibility to repress transcription in vitro. *Mol Cell Biol* **22**, 7919-7928 (2002).
10. Shao, Z. *et al.* Stabilization of chromatin structure by PRC1, a Polycomb complex. *Cell* **98**, 37-46 (1999).
11. Voncken, J.W. *et al.* Rnf2 (Ring1b) deficiency causes gastrulation arrest and cell cycle inhibition. *Proc Natl Acad Sci U S A* **100**, 2468-2473 (2003).
12. van der Lugt, N.M. *et al.* Posterior transformation, neurological abnormalities, and severe hematopoietic defects in mice with a targeted deletion of the bmi-1 proto-oncogene. *Genes Dev* **8**, 757-769 (1994).
13. Cao, R. *et al.* Role of histone H3 lysine 27 methylation in Polycomb-group silencing. *Science* **298**, 1039-1043 (2002).
14. Czermin, B. *et al.* Drosophila enhancer of Zeste/ESC complexes have a histone H3 methyltransferase activity that marks chromosomal Polycomb sites. *Cell* **111**, 185-196 (2002).
15. Kuzmichev, A., Nishioka, K., Erdjument-Bromage, H., Tempst, P. & Reinberg, D. Histone methyltransferase activity associated with a human multiprotein complex containing the Enhancer of Zeste protein. *Genes Dev* **16**, 2893-2905 (2002).
16. Muller, J. *et al.* Histone methyltransferase activity of a Drosophila Polycomb group repressor complex. *Cell* **111**, 197-208 (2002).
17. Faust, C., Lawson, K.A., Schork, N.J., Thiel, B. & Magnuson, T. The Polycomb-group gene eed is required for normal morphogenetic movements during gastrulation in the mouse embryo. *Development* **125**, 4495-4506 (1998).
18. O'Carroll, D. *et al.* The polycomb-group gene Ezh2 is required for early mouse development. *Mol Cell Biol* **21**, 4330-4336. (2001).
19. Pasini, D., Bracken, A.P., Jensen, M.R., Denchi, E.L. & Helin, K. Suz12 is essential for mouse development and for EZH2 histone methyltransferase activity. *Embo J* **23**, 4061-4071 (2004).
20. Cao, R. *et al.* Role of hPHF1 in H3K27 methylation and Hox gene silencing. *Mol Cell Biol* **28**, 1862-1872 (2008).

21. Sarma, K., Margueron, R., Ivanov, A., Pirrotta, V. & Reinberg, D. Ezh2 requires PHF1 to efficiently catalyze H3 lysine 27 trimethylation in vivo. *Mol Cell Biol* **28**, 2718-2731 (2008).
22. Li, G. *et al.* Jarid2 and PRC2, partners in regulating gene expression. *Genes Dev* **24**, 368-380 (2010).
23. Shen, X. *et al.* Jumonji modulates polycomb activity and self-renewal versus differentiation of stem cells. *Cell* **139**, 1303-1314 (2009).
24. Walker, E. *et al.* Polycomb-like 2 associates with PRC2 and regulates transcriptional networks during mouse embryonic stem cell self-renewal and differentiation. *Cell Stem Cell* **6**, 153-166 (2010).
25. Landeira, D. *et al.* Jarid2 is a PRC2 component in embryonic stem cells required for multi-lineage differentiation and recruitment of PRC1 and RNA Polymerase II to developmental regulators. *Nat Cell Biol* **12**, 618-624 (2010).
26. Pasini, D. *et al.* JARID2 regulates binding of the Polycomb repressive complex 2 to target genes in ES cells. *Nature* **464**, 306-310 (2010).
27. Peng, J.C. *et al.* Jarid2/Jumonji coordinates control of PRC2 enzymatic activity and target gene occupancy in pluripotent cells. *Cell* **139**, 1290-1302 (2009).
28. Bernstein, B.E. *et al.* A bivalent chromatin structure marks key developmental genes in embryonic stem cells. *Cell* **125**, 315-326 (2006).
29. Boyer, L.A. *et al.* Polycomb complexes repress developmental regulators in murine embryonic stem cells. *Nature* **441**, 349-353 (2006).
30. Bracken, A.P., Dietrich, N., Pasini, D., Hansen, K.H. & Helin, K. Genome-wide mapping of Polycomb target genes unravels their roles in cell fate transitions. *Genes Dev* **20**, 1123-1136 (2006).
31. Lee, T.I. *et al.* Control of developmental regulators by Polycomb in human embryonic stem cells. *Cell* **125**, 301-313 (2006).
32. Mohn, F. *et al.* Lineage-specific polycomb targets and de novo DNA methylation define restriction and potential of neuronal progenitors. *Mol Cell* **30**, 755-766 (2008).
33. Squazzo, S.L. *et al.* Suz12 binds to silenced regions of the genome in a cell-type-specific manner. *Genome Res* **16**, 890-900 (2006).
34. Luger, K. Structure and dynamic behavior of nucleosomes. *Curr Opin Genet Dev* **13**, 127-135 (2003).
35. Jenuwein, T. & Allis, C.D. Translating the histone code. *Science* **293**, 1074-1080 (2001).
36. Hansen, K.H. & Helin, K. Epigenetic inheritance through self-recruitment of the polycomb repressive complex 2. *Epigenetics* **4**, 133-138 (2009).
37. Waddington, C.H. The Epigenotype. *Endeavour*, 18-20 (1942).
38. Levenson, J.M. & Sweatt, J.D. Epigenetic mechanisms in memory formation. *Nat Rev Neurosci* **6**, 108-118 (2005).
39. Keverne, B. Monoallelic gene expression and mammalian evolution. *Bioessays* **31**, 1318-1326 (2009).
40. Sparmann, A. & van Lohuizen, M. Polycomb silencers control cell fate, development and cancer. *Nat Rev Cancer* **6**, 846-856 (2006).
41. Cao, R. & Zhang, Y. SUZ12 is required for both the histone methyltransferase activity and the silencing function of the EED-EZH2 complex. *Mol Cell* **15**, 57-67 (2004).
42. Cao, R., Tsukada, Y. & Zhang, Y. Role of Bmi-1 and Ring1A in H2A ubiquitylation and Hox gene silencing. *Mol Cell* **20**, 845-854 (2005).
43. Bernstein, E. *et al.* Mouse polycomb proteins bind differentially to methylated histone H3 and RNA and are enriched in facultative heterochromatin. *Mol Cell Biol* **26**, 2560-2569 (2006).

44. Wang, H. *et al.* Role of histone H2A ubiquitination in Polycomb silencing. *Nature* **431**, 873-878 (2004).
45. Francis, N.J., Kingston, R.E. & Woodcock, C.L. Chromatin compaction by a polycomb group protein complex. *Science* **306**, 1574-1577 (2004).
46. Hanahan, D. & Weinberg, R.A. The hallmarks of cancer. *Cell* **100**, 57-70 (2000).
47. Mantovani, A. Cancer: Inflaming metastasis. *Nature* **457**, 36-37 (2009).
48. Carver, B.S. & Pandolfi, P.P. Mouse modeling in oncologic preclinical and translational research. *Clin Cancer Res* **12**, 5305-5311 (2006).
49. Degenhardt, K. & White, E. A mouse model system to genetically dissect the molecular mechanisms regulating tumorigenesis. *Clin Cancer Res* **12**, 5298-5304 (2006).
50. Fomchenko, E.I. & Holland, E.C. Mouse models of brain tumors and their applications in preclinical trials. *Clin Cancer Res* **12**, 5288-5297 (2006).
51. Olive, K.P. & Tuveson, D.A. The use of targeted mouse models for preclinical testing of novel cancer therapeutics. *Clin Cancer Res* **12**, 5277-5287 (2006).
52. Rangarajan, A. & Weinberg, R.A. Opinion: Comparative biology of mouse versus human cells: modelling human cancer in mice. *Nat Rev Cancer* **3**, 952-959 (2003).
53. Karakosta, A. *et al.* Genetic models of human cancer as a multistep process. Paradigm models of colorectal cancer, breast cancer, and chronic myelogenous and acute lymphoblastic leukaemia. *J Exp Clin Cancer Res* **24**, 505-514 (2005).
54. Krivtsov, A.V. & Armstrong, S.A. MLL translocations, histone modifications and leukaemia stem-cell development. *Nat Rev Cancer* **7**, 823-833 (2007).
55. Bracken, A.P. & Helin, K. Polycomb group proteins: navigators of lineage pathways led astray in cancer. *Nat Rev Cancer* **9**, 773-784 (2009).
56. Piunti, A. & Pasini, D. Epigenetic factors in cancer development: polycomb group proteins. *Future Oncol* **7**, 57-75 (2011).
57. van Lohuizen, M. *et al.* Identification of cooperating oncogenes in E mu-myc transgenic mice by provirus tagging. *Cell* **65**, 737-752 (1991).
58. Varambally, S. *et al.* The polycomb group protein EZH2 is involved in progression of prostate cancer. *Nature* **419**, 624-629 (2002).
59. Bracken, A.P. *et al.* EZH2 is downstream of the pRB-E2F pathway, essential for proliferation and amplified in cancer. *Embo J* **22**, 5323-5335 (2003).
60. Oguro, H. *et al.* Lethal myelofibrosis induced by Bmi1-deficient hematopoietic cells unveils a tumor suppressor function of the polycomb group genes. *The Journal of experimental medicine* **209**, 445-454 (2012).
61. Ntziachristos, P. *et al.* Genetic inactivation of the polycomb repressive complex 2 in T cell acute lymphoblastic leukemia. *Nature medicine* **18**, 298-301 (2012).
62. Simon, C. *et al.* A key role for EZH2 and associated genes in mouse and human adult T-cell acute leukemia. *Genes & development* **26**, 651-656 (2012).
63. Bernard, D. *et al.* CBX7 controls the growth of normal and tumor-derived prostate cells by repressing the Ink4a/Arf locus. *Oncogene* **24**, 5543-5551 (2005).
64. van Leenders, G.J. *et al.* Polycomb-group oncogenes EZH2, BMI1, and RING1 are overexpressed in prostate cancer with adverse pathologic and clinical features. *Eur Urol* **52**, 455-463 (2007).
65. Karanikolas, B.D., Figueiredo, M.L. & Wu, L. Comprehensive evaluation of the role of EZH2 in the growth, invasion, and aggression of a panel of prostate cancer cell lines. *Prostate* **70**, 675-688 (2010).
66. Yu, J. *et al.* Integrative genomics analysis reveals silencing of beta-adrenergic signaling by polycomb in prostate cancer. *Cancer Cell* **12**, 419-431 (2007).

67. Karanikolas, B.D., Figueiredo, M.L. & Wu, L. Polycomb group protein enhancer of zeste 2 is an oncogene that promotes the neoplastic transformation of a benign prostatic epithelial cell line. *Mol Cancer Res* **7**, 1456-1465 (2009).
68. Wang, W. *et al.* The novel tumor-suppressor Mel-18 in prostate cancer: its functional polymorphism, expression and clinical significance. *Int J Cancer* **125**, 2836-2843 (2009).
69. Guo, W.J., Datta, S., Band, V. & Dimri, G.P. Mel-18, a polycomb group protein, regulates cell proliferation and senescence via transcriptional repression of Bmi-1 and c-Myc oncoproteins. *Mol Biol Cell* **18**, 536-546 (2007).
70. Kajiume, T., Ninomiya, Y., Ishihara, H., Kanno, R. & Kanno, M. Polycomb group gene mel-18 modulates the self-renewal activity and cell cycle status of hematopoietic stem cells. *Exp Hematol* **32**, 571-578 (2004).
71. Park, I.K. *et al.* Bmi-1 is required for maintenance of adult self-renewing haematopoietic stem cells. *Nature* **423**, 302-305 (2003).
72. Nacerddine, K. *et al.* Akt-mediated phosphorylation of Bmi1 modulates its oncogenic potential, E3 ligase activity, and DNA damage repair activity in mouse prostate cancer. *J Clin Invest* **122**, 1920-1932 (2012).
73. Berezovska, O.P. *et al.* Essential role for activation of the Polycomb group (PcG) protein chromatin silencing pathway in metastatic prostate cancer. *Cell Cycle* **5**, 1886-1901 (2006).
74. Saramaki, O.R., Tammela, T.L., Martikainen, P.M., Vessella, R.L. & Visakorpi, T. The gene for polycomb group protein enhancer of zeste homolog 2 (EZH2) is amplified in late-stage prostate cancer. *Genes Chromosomes Cancer* **45**, 639-645 (2006).
75. Varambally, S. *et al.* Genomic loss of microRNA-101 leads to overexpression of histone methyltransferase EZH2 in cancer. *Science* **322**, 1695-1699 (2008).
76. Beke, L., Nuytten, M., Van Eynde, A., Beullens, M. & Bollen, M. The gene encoding the prostatic tumor suppressor PSP94 is a target for repression by the Polycomb group protein EZH2. *Oncogene* **26**, 4590-4595 (2007).
77. Min, J. *et al.* An oncogene-tumor suppressor cascade drives metastatic prostate cancer by coordinately activating Ras and nuclear factor-kappaB. *Nat Med* **16**, 286-294 (2010).
78. Yu, J. *et al.* A polycomb repression signature in metastatic prostate cancer predicts cancer outcome. *Cancer Res* **67**, 10657-10663 (2007).
79. Cao, Q. *et al.* Coordinated regulation of polycomb group complexes through microRNAs in cancer. *Cancer cell* **20**, 187-199 (2011).
80. Xu, K. *et al.* EZH2 oncogenic activity in castration-resistant prostate cancer cells is Polycomb-independent. *Science* **338**, 1465-1469 (2012).
81. Cavalli, G. Molecular biology. EZH2 goes solo. *Science* **338**, 1430-1431 (2012).
82. Zhao, J.C. *et al.* Cooperation between Polycomb and androgen receptor during oncogenic transformation. *Genome research* **22**, 322-331 (2012).
83. Furnari, F.B. *et al.* Malignant astrocytic glioma: genetics, biology, and paths to treatment. *Genes Dev* **21**, 2683-2710 (2007).
84. Abdouh, M. *et al.* BMI1 sustains human glioblastoma multiforme stem cell renewal. *J Neurosci* **29**, 8884-8896 (2009).
85. Godlewski, J. *et al.* Targeting of the Bmi-1 oncogene/stem cell renewal factor by microRNA-128 inhibits glioma proliferation and self-renewal. *Cancer Res* **68**, 9125-9130 (2008).
86. Korur, S. *et al.* GSK3beta regulates differentiation and growth arrest in glioblastoma. *PLoS One* **4**, e7443 (2009).
87. Suva, M.L. *et al.* EZH2 is essential for glioblastoma cancer stem cell maintenance. *Cancer Res* **69**, 9211-9218 (2009).

88. Bruggeman, S.W. *et al.* Bmi1 controls tumor development in an Ink4a/Arf-independent manner in a mouse model for glioma. *Cancer Cell* **12**, 328-341 (2007).
89. Fasano, C.A. *et al.* shRNA knockdown of Bmi-1 reveals a critical role for p21-Rb pathway in NSC self-renewal during development. *Cell stem cell* **1**, 87-99 (2007).
90. Ochiai, H. *et al.* Bmi1 is a MYCN target gene that regulates tumorigenesis through repression of KIF1Bbeta and TSLC1 in neuroblastoma. *Oncogene* **29**, 2681-2690 (2010).
91. Bruggeman, S.W., Hulsman, D. & van Lohuizen, M. Bmi1 deficient neural stem cells have increased integrin dependent adhesion to self-secreted matrix. *Biochim Biophys Acta* **1790**, 351-360 (2009).
92. Wiederschain, D. *et al.* Contribution of polycomb homologues Bmi-1 and Mel-18 to medulloblastoma pathogenesis. *Mol Cell Biol* **27**, 4968-4979 (2007).
93. Pengelly, A.R., Copur, O., Jackle, H., Herzig, A. & Muller, J. A histone mutant reproduces the phenotype caused by loss of histone-modifying factor Polycomb. *Science* **339**, 698-699 (2013).
94. Kim, E. *et al.* Phosphorylation of EZH2 activates STAT3 signaling via STAT3 methylation and promotes tumorigenicity of glioblastoma stem-like cells. *Cancer cell* **23**, 839-852 (2013).
95. Gargiulo, G. *et al.* In vivo RNAi screen for BMI1 targets identifies TGF-beta/BMP-ER stress pathways as key regulators of neural- and malignant glioma-stem cell homeostasis. *Cancer cell* **23**, 660-676 (2013).
96. Burgess, D.J. Histone modification at the gene level. *Nature reviews. Cancer* **12**, 156 (2012).
97. Burgess, D.J. Cancer genomics: Histone modification at the gene level. *Nature reviews. Genetics* **13**, 148-149 (2012).
98. Wu, G. *et al.* Somatic histone H3 alterations in pediatric diffuse intrinsic pontine gliomas and non-brainstem glioblastomas. *Nature genetics* **44**, 251-253 (2012).
99. Schwartzentruber, J. *et al.* Driver mutations in histone H3.3 and chromatin remodelling genes in paediatric glioblastoma. *Nature* **482**, 226-231 (2012).
100. Sturm, D. *et al.* Hotspot mutations in H3F3A and IDH1 define distinct epigenetic and biological subgroups of glioblastoma. *Cancer cell* **22**, 425-437 (2012).
101. Lewis, P.W. *et al.* Inhibition of PRC2 activity by a gain-of-function H3 mutation found in pediatric glioblastoma. *Science* **340**, 857-861 (2013).
102. Chan, K.M. *et al.* The histone H3.3K27M mutation in pediatric glioma reprograms H3K27 methylation and gene expression. *Genes & development* **27**, 985-990 (2013).
103. Collett, K. *et al.* Expression of enhancer of zeste homologue 2 is significantly associated with increased tumor cell proliferation and is a marker of aggressive breast cancer. *Clin Cancer Res* **12**, 1168-1174 (2006).
104. Kleer, C.G. *et al.* EZH2 is a marker of aggressive breast cancer and promotes neoplastic transformation of breast epithelial cells. *Proc Natl Acad Sci U S A* **100**, 11606-11611 (2003).
105. Ding, L., Erdmann, C., Chinnaiyan, A.M., Merajver, S.D. & Kleer, C.G. Identification of EZH2 as a molecular marker for a precancerous state in morphologically normal breast tissues. *Cancer Res* **66**, 4095-4099 (2006).
106. Silva, J. *et al.* Implication of polycomb members Bmi-1, Mel-18, and Hpc-2 in the regulation of p16INK4a, p14ARF, h-TERT, and c-Myc expression in primary breast carcinomas. *Clin Cancer Res* **12**, 6929-6936 (2006).

107. Lee, J.Y. *et al.* Mel-18 negatively regulates INK4a/ARF-independent cell cycle progression via Akt inactivation in breast cancer. *Cancer Res* **68**, 4201-4209 (2008).
108. Hoenerhoff, M.J. *et al.* BMI1 cooperates with H-RAS to induce an aggressive breast cancer phenotype with brain metastases. *Oncogene* **28**, 3022-3032 (2009).
109. Puppe, J. *et al.* BRCA1-deficient mammary tumor cells are dependent on EZH2 expression and sensitive to Polycomb Repressive Complex 2-inhibitor 3-deazaneplanocin A. *Breast Cancer Res* **11**, R63 (2009).
110. Li, X. *et al.* Targeted overexpression of EZH2 in the mammary gland disrupts ductal morphogenesis and causes epithelial hyperplasia. *Am J Pathol* **175**, 1246-1254 (2009).
111. Ben-Porath, I. *et al.* An embryonic stem cell-like gene expression signature in poorly differentiated aggressive human tumors. *Nat Genet* **40**, 499-507 (2008).
112. Gupta, R.A. *et al.* Long non-coding RNA HOTAIR reprograms chromatin state to promote cancer metastasis. *Nature* **464**, 1071-1076 (2010).
113. Rinn, J.L. *et al.* Functional demarcation of active and silent chromatin domains in human HOX loci by noncoding RNAs. *Cell* **129**, 1311-1323 (2007).
114. Wang, L. *et al.* BRCA1 is a negative modulator of the PRC2 complex. *The EMBO journal* **32**, 1584-1597 (2013).
115. Lessard, J. *et al.* Functional antagonism of the Polycomb-Group genes eed and Bmi1 in hemopoietic cell proliferation. *Genes Dev* **13**, 2691-2703 (1999).
116. Su, I.H. *et al.* Ezh2 controls B cell development through histone H3 methylation and Igh rearrangement. *Nat Immunol* **4**, 124-131 (2003).
117. Bea, S. *et al.* BMI-1 gene amplification and overexpression in hematological malignancies occur mainly in mantle cell lymphomas. *Cancer Res* **61**, 2409-2412 (2001).
118. Raaphorst, F.M. *et al.* Coexpression of BMI-1 and EZH2 polycomb group genes in Reed-Sternberg cells of Hodgkin's disease. *Am J Pathol* **157**, 709-715 (2000).
119. van Kemenade, F.J. *et al.* Coexpression of BMI-1 and EZH2 polycomb-group proteins is associated with cycling cells and degree of malignancy in B-cell non-Hodgkin lymphoma. *Blood* **97**, 3896-3901 (2001).
120. Visser, H.P. *et al.* The Polycomb group protein EZH2 is upregulated in proliferating, cultured human mantle cell lymphoma. *Br J Haematol* **112**, 950-958 (2001).
121. van Galen, J.C. *et al.* Expression of the polycomb-group gene BMI1 is related to an unfavourable prognosis in primary nodal DLBCL. *J Clin Pathol* **60**, 167-172 (2007).
122. Alkema, M.J., Jacobs, H., van Lohuizen, M. & Berns, A. Pertubation of B and T cell development and predisposition to lymphomagenesis in Emu Bmi1 transgenic mice require the Bmi1 RING finger. *Oncogene* **15**, 899-910 (1997).
123. Morin, R.D. *et al.* Somatic mutations altering EZH2 (Tyr641) in follicular and diffuse large B-cell lymphomas of germinal-center origin. *Nat Genet* **42**, 181-185 (2010).
124. Sneeringer, C.J. *et al.* Coordinated activities of wild-type plus mutant EZH2 drive tumor-associated hypertrimethylation of lysine 27 on histone H3 (H3K27) in human B-cell lymphomas. *Proceedings of the National Academy of Sciences of the United States of America* **107**, 20980-20985 (2010).
125. Yap, D.B. *et al.* Somatic mutations at EZH2 Y641 act dominantly through a mechanism of selectively altered PRC2 catalytic activity, to increase H3K27 trimethylation. *Blood* **117**, 2451-2459 (2011).

126. Verma, S.K. & Knight, S.D. Recent progress in the discovery of small-molecule inhibitors of the HMT EZH2 for the treatment of cancer. *Future medicinal chemistry* **5**, 1661-1670 (2013).
127. McCabe, M.T. *et al.* EZH2 inhibition as a therapeutic strategy for lymphoma with EZH2-activating mutations. *Nature* **492**, 108-112 (2012).
128. Knutson, S.K. *et al.* A selective inhibitor of EZH2 blocks H3K27 methylation and kills mutant lymphoma cells. *Nat Chem Biol* **8**, 890-896 (2012).
129. Qi, W. *et al.* Selective inhibition of Ezh2 by a small molecule inhibitor blocks tumor cells proliferation. *Proceedings of the National Academy of Sciences of the United States of America* **109**, 21360-21365 (2012).
130. Ernst, T. *et al.* Inactivating mutations of the histone methyltransferase gene EZH2 in myeloid disorders. *Nature genetics* **42**, 722-726 (2010).
131. Beguelin, W. *et al.* EZH2 is required for germinal center formation and somatic EZH2 mutations promote lymphoid transformation. *Cancer cell* **23**, 677-692 (2013).
132. Herrera-Merchan, A. *et al.* Ectopic expression of the histone methyltransferase Ezh2 in haematopoietic stem cells causes myeloproliferative disease. *Nature communications* **3**, 623 (2012).
133. Scott, C.L. *et al.* Role of the chromobox protein CBX7 in lymphomagenesis. *Proc Natl Acad Sci U S A* **104**, 5389-5394 (2007).
134. Redner, R.L. Variations on a theme: the alternate translocations in APL. *Leukemia* **16**, 1927-1932 (2002).
135. Villa, R. *et al.* Role of the polycomb repressive complex 2 in acute promyelocytic leukemia. *Cancer Cell* **11**, 513-525 (2007).
136. Boukarabila, H. *et al.* The PRC1 Polycomb group complex interacts with PLZF/RARA to mediate leukemic transformation. *Genes Dev* **23**, 1195-1206 (2009).
137. Chowdhury, M. *et al.* Expression of Polycomb-group (PcG) protein BMI-1 predicts prognosis in patients with acute myeloid leukemia. *Leukemia* **21**, 1116-1122 (2007).
138. Mohty, M., Yong, A.S., Szydlo, R.M., Apperley, J.F. & Melo, J.V. The polycomb group BMI1 gene is a molecular marker for predicting prognosis of chronic myeloid leukemia. *Blood* **110**, 380-383 (2007).
139. Sawa, M. *et al.* BMI-1 is highly expressed in M0-subtype acute myeloid leukemia. *Int J Hematol* **82**, 42-47 (2005).
140. Lessard, J. & Sauvageau, G. Bmi-1 determines the proliferative capacity of normal and leukaemic stem cells. *Nature* **423**, 255-260 (2003).
141. Fiskus, W. *et al.* Combined epigenetic therapy with the histone methyltransferase EZH2 inhibitor 3-deazaneplanocin A and the histone deacetylase inhibitor panobinostat against human AML cells. *Blood* **114**, 2733-2743 (2009).
142. Tokimasa, S. *et al.* Lack of the Polycomb-group gene rae28 causes maturation arrest at the early B-cell developmental stage. *Exp Hematol* **29**, 93-103 (2001).
143. Nikoloski, G. *et al.* Somatic mutations of the histone methyltransferase gene EZH2 in myelodysplastic syndromes. *Nat Genet* **42**, 665-667 (2010).
144. Breuer, R.H. *et al.* Increased expression of the EZH2 polycomb group gene in BMI-1-positive neoplastic cells during bronchial carcinogenesis. *Neoplasia* **6**, 736-743 (2004).
145. Breuer, R.H. *et al.* Expression of the p16(INK4a) gene product, methylation of the p16(INK4a) promoter region and expression of the polycomb-group gene BMI-1 in squamous cell lung carcinoma and premalignant endobronchial lesions. *Lung Cancer* **48**, 299-306 (2005).

146. Dovey, J.S., Zacharek, S.J., Kim, C.F. & Lees, J.A. Bmi1 is critical for lung tumorigenesis and bronchioalveolar stem cell expansion. *Proc Natl Acad Sci U S A* **105**, 11857-11862 (2008).
147. Hussain, M. *et al.* Tobacco smoke induces polycomb-mediated repression of Dickkopf-1 in lung cancer cells. *Cancer Res* **69**, 3570-3578 (2009).
148. Sasaki, M. *et al.* The overexpression of polycomb group proteins Bmi1 and EZH2 is associated with the progression and aggressive biological behavior of hepatocellular carcinoma. *Lab Invest* **88**, 873-882 (2008).
149. Steele, J.C. *et al.* The polycomb group proteins, BMI-1 and EZH2, are tumour-associated antigens. *Br J Cancer* **95**, 1202-1211 (2006).
150. Kang, M.K. *et al.* Elevated Bmi-1 expression is associated with dysplastic cell transformation during oral carcinogenesis and is required for cancer cell replication and survival. *Br J Cancer* **96**, 126-133 (2007).
151. Kidani, K. *et al.* High expression of EZH2 is associated with tumor proliferation and prognosis in human oral squamous cell carcinomas. *Oral Oncol* **45**, 39-46 (2009).
152. Cai, G.H., Wang, K., Miao, Q., Peng, Y.S. & Chen, X.Y. Expression of polycomb protein EZH2 in multi-stage tissues of gastric carcinogenesis. *J Dig Dis* **11**, 88-93 (2010).
153. Li, W., Li, Y., Tan, Y., Ma, K. & Cui, J. Bmi-1 is critical for the proliferation and invasiveness of gastric carcinoma cells. *J Gastroenterol Hepatol* **25**, 568-575 (2010).
154. Mimori, K. *et al.* Clinical significance of enhancer of zeste homolog 2 expression in colorectal cancer cases. *Eur J Surg Oncol* **31**, 376-380 (2005).
155. Tateishi, K. *et al.* Dysregulated expression of stem cell factor Bmi1 in precancerous lesions of the gastrointestinal tract. *Clin Cancer Res* **12**, 6960-6966 (2006).
156. Sasaki, H. *et al.* The knock-down of overexpressed EZH2 and BMI-1 does not prevent osteosarcoma growth. *Oncol Rep* **23**, 677-684 (2010).
157. Arisan, S. *et al.* Increased expression of EZH2, a polycomb group protein, in bladder carcinoma. *Urol Int* **75**, 252-257 (2005).
158. Raman, J.D. *et al.* Increased expression of the polycomb group gene, EZH2, in transitional cell carcinoma of the bladder. *Clin Cancer Res* **11**, 8570-8576 (2005).
159. Shafaroudi, A.M. *et al.* Overexpression of BMI1, a polycomb group repressor protein, in bladder tumors: a preliminary report. *Urol J* **5**, 99-105 (2008).
160. Weikert, S. *et al.* Expression levels of the EZH2 polycomb transcriptional repressor correlate with aggressiveness and invasive potential of bladder carcinomas. *Int J Mol Med* **16**, 349-353 (2005).
161. McHugh, J.B., Fullen, D.R., Ma, L., Kleer, C.G. & Su, L.D. Expression of polycomb group protein EZH2 in nevi and melanoma. *J Cutan Pathol* **34**, 597-600 (2007).
162. Bachmann, I.M., Puntervoll, H.E., Otte, A.P. & Akslen, L.A. Loss of BMI-1 expression is associated with clinical progress of malignant melanoma. *Mod Pathol* **21**, 583-590 (2008).
163. Song, L.B. *et al.* The polycomb group protein Bmi-1 represses the tumor suppressor PTEN and induces epithelial-mesenchymal transition in human nasopharyngeal epithelial cells. *J Clin Invest* **119**, 3626-3636 (2009).
164. Friedman, J.M. *et al.* The putative tumor suppressor microRNA-101 modulates the cancer epigenome by repressing the polycomb group protein EZH2. *Cancer Res* **69**, 2623-2629 (2009).

165. Hinz, S. *et al.* EZH2 polycomb transcriptional repressor expression correlates with methylation of the APAF-1 gene in superficial transitional cell carcinoma of the bladder. *Tumour Biol* **28**, 151-157 (2007).
166. Mallen-St Clair, J. *et al.* EZH2 couples pancreatic regeneration to neoplastic progression. *Genes & development* **26**, 439-444 (2012).
167. Karamitopoulou, E. *et al.* Loss of the CBX7 protein expression correlates with a more aggressive phenotype in pancreatic cancer. *Eur J Cancer* **46**, 1438-1444 (2010).
168. Deshpande, A.M. *et al.* PHC3, a component of the hPRC-H complex, associates with E2F6 during G0 and is lost in osteosarcoma tumors. *Oncogene* **26**, 1714-1722 (2007).
169. Koontz, J.I. *et al.* Frequent fusion of the JAZF1 and JJAZ1 genes in endometrial stromal tumors. *Proc Natl Acad Sci U S A* **98**, 6348-6353 (2001).
170. Micci, F., Panagopoulos, I., Bjerkehagen, B. & Heim, S. Consistent rearrangement of chromosomal band 6p21 with generation of fusion genes JAZF1/PHF1 and EPC1/PHF1 in endometrial stromal sarcoma. *Cancer Res* **66**, 107-112 (2006).
171. Li, H., Wang, J., Mor, G. & Sklar, J. A neoplastic gene fusion mimics trans-splicing of RNAs in normal human cells. *Science* **321**, 1357-1361 (2008).
172. Ringrose, L. & Paro, R. Polycomb/Trithorax response elements and epigenetic memory of cell identity. *Development* **134**, 223-232 (2007).
173. Ringrose, L., Rehmsmeier, M., Dura, J.M. & Paro, R. Genome-wide prediction of Polycomb/Trithorax response elements in Drosophila melanogaster. *Dev Cell* **5**, 759-771 (2003).
174. Negre, N. *et al.* Chromosomal distribution of PcG proteins during Drosophila development. *PLoS Biol* **4**, e170 (2006).
175. Sing, A. *et al.* A vertebrate Polycomb response element governs segmentation of the posterior hindbrain. *Cell* **138**, 885-897 (2009).
176. Woo, C.J., Kharchenko, P.V., Daheron, L., Park, P.J. & Kingston, R.E. A region of the human HOXD cluster that confers polycomb-group responsiveness. *Cell* **140**, 99-110.
177. Pasini, D. *et al.* Coordinated regulation of transcriptional repression by the RBP2 H3K4 demethylase and Polycomb-Repressive Complex 2. *Genes Dev* **22**, 1345-1355 (2008).
178. Herranz, N. *et al.* Polycomb complex 2 is required for E-cadherin repression by the Snail1 transcription factor. *Mol Cell Biol* **28**, 4772-4781 (2008).
179. Shi, B. *et al.* Integration of estrogen and Wnt signaling circuits by the polycomb group protein EZH2 in breast cancer cells. *Mol Cell Biol* **27**, 5105-5119 (2007).
180. Zhao, J., Sun, B.K., Erwin, J.A., Song, J.J. & Lee, J.T. Polycomb proteins targeted by a short repeat RNA to the mouse X chromosome. *Science* **322**, 750-756 (2008).
181. Yap, K.L. *et al.* Molecular interplay of the noncoding RNA ANRIL and methylated histone H3 lysine 27 by polycomb CBX7 in transcriptional silencing of INK4a. *Mol Cell* **38**, 662-674 (2010).
182. Tsai, M.C. *et al.* Long noncoding RNA as modular scaffold of histone modification complexes. *Science* **329**, 689-693 (2010).
183. Davidovich, C., Zheng, L., Goodrich, K.J. & Cech, T.R. Promiscuous RNA binding by Polycomb repressive complex 2. *Nature structural & molecular biology* **20**, 1250-1257 (2013).
184. Barrero, M.J. & Izpisua Belmonte, J.C. Polycomb complex recruitment in pluripotent stem cells. *Nature cell biology* **15**, 348-350 (2013).

185. Min, J., Zhang, Y. & Xu, R.M. Structural basis for specific binding of Polycomb chromodomain to histone H3 methylated at Lys 27. *Genes & development* **17**, 1823-1828 (2003).
186. Tavares, L. *et al.* RYBP-PRC1 complexes mediate H2A ubiquitylation at polycomb target sites independently of PRC2 and H3K27me3. *Cell* **148**, 664-678 (2012).
187. Wu, X., Johansen, J.V. & Helin, K. Fbxl10/Kdm2b recruits polycomb repressive complex 1 to CpG islands and regulates H2A ubiquitylation. *Molecular cell* **49**, 1134-1146 (2013).
188. He, J. *et al.* Kdm2b maintains murine embryonic stem cell status by recruiting PRC1 complex to CpG islands of developmental genes. *Nature cell biology* **15**, 373-384 (2013).
189. Farcas, A.M. *et al.* KDM2B links the Polycomb Repressive Complex 1 (PRC1) to recognition of CpG islands. *eLife* **1**, e00205 (2012).
190. Melnick, A. Epigenetic therapy leaps ahead with specific targeting of EZH2. *Cancer cell* **22**, 569-570 (2012).
191. Tan, J. *et al.* Pharmacologic disruption of Polycomb-repressive complex 2-mediated gene repression selectively induces apoptosis in cancer cells. *Genes Dev* **21**, 1050-1063 (2007).
192. Sun, F. *et al.* Combinatorial pharmacologic approaches target EZH2-mediated gene repression in breast cancer cells. *Mol Cancer Ther* **8**, 3191-3202 (2009).
193. Miranda, T.B. *et al.* DZNep is a global histone methylation inhibitor that reactivates developmental genes not silenced by DNA methylation. *Mol Cancer Ther* **8**, 1579-1588 (2009).
194. Margueron, R. *et al.* Role of the polycomb protein EED in the propagation of repressive histone marks. *Nature* **461**, 762-767 (2009).
195. Kim, W. *et al.* Targeted disruption of the EZH2-EED complex inhibits EZH2-dependent cancer. *Nature chemical biology* **9**, 643-650 (2013).
196. Bracken, A.P. *et al.* The Polycomb group proteins bind throughout the INK4A-ARF locus and are disassociated in senescent cells. *Genes Dev* **21**, 525-530 (2007).
197. Dietrich, N. *et al.* Bypass of senescence by the polycomb group protein CBX8 through direct binding to the INK4A-ARF locus. *EMBO J* **26**, 1637-1648 (2007).
198. Jacobs, J.J., Kieboom, K., Marino, S., DePinho, R.A. & van Lohuizen, M. The oncogene and Polycomb-group gene bmi-1 regulates cell proliferation and senescence through the ink4a locus. *Nature* **397**, 164-168 (1999).
199. Gil, J. & Peters, G. Regulation of the INK4b-ARF-INK4a tumour suppressor locus: all for one or one for all. *Nat Rev Mol Cell Biol* **7**, 667-677 (2006).
200. Gil, J., Bernard, D., Martinez, D. & Beach, D. Polycomb CBX7 has a unifying role in cellular lifespan. *Nat Cell Biol* **6**, 67-72 (2004).
201. Jacobs, J.J. *et al.* Bmi-1 collaborates with c-Myc in tumorigenesis by inhibiting c-Myc-induced apoptosis via INK4a/ARF. *Genes Dev* **13**, 2678-2690 (1999).
202. Forzati, F. *et al.* CBX7 is a tumor suppressor in mice and humans. *The Journal of clinical investigation* **122**, 612-623 (2012).
203. Bruggeman, S.W. *et al.* Ink4a and Arf differentially affect cell proliferation and neural stem cell self-renewal in Bmi1-deficient mice. *Genes Dev* **19**, 1438-1443 (2005).
204. Chen, H. *et al.* Polycomb protein Ezh2 regulates pancreatic beta-cell Ink4a/Arf expression and regeneration in diabetes mellitus. *Genes Dev* **23**, 975-985 (2009).

205. Dhawan, S., Tschen, S.I. & Bhushan, A. Bmi-1 regulates the Ink4a/Arf locus to control pancreatic beta-cell proliferation. *Genes & development* **23**, 906-911 (2009).
206. Zhou, J.X. *et al.* Combined modulation of polycomb and trithorax genes rejuvenates beta cell replication. *The Journal of clinical investigation* (2013).
207. Ezhkova, E. *et al.* Ezh2 orchestrates gene expression for the stepwise differentiation of tissue-specific stem cells. *Cell* **136**, 1122-1135 (2009).
208. Hidalgo, I. *et al.* Ezh1 is required for hematopoietic stem cell maintenance and prevents senescence-like cell cycle arrest. *Cell stem cell* **11**, 649-662 (2012).
209. Biehs, B. *et al.* BMI1 represses Ink4a/Arf and Hox genes to regulate stem cells in the rodent incisor. *Nature cell biology* **15**, 846-852 (2013).
210. Liu, J. *et al.* Bmi1 regulates mitochondrial function and the DNA damage response pathway. *Nature* **459**, 387-392 (2009).
211. Vonlanthen, S. *et al.* The bmi-1 oncoprotein is differentially expressed in non-small cell lung cancer and correlates with INK4A-ARF locus expression. *Br J Cancer* **84**, 1372-1376 (2001).
212. Dukers, D.F. *et al.* Unique polycomb gene expression pattern in Hodgkin's lymphoma and Hodgkin's lymphoma-derived cell lines. *Am J Pathol* **164**, 873-881 (2004).
213. Young, N.P. & Jacks, T. Tissue-specific p19Arf regulation dictates the response to oncogenic K-ras. *Proc Natl Acad Sci U S A* **107**, 10184-10189.
214. Douglas, D. *et al.* BMI-1 promotes ewing sarcoma tumorigenicity independent of CDKN2A repression. *Cancer Res* **68**, 6507-6515 (2008).
215. Hanahan, D. & Weinberg, R.A. Hallmarks of cancer: the next generation. *Cell* **144**, 646-674 (2011).
216. Medema, R.H. & Macurek, L. Checkpoint control and cancer. *Oncogene* **31**, 2601-2613 (2012).
217. Hahn, W.C. *et al.* Creation of human tumour cells with defined genetic elements. *Nature* **400**, 464-468 (1999).
218. Ventura, A. *et al.* Restoration of p53 function leads to tumour regression in vivo. *Nature* **445**, 661-665 (2007).
219. Serrano, M. *et al.* Role of the INK4a locus in tumor suppression and cell mortality. *Cell* **85**, 27-37 (1996).
220. Kamijo, T. *et al.* Tumor suppression at the mouse INK4a locus mediated by the alternative reading frame product p19ARF. *Cell* **91**, 649-659 (1997).
221. Sperka, T., Wang, J. & Rudolph, K.L. DNA damage checkpoints in stem cells, ageing and cancer. *Nat Rev Mol Cell Biol* **13**, 579-590 (2012).
222. Kim, W.Y. & Sharpless, N.E. The regulation of INK4/ARF in cancer and aging. *Cell* **127**, 265-275 (2006).
223. Yang, M.H. *et al.* Bmi1 is essential in Twist1-induced epithelial-mesenchymal transition. *Nat Cell Biol* **12**, 982-992 (2010).
224. Miyazaki, M. *et al.* Thymocyte proliferation induced by pre-T cell receptor signaling is maintained through polycomb gene product Bmi-1-mediated Cdkn2a repression. *Immunity* **28**, 231-245 (2008).
225. Smith, K.S. *et al.* Bmi-1 regulation of INK4A-ARF is a downstream requirement for transformation of hematopoietic progenitors by E2a-Pbx1. *Mol Cell* **12**, 393-400 (2003).
226. Wen, W. *et al.* Knockdown of RNF2 induces apoptosis by regulating MDM2 and p53 stability. *Oncogene* (2013).
227. Su, W.J. *et al.* RNF2/Ring1b negatively regulates p53 expression in selective cancer cell types to promote tumor development. *Proceedings of the National Academy of Sciences of the United States of America* **110**, 1720-1725 (2013).

228. Calao, M. *et al.* Direct effects of Bmi1 on p53 protein stability inactivates oncoprotein stress responses in embryonal cancer precursor cells at tumor initiation. *Oncogene* (2012).
229. Datta, S. *et al.* Bmi-1 cooperates with H-Ras to transform human mammary epithelial cells via dysregulation of multiple growth-regulatory pathways. *Cancer Res* **67**, 10286-10295 (2007).
230. Serrano, M. The INK4a/ARF locus in murine tumorigenesis. *Carcinogenesis* **21**, 865-869 (2000).
231. Parrinello, S. *et al.* Oxygen sensitivity severely limits the replicative lifespan of murine fibroblasts. *Nat Cell Biol* **5**, 741-747 (2003).
232. Seibler, J. *et al.* Rapid generation of inducible mouse mutants. *Nucleic Acids Res* **31**, e12 (2003).
233. Pasini, D., Bracken, A.P., Jensen, M.R., Lazzerini Denchi, E. & Helin, K. Suz12 is essential for mouse development and for EZH2 histone methyltransferase activity. *EMBO J* **23**, 4061-4071 (2004).
234. Margueron, R. & Reinberg, D. The Polycomb complex PRC2 and its mark in life. *Nature* **469**, 343-349 (2011).
235. de Napoles, M. *et al.* Polycomb group proteins Ring1A/B link ubiquitylation of histone H2A to heritable gene silencing and X inactivation. *Dev Cell* **7**, 663-676 (2004).
236. Francis, N.J., Follmer, N.E., Simon, M.D., Aghia, G. & Butler, J.D. Polycomb proteins remain bound to chromatin and DNA during DNA replication in vitro. *Cell* **137**, 110-122 (2009).
237. Hansen, K.H. *et al.* A model for transmission of the H3K27me3 epigenetic mark. *Nat Cell Biol* **10**, 1291-1300 (2008).
238. Duhamel, S. *et al.* Sef downregulation by Ras causes MEK1/2 to become aberrantly nuclear localized leading to polyploidy and neoplastic transformation. *Cancer Res* **72**, 626-635 (2012).
239. Li, Q. & Dang, C.V. c-Myc overexpression uncouples DNA replication from mitosis. *Mol Cell Biol* **19**, 5339-5351 (1999).
240. Michalet, X. *et al.* Dynamic molecular combing: stretching the whole human genome for high-resolution studies. *Science* **277**, 1518-1523 (1997).
241. Doksani, Y., Bermejo, R., Fiorani, S., Haber, J.E. & Foiani, M. Replicon dynamics, dormant origin firing, and terminal fork integrity after double-strand break formation. *Cell* **137**, 247-258 (2009).
242. Bianco, J.N. *et al.* Analysis of DNA replication profiles in budding yeast and mammalian cells using DNA combing. *Methods* **57**, 149-157 (2012).
243. Lukas, C. *et al.* 53BP1 nuclear bodies form around DNA lesions generated by mitotic transmission of chromosomes under replication stress. *Nat Cell Biol* **13**, 243-253 (2011).
244. Tai, Y.C., Tan, J.A. & Peh, S.C. Higher frequency of p53 gene mutations in diffuse large B-cell lymphoma with MALT component. *Pathol Int* **54**, 811-818 (2004).
245. Simonitsch-Klupp, I. *et al.* Diffuse large B-cell lymphomas with plasmablastic/plasmacytoid features are associated with TP53 deletions and poor clinical outcome. *Leukemia* **18**, 146-155 (2004).
246. Di Micco, R. *et al.* Oncogene-induced senescence is a DNA damage response triggered by DNA hyper-replication. *Nature* **444**, 638-642 (2006).
247. Herold, S., Herkert, B. & Eilers, M. Facilitating replication under stress: an oncogenic function of MYC? *Nat Rev Cancer* **9**, 441-444 (2009).
248. Zheng, L. *et al.* Polyploid cells rewire DNA damage response networks to overcome replication stress-induced barriers for tumour progression. *Nat Commun* **3**, 815 (2012).

249. Lehmann, L. *et al.* Polycomb repressive complex 1 (PRC1) disassembles RNA polymerase II preinitiation complexes. *J Biol Chem* **287**, 35784-35794 (2012).
250. Helmrich, A., Ballarino, M., Nudler, E. & Tora, L. Transcription-replication encounters, consequences and genomic instability. *Nature structural & molecular biology* **20**, 412-418 (2013).
251. Pasini, D., Bracken, A.P., Hansen, J.B., Capillo, M. & Helin, K. The polycomb group protein Suz12 is required for embryonic stem cell differentiation. *Mol Cell Biol* **27**, 3769-3779 (2007).
252. Campaner, S. *et al.* Cdk2 suppresses cellular senescence induced by the c-myc oncogene. *Nat Cell Biol* **12**, 54-59; sup pp 51-14 (2010).
253. Vella, P. *et al.* Tet proteins connect the O-linked N-acetylglucosamine transferase Ogt to chromatin in embryonic stem cells. *Mol Cell* **49**, 645-656 (2013).
254. Lebofsky, R. & Bensimon, A. Single DNA molecule analysis: applications of molecular combing. *Brief Funct Genomic Proteomic* **1**, 385-396 (2003).
255. Olsen, J.V. *et al.* Parts per million mass accuracy on an Orbitrap mass spectrometer via lock mass injection into a C-trap. *Mol Cell Proteomics* **4**, 2010-2021 (2005).
256. Kall, L., Storey, J.D., MacCoss, M.J. & Noble, W.S. Assigning significance to peptides identified by tandem mass spectrometry using decoy databases. *J Proteome Res* **7**, 29-34 (2008).
257. Elias, J.E., Haas, W., Faherty, B.K. & Gygi, S.P. Comparative evaluation of mass spectrometry platforms used in large-scale proteomics investigations. *Nat Methods* **2**, 667-675 (2005).
258. Cox, J. *et al.* Andromeda: a peptide search engine integrated into the MaxQuant environment. *J Proteome Res* **10**, 1794-1805 (2011).
259. Arike, L. *et al.* Comparison and applications of label-free absolute proteome quantification methods on Escherichia coli. *Journal of proteomics* **75**, 5437-5448 (2012).